UNIVERSITY OF SOUTHAMPTON

FACULTY OF SOCIAL AND HUMAN SCIENCES

Mathematical Sciences

Neutron star oscillations from starquakes

by

Lucy Keer

Thesis for the degree of Doctor of Philosophy

January 2014

UNIVERSITY OF SOUTHAMPTON

ABSTRACT

FACULTY OF SOCIAL AND HUMAN SCIENCES
Mathematical Sciences

Doctor of Philosophy

NEUTRON STAR OSCILLATIONS FROM STARQUAKES

by Lucy Keer

Glitches are sudden increases in the otherwise extremely regular spin rate of pulsars. One theory proposed to account for these glitches is the starquake model, in which the spinup is caused by a sudden rearrangement of the neutron star crust.

Starquakes can be expected to excite some of the oscillation modes of the neutron star. These oscillations are of interest as a source of gravitational waves, and may also modify the pulsar radio emission. In this thesis we develop a toy model of the starquake and calculate which modes of the star are excited.

We start by making some order-of-magnitude upper estimates on the energy made available by the starquake and the amplitude of the modes excited, before moving on to a more detailed calculation based on a specific model of the starquake in which all strain is lost instantaneously from the star at the glitch. To find out which modes are excited by the starquake, we construct initial data describing the change in the star at the glitch, and then project this against the basis of normal modes of the star.

We first carry out this procedure for a simplified model in which the star has spun down to zero angular velocity before the starquake. We find that the majority of the energy released goes into a mode similar to the fundamental mode of a fluid star.

Finally, we describe the extension of this model to the more realistic case where the star is rotating before the glitch. We calculate the change in the normal modes of the star to first order in the rotation; these are no longer orthogonal, but we construct a scheme that still enables us to project our initial data against this set of modes, and discuss some preliminary results of the model.

Contents

List of Figures

Acknowledgements

First of all, I'd like to thank my supervisor, Ian Jones, for all his help throughout, and his intuition for always finding the simplest problem that will give insight into the physics. I hope that along the way I've learnt to think at least a bit less like a maths student and more like a physicist. Thanks also to my my adviser Ian Hawke, for very detailed and useful comments on my earlier work, all of which helped to improve the final thesis a great deal. Writing these acknowledgements at the last minute does at least mean I also have the opportunity to thank my examiners, Leor Barack and Nikolaos Stergioulas, for the thorough reading of my thesis and the very constructive suggestions and corrections – it is much appreciated.

The Southampton general relativity group has been a very enjoyable place to work, and to learn and discuss new physics. Thanks in particular to Sam Lander for all the helpful comments, and even more for all the unhelpful but entertaining ones. Also to Mike Hogg and Cesár Merlín González for moral support during the many weekend hours spent slowly losing the plot in the maths department towards the end.

I've been lucky to have family who have been extremely supportive throughout. Special thanks to my parents, Peter and Val Keer, for never asking me when I'm going to go and get a real job. Lots of thanks as well to Andrew, Andrea and Laura Keer, and in particular to Eugene Gill for lending me all those popular science books and getting me interested in this physics nonsense in the first place. I also hope my nephew James Gill will read this some time and point out all the mistakes to me!

Declaration of Authorship

I, Lucy Keer, declare that the thesis entitled *Neutron star oscillations from starquakes* and the work presented in the thesis are both my own, and have been generated by me as the result of my own original research. I confirm that:

- this work was done wholly or mainly while in candidature for a research degree at this University;
- where any part of this thesis has previously been submitted for a degree or any other qualification at this University or any other institution, this has been clearly stated;
- where I have consulted the published work of others, this is always clearly attributed;
- where I have quoted from the work of others, the source is always given. With the exception of such quotations, this thesis is entirely my own work;
- I have acknowledged all main sources of help;
- where the thesis is based on work done by myself jointly with others, I have made clear exactly what was done by others and what I have contributed myself;
- none of this work has been published before submission

Signed:.....

Date:.....

Chapter 1

Introduction

1.1 Neutron star physics

Neutron stars are complicated. These dense remnants, formed by the gravitational collapse of some massive stars, contain a mass of one or two times the mass of the Sun within a radius of only around 10 km. For an object this compact, the effects of general relativity become important, making neutron stars a good candidate for the emission of gravitational waves. Neutron stars have a stratified structure, with a solid crust and an outer core composed of superfluid neutrons and superconducting protons, while the properties of matter at the high densities of the inner core are still poorly understood. Further complications are introduced to the stellar structure by the extremely high magnetic fields of some neutron stars, of up to around 10^{14} gauss, and by their rotation, which can reach frequencies of up to around 700 Hz.

Disentangling these effects is a challenging problem. One of the most promising approaches is to use the methods of *seismology*: the determination of an object's properties from its characteristic modes of oscillation after a disturbance from equilibrium. Originally used with great success to determine the composition of the Earth through measurement of the waves produced by large earthquakes, seismology has since been adapted to study the interior of the Sun (*helioseismology*) and other stars (*asteroseismology*).

In this thesis, we will study a scenario which is in fact highly analogous to that in geophysics: the generation of stellar oscillations by *starquakes*, sudden, catastrophic losses of strain in the solid crust. These have been suggested as an explanation for the sudden speed-ups in rotation, or *glitches*, observed in many younger neutron stars.

We will develop a simple toy model for a starquake and study the spectra of oscillations produced. The properties of these oscillations will be affected by the elastic crust and

the fluid core, as well as the rotation of the star. We will also briefly discuss the potential for observing these observations through the detection of gravitational waves.

This introductory chapter will concentrate on the observational and theoretical background that will be needed throughout the rest of the thesis. After a brief overview in this section of some of the main relevant areas of neutron star physics, we move on to summarise basic equations and results in fluid dynamics, elasticity and gravitational wave theory that will be useful for later chapters.

1.1.1 Observing neutron stars

The idea of a star composed of tightly packed neutrons was proposed by Baade and Zwicky as early as 1934 [12], only two years after the neutron was discovered. The possibility of making any electromagnetic observation of such a small, cold object seemed unlikely, but theoretical speculation continued until the unexpected discovery by Bell and Hewish in 1967 of a 'pulsar': a new celestial source of regular radio pulses. The small inferred size of the source region suggested a neutron star as a possible origin [37].

The picture that gradually emerged was of a rotating, magnetised neutron star [34], [64], slowly spinning down as it loses energy to magnetic dipole radiation. The radio pulses were identified with a 'lighthouse beam' of radiation sweeping across the earth as the star rotates.

Since then, neutron star observations have been made across the electromagnetic spectrum, in optical, X-ray and gamma ray wavelengths. In addition, many neutron stars have been found that have binary companions. These new sources of information have helped us further constrain the properties of neutron stars. In this section we will briefly discuss some of the observational characteristics of neutron stars most relevant to this thesis.

1.1.1.1 Radio observations

Radio emission is still the richest source of information about neutron stars. Around 1900 pulsars have been discovered [88], and almost all known neutron stars are observed in the radio band. Distance measurements show that the majority of pulsars are concentrated in the plane of the galaxy, within a radial distance of about 10 kiloparsecs from the centre [54].

The most obvious feature of the radio pulse is the extremely regular period P of the signal. It is also possible to observe a steady period increase $\dot{P}$. This fits with a slowing down of the star's rotation due to the torque produced by magnetic dipole radiation.

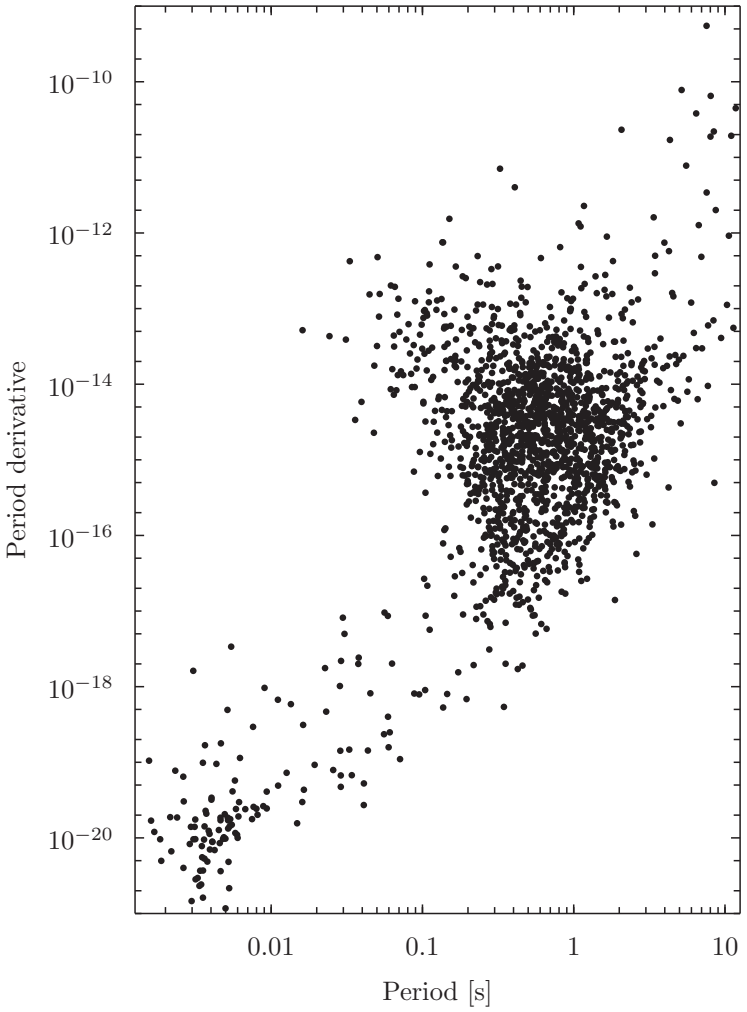

Figure 1.1: $P - \dot{P}$ diagram showing period of rotation of pulsars in seconds against dimensionless period derivative.

The magnetic dipole model predicts a magnetic field strength of $B \sim \sqrt{P\dot{P}}$, and an approximate age (the 'characteristic age') of the pulsar $\tau_c \approx \frac{P}{2\dot{P}}$. These two properties can therefore be seen to give important information about the properties of the star and are often plotted in a $P - \dot{P}$ diagram. This is done in Figure 1.1 using data from the ATNF Pulsar Database [57].

Perhaps the most immediately striking feature of the diagram is that pulsars split roughly into two populations, with short-period, low-magnetic-field stars as a separate group in the bottom left. These *millisecond pulsars* are found in binary systems and are thought to be older pulsars spun up by the accretion of matter on to their surface from the companion star [51].

1.1.1.2 Binary systems

Around 80% of millisecond pulsars, and 1% of normal pulsars, are observed to be in a binary system [50]. The companion star may be an ordinary star, a white dwarf or another neutron star. These systems can provide new information about neutron stars that is impossible to infer from isolated stars.

One of the most important features of binary systems is that for a few special cases it is possible to constrain the mass of the stars in the system from information contained in the pulse signal. For an accurate determination, it is necessary to have good knowledge of the inclination angle of the binary system. In those systems where this can be done, mass measurements range from $1M_{\odot}$ to a recent high measurement of $2M_{\odot}$ [27]. A summary of current measurements is provided in [47].

1.1.2 Formation of a neutron star

Neutron stars are remnants formed from the gravitational collapse of a massive star. This collapse occurs when a star has run out of energy gained from the fusion of elements within its core, and its thermal pressure can no longer stay in equilibrium with the gravitational force.

At this point, the majority of stars will evolve to a point where the gravitational forces are instead balanced by the electron degeneracy pressure: this pressure is a consequence of the Pauli exclusion principle stating that no two electrons can occupy the same quantum state. A star supported by this type of pressure is called a *white dwarf*.

However, there is a maximum mass sustainable by an object supported by relativistic, degenerate electrons; stars that exceed this *Chandrasekhar limit* [20] are no longer stable. This is the case for more massive stars of typically around $8M_{\odot}$ and over, where nuclear fusion in the core proceeds all the way to the endpoint of iron nuclei.

At this point, the core implodes rapidly, triggering a complex process of shock formation and ultimately a *supernova explosion* [33]. This explosion expels all the outer matter of the progenitor star, leaving only the core. This core cools fast, soon reaching a new equilibrium at *nuclear density*, the density at which the mean density of matter reaches the density of an atomic nucleus. Matter is then expelled outwards in a Type II supernova, leaving a compact core behind. This core is the *neutron star*, and is supported by the degeneracy pressure of neutrons. The neutron star has a typical mass of around $1.4M_{\odot}$ and a radius of around 10km. This scenario may occur for stars with initial masses in the region of $8 - 20M_{\odot}$ [75].

For some of the most massive stars, the supernova explosion fails to eject enough material and the star reaches the *Oppenheimer-Volkoff mass limit* [62], the maximum mass

sustainable by degenerate neutrons. In this case the star can undergo complete collapse to a *black hole.*

1.1.3 Structure of a neutron star

Neutron star matter spans a huge range of densities, from a surface density of around 10^6 g cm^{-3} up to extremely high densities of around 10^{15} g cm^{-3} in the inner core, higher than the *nuclear density* $\rho_0 = 2.8 \times 10^{14}$ g cm^{-3} of a heavy atomic nucleus [88].

Laboratory measurements of nuclear properties are only available up to just below nuclear density, where the nuclei predicted to occur are ones that can be produced experimentally [68]. Beyond this point, theoretical models of the interaction between nucleons can be used to predict the properties of the matter up to just above nuclear density. The dense nuclear matter in the inner core is still not well understood theoretically.

Figure 1.2 shows the composition of a neutron star. The star can be divided into two main regions, a solid crust and a liquid interior. The outer part of the crust consists of a rigid, crystal lattice of atomic nuclei. Near the surface, these are mainly ordinary nuclei, and at low densities the most energetically favourable nucleus is iron. At increasing densities it instead becomes energetically favourable to reduce the number of electrons by converting protons to neutrons through inverse beta decay. This leads to the creation of increasingly neutron-rich nuclei, up to the point of *neutron drip* at a density of around 4×10^{11} gcm^{-3}, where neutron states become unbound [68]. The density of free neutrons between nuclei then increases until it is comparable to that of the nuclei: at this point the nuclei merge to create a fluid of neutrons together with a small fraction of protons and electrons. This marks the crust-core transition and occurs at a density of around ρ_0, around 1 km below the surface.

In the fluid core, the neutrons are expected to be superfluid and the protons superconducting [14]. The properties of the dense nuclear matter in the inner core are not well understood, but the star may contain exotic material. This could consist of hyperons, a Bose condensate of pions or kaons, or deconfined quark matter [88], [46].

1.1.4 The neutron star equation of state

The thermodynamic properties of a neutron star are encoded in the *equation of state*, a relation $P = P(\rho, T)$ between the pressure P, density ρ and temperature T of the star. For low temperatures, we can take the $T = 0$ *barotropic* limit, obtaining an equation of state $P = P(\rho)$.

Realistic equations of state are calculated numerically, and take into account the detailed physics of interactions between nucleons in the neutron star core. The equation of state

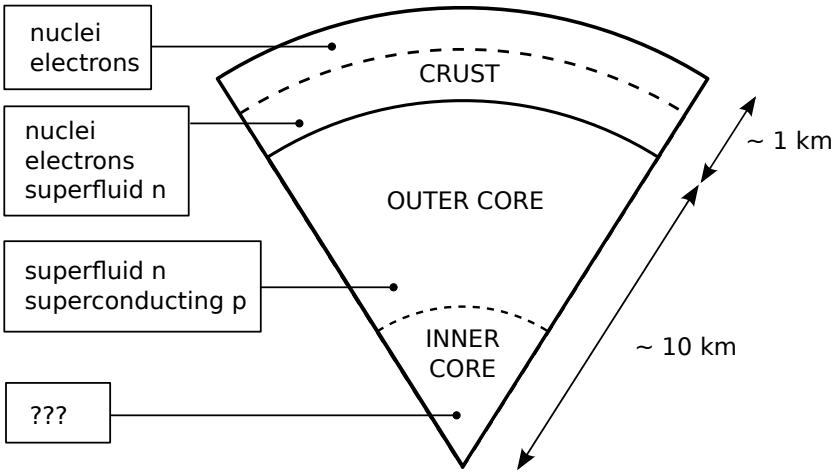

Figure 1.2: Cross-section of a neutron star, showing the composition of the main regions of the star. The outer crust is a lattice of atomic nuclei. At higher densities the proportion of free neutrons increases. The core is a fluid of superfluid neutrons and superconducting protons, while the composition of the inner core is unknown.

depends strongly on the unknown properties of the inner core, so there is wide variation in possible equations of state; a survey is provided by Haensel, Potekhin and Yakovlev [35].

It is also common to use simpler analytic models which capture some of the qualitative features of the equation of state. Polytropes have an equation of state of the form $P = k\rho^{\Gamma}$. Polytropic equations of state govern some idealised systems such as an ideal Fermi gas of nonrelativistic ($\Gamma = \frac{5}{3}$) or ultrarelativistic ($\Gamma = \frac{4}{3}$) neutrons, and so equations of state of this type can be a useful approximation to the more complicated physics of a realistic neutron star model.

Given a barotropic equation of state $P = P(\rho)$, each pressure-density equation of state uniquely determines a relationship between masses and radii for neutron stars [49], and also fixes the maximum allowed mass. This means that observational data on the masses of neutron stars is very useful in constraining the neutron star equation of state [48].

1.2 Gravitational waves

General relativity predicts the existence of gravitational waves, propagating waves of spacetime curvature generated by varying mass distributions. As well as providing a test of general relativity, direct detection of gravitational waves would be of great use to astronomy, as these waves can provide information complementary to that currently available from electromagnetic observations.

In particular, gravitational waves are generated by the bulk movement of a source rather than being radiated by individual particles. This means that gravitational wave frequencies are directly related to the dynamical timescales of the source. Gravitational waves are not scattered by matter in the same way as electromagnetic waves, so can provide more direct information about the source. For neutron stars, this could be extremely useful as a way to probe the physics of the dense matter interior.

In this section we will first outline the basic theory of gravitational wave generation, and then briefly discuss the outlook for detection of gravitational waves.

For convenience, throughout this section we will work in geometrised units where $G = c = 1$. This simplifies many formulae, and we can convert back to SI or cgs units when calculating physical quantities. We will use Greek indices for spacetime tensors, and Latin ones when we are using only the spatial part.

1.2.1 Gravitational wave theory

Before discussing gravitational wave generation, it will be useful to summarise some basic equations of general relativity. In this theory, spacetime is described by a metric $g_{\alpha\beta}$. The tidal gravitational forces experienced by particles in this spacetime are governed by the curvature of the metric. This curvature can be quantified through the *Riemann curvature tensor* $R_{\alpha\beta\gamma\delta}$. In a local inertial frame the Riemann curvature tensor can be written in terms of the metric as

$$R_{\alpha\beta\gamma\delta} = \frac{1}{2}\left(g_{\alpha\delta,\beta\gamma} + g_{\alpha\gamma,\beta\delta} - g_{\beta\gamma,\alpha\delta} - g_{\beta\delta,\alpha\gamma}\right). \tag{1.1}$$

Einstein's field equations

$$G_{\alpha\beta} = 8\pi T_{\alpha\beta} \tag{1.2}$$

then relate the stress-energy tensor $T_{\alpha\beta}$ of the matter distribution to the curvature of the metric through the Einstein tensor $G_{\alpha\beta}$, where

$$G_{\alpha\beta} = R_{\alpha\beta} - \frac{1}{2}R\, g_{\alpha\beta}. \tag{1.3}$$

The *Ricci tensor* $R_{\alpha\beta}$ is constructed from the Riemann curvature tensor as

$$R_{\alpha\beta} = R^{\lambda}{}_{\alpha\lambda\beta}, \tag{1.4}$$

while R is the *Ricci scalar* $R := g^{\alpha\beta}R_{\alpha\beta}$.

1.2.1.1 The linearised Einstein equations

In this section, we will largely follow the presentation in Schutz [75]. Our aim is to find the wave field far from the source, where we can expect the amplitude of the waves to be very small. This allows us to find coordinates where we can split the spacetime into a background piece, which we take as flat Minkowski spacetime $\eta_{\alpha\beta}$, and a piece describing small perturbations:

$$g_{\alpha\beta} = \eta_{\alpha\beta} + h_{\alpha\beta}, \tag{1.5}$$

where $|h_{\alpha\beta}| \ll 1$. The linearised Einstein field equations (1.2) then become

$$G_{\alpha\beta} = -\frac{1}{2}\left[\bar{h}_{\alpha\beta,\mu}{}^{,\mu} + \eta_{\alpha\beta}\bar{h}_{\mu\nu}{}^{,\mu\nu} - \bar{h}_{\alpha\mu,\beta}{}^{,\mu} - \bar{h}_{\beta\mu,\alpha}{}^{,\mu}\right] = 8\pi T_{\alpha\beta} \tag{1.6}$$

to first order in $h_{\alpha\beta}$. Here $\bar{h}_{\alpha\beta}$ is the *trace reverse* of the metric perturbation, $\bar{h}_{\alpha\beta} = h_{\alpha\beta} - \frac{1}{2}\eta^{\alpha\beta}h^{\mu}{}_{\mu}$.

This can be simplified using the freedom we have to change the metric. We can stay within the regime of small perturbations by making a *gauge transformation*: a coordinate change $x^{\alpha} \to x'^{\alpha} = x^{\alpha} + \xi^{\alpha}$, where ξ^{α} is a small vector. This is equivalent to switching to a new metric perturbation

$$\bar{h}'_{\alpha\beta} = \bar{h}_{\alpha\beta} - \xi_{\alpha,\beta} - \xi_{\beta,\alpha} + \eta_{\alpha\beta}\xi^{\mu}{}_{,\mu}. \tag{1.7}$$

We will now use up some of this gauge freedom to pick ξ^{α} so that it satisfies the gauge condition $\xi^{\mu,\nu}_{\nu} = \bar{h}^{\mu\nu}{}_{,\nu}$. This puts us into *Lorenz gauge*, where

$$\bar{h}'^{\alpha\beta}{}_{,\beta} = 0, \tag{1.8}$$

and so the linearised Einstein field equations (1.6) simplify to

$$\left(-\frac{\partial^2}{\partial t^2} + \nabla^2\right)\bar{h}'^{\alpha\beta} = -16\pi T^{\alpha\beta}. \tag{1.9}$$

This has the form of an inhomogeneous wave equation with the stress-energy tensor $T_{\alpha\beta}$ as its source.

1.2.1.2 Generation of gravitational waves

To find the wave field produced by a source, we will need to solve the weak-field Einstein equation above. Using the coordinates (t, x^i) for the background Minkowski metric $\eta_{\alpha\beta}$, this has a formal integral solution

$$\bar{h}_{\alpha\beta}(t, x^i) = 4 \int_\Lambda \frac{T_{\alpha\beta}(t - R)}{R} d^3y, \tag{1.10}$$

where $R = |x^i - y^i|$, and the integral is taken over the past light cone Λ of the event (t, x^i) [85]. To make further progress, though, we will have to make some simplifying approximations.

We choose the origin of coordinates to be inside the source, far from the observer at (t, x^i). Because we are far from the source, $|y^i| \ll |x^i|$, and so we can take $R \approx r := |x^i|$ in the denominator of the integral. We also make the *slow motion approximation*, which is that the typical velocity v in the source region is much smaller than the speed of light: $v \ll 1$ [75]. We can then take $t - R \approx t - r$, and so our approximate integral solution is

$$\bar{h}_{\alpha\beta}(t, x^i) \approx \frac{4}{r} \int T_{\alpha\beta}(t - r) d^3y. \tag{1.11}$$

We are mainly interested in the spatial part $\bar{h}_{ij}$. Using conservation of the stress-energy tensor, $T^{\alpha\beta}{}_{,\beta} = 0$, we can show that

$$\frac{d^2}{dt^2} \int T^{00} x^i x^j d^3x = 2 \int T^{ij} d^3x, \tag{1.12}$$

and so

$$\bar{h}^{jk}(t, x^i) \approx \frac{2}{r} \frac{d^2}{dt^2} \int T^{00} x^j x^k d^3x. \tag{1.13}$$

This is the *quadrupole approximation*, and $\int T^{00} x^i x^j d^3x$ is called the *mass quadrupole moment* of the source,

$$I^{jk} = \int_V T^{00}(t - r) x^j x^k d^3x. \tag{1.14}$$

1.2.1.3 Transverse-traceless gauge

We have not yet used all our available gauge freedom: we can remain in the Lorenz class of gauges by adding to ξ^α any vector ζ^α with $\left(-\frac{\partial^2}{\partial t^2} + \nabla^2\right) \zeta^\alpha = 0$. We will now fix our gauge completely, by specialising to *transverse-traceless gauge*, where the wavefield takes on a particularly simple form:

- First we will choose $h_{\alpha\beta}U^0 = 0$, where U^0 is the time basis vector of our coordinate system. This means that $h_{\alpha 0} = 0$ for all indices α.
- We then keep only the spatial part of $h_{\alpha\beta}$ which is transverse to the direction of propagation n^j, using the projection tensor

$$P^j{}_k = \delta^j{}_k - n^j n_k \tag{1.15}$$

  orthogonal to n^j. This is achieved automatically if the perturbation is already in Lorenz gauge.
- Finally we remove the trace of $h_{\alpha\beta}$.

Together these conditions give us the transverse-traceless wavefield

$$\bar{h}^{TT}_{\alpha 0} = 0, \tag{1.16}$$

$$\bar{h}^{TT}_{ij} = P^k{}_i P^l{}_j \bar{h}_{kl} - \frac{1}{2} P_{ij}(P^{kl}\bar{h}_{kl}). \tag{1.17}$$

For example, if we choose our axes so that the wave propagates in the $z-$direction, the metric perturbation becomes

$$h^{TT}_{\alpha\beta} = \begin{pmatrix} 0 & 0 & 0 & 0 \\ 0 & h_+ & h_\times & 0 \\ 0 & h_\times & -h_+ & 0 \\ 0 & 0 & 0 & 0 \end{pmatrix}. \tag{1.18}$$

From this we can see that there are only two independent components, corresponding to two independent polarisations of the wave. These are called the 'plus' and 'cross' polarisations because of their effect on a circle of test particles in the $x - y$ plane (see Figure 1.3).

1.2.1.4 The energy carried away by gravitational waves

In general relativity, we can always choose a local frame in which the gravitational field vanishes; we can only see the effect of the field by looking at how the proper separation between two particles changes. This means that there is no way of unambiguously defining the energy in a gravitational wave at one spacetime point. However, it is possible to define an averaged stress-energy tensor for the waves [40],[41].

This can be found by expanding the Einstein tensor to second order in the $h_{\alpha\beta}$ and averaging over one wavelength in spatial directions and over one period of the wave in time:

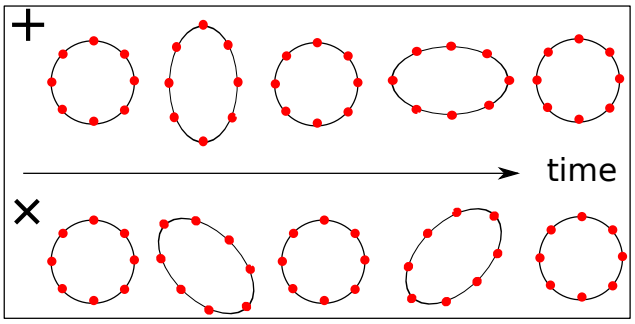

Figure 1.3: Diagram showing the effect of a passing gravitational wave on a circle of test particles perpendicular to the direction of propagation of the wave, for a purely 'plus' polarised wave *(top)* and a purely 'cross' polarised wave *(bottom)*.

$$\langle G_{\alpha\beta}\rangle = G^{(0)}_{\alpha\beta} + \langle G^{(1)}_{\alpha\beta}\rangle + \langle G^{(2)}_{\alpha\beta}\rangle + O(h^3). \tag{1.19}$$

The background $G^{(0)}$ term is zero for flat space, and the $G^{(1)}$ term linear in h will vanish when averaged over a wavelength. This leaves

$$\langle G^{(2)}_{\alpha\beta}\rangle := -8\pi T^{GW}_{\alpha\beta}, \tag{1.20}$$

which defines the stress-energy tensor for the gravitational waves. In TT gauge

$$T^{GW}_{\alpha\beta} = \frac{1}{32\pi}\langle \bar{h}^{TT}_{\mu\nu,\alpha}\bar{h}^{TT\mu\nu}{}_{,\beta}\rangle. \tag{1.21}$$

The energy flux in, for example, the z-direction is then

$$F = T_{0z} = \frac{\omega^2}{32\pi}\langle \bar{h}^{TT}_{ij}\bar{h}^{TTij}\rangle. \tag{1.22}$$

1.2.2 Detection of gravitational waves

Indirect evidence for gravitational waves already exists: the effects of energy loss from gravitational wave emission were first seen in the double neutron star system discovered by Hulse and Taylor [39],[81]. The decrease in orbit period observed in this system matches the predictions of general relativity to within 1% and so provides an important test for the theory. Even more stringent recent tests include the double pulsar system PSR J0737-3039A/B, which has been found to agree to within 0.1% [42].

The direct detection of gravitational waves using an Earth-based detector is a huge technical challenge. The current network of ground-based detectors includes LIGO Livingston and Hanford, VIRGO and GEO600. These use laser interferometry to detect changes in the lengths of the two arms of the detectors. LIGO is now sensitive to fractional changes in length of order 10^{-22}, [69], with maximum sensitivity at frequencies

of around $100 - 1000$ Hz. The LIGO detectors are currently being updated, and Advanced LIGO should have sensitivity increased by a factor of around 10, depending on the chosen detector configuration [77].

There are a wide range of possible gravitational wave sources which may be detected; for the purposes of detection these are normally split into inspiral, continuous, burst and stochastic signals [6]. Inspiral signals come from the final stages of a neutron star or black hole binary, as the compact objects merge together [2]. This should produce a distinctive signal, increasing in frequency until the merger.

Other types of signal from single compact stars or binaries are divided into continuous and burst types. Continuous signals can be produced from spinning neutron stars. These could generate a gravitational wave signal if they are deformed from an axisymmetric rotation shape by crustal 'mountains' [4]. Another possible source of continuous gravitational radiation would be a secular instability such as the r-mode instability [10].

Bursts are, as the name implies, short-lived signals produced by a variety of violent astrophysical events such as core-collapse supernovae or neutron star collapse to black holes [1]. This type of signal is particularly interesting to us, as a neutron star glitch should produce a rapidly damped burst of radiation.

The fourth class, stochastic signals, are those produced by a large population of independent sources, which would be expected to show up as noisy 'gravitational wave background radiation'. A stochastic signal may be produced as a relic of events in the early universe after the Big Bang [5].

1.3 Equations of motion for an ideal fluid

As we saw in Section 1.1.3, the core of a neutron star is fluid. The defining property of a fluid is that it shows very little resistance to shear strain – in fact, we will consider *ideal fluids*, in the zero viscosity limit of *no* strain. We will also be modelling our fluid as non-relativistic, so will use a Newtonian description throughout.

We will derive a few of the most important equations governing fluid flow below, which will be needed throughout this thesis. The derivations here follow those in Landau and Lifshitz [44].

1.3.1 Conservation of mass

A basic property of a fluid is that mass is conserved (at least in Newtonian gravity, where there is no gravitational radiation). We will consider what happens in a 'test volume' V fixed with respect to the observer measuring the properties of the fluid. Conservation of

mass means that the decrease per unit time of the mass of the fluid in V is equal to the flux of mass flowing through its surface ∂V in unit time. For a fluid of density $\rho(x^i, t)$,

$$-\frac{d}{dt}\int_V \rho dV = \int_{\partial V} \rho v^i dS_i. \tag{1.23}$$

Here dS_i is a surface element defined to be positive pointing out of the volume. We can rewrite this as

$$\int_V \left(\frac{\partial \rho}{\partial t} + \nabla_i \left(\rho v^i\right)\right) dV = 0, \tag{1.24}$$

and since this equation holds for any volume V, we have the *equation of continuity*,

$$\frac{\partial \rho}{\partial t} + \nabla_i \left(\rho v^i\right) = 0. \tag{1.25}$$

1.3.2 Euler's equations

We next consider the forces acting on a small volume of fluid. In this case we will take the small volume δV moving with the fluid element, so that

$$\rho \frac{Dv_i}{Dt}\delta V = f_i \delta V, \tag{1.26}$$

where f_i is the force per unit volume acting on the fluid element. Here the derivative $\frac{D}{Dt}$ is the derivative taken with respect to the moving fluid, known as the *convective derivative*. This can be written as

$$\frac{D}{Dt} \equiv \frac{\partial}{\partial t} + \frac{dx^i}{dt}\frac{\partial}{\partial x^i} = \frac{\partial}{\partial t} + (v^i \nabla_i), \tag{1.27}$$

leading to *Euler's equation*,

$$\frac{\partial v_i}{\partial t} + (v^j \nabla_j) v_i = \frac{f_i}{\rho}. \tag{1.28}$$

1.3.3 Eulerian and Lagrangian perturbations

Most of our work will be within the framework of perturbation theory, where we study the behaviour of solutions under small perturbations to the background properties of the star. There are two important descriptions of a fluid perturbation that we will use. These are the *Eulerian* and *Lagrangian* perturbations (see, for example, [76] or [26]).

The Eulerian description takes a 'macroscopic' perspective, measuring the change in a quantity Q_0 at a fixed point in space. If $Q_0(x^i, t)$ describes the quantity before the perturbation and $Q(x^i, t)$ describes it afterwards, then the Eulerian perturbation is defined as

$$\delta Q \equiv Q(x^i, t) - Q_0(x^i, t). \tag{1.29}$$

The Lagrangian description takes the 'microscopic' approach, following the fluid elements as they are displaced by the perturbation. To do this, we introduce a *displacement vector* ξ^i mapping fluid elements in the unperturbed star to their new locations in the perturbed one. The Lagrangian perturbation is then defined as

$$\Delta Q \equiv Q(x^i + \xi^i, t) - Q_0(x^i, t). \tag{1.30}$$

The two types of perturbation can be related by

$$\Delta Q = \delta Q + \xi^i \nabla_i Q. \tag{1.31}$$

In the case of the Lagrangian change in the velocity Δv^i, we can also obtain a useful expression in terms of the displacement field ξ^i. The Lagrangian change in the velocity of a fluid element is its velocity in the perturbed flow relative to that in the unperturbed flow, i.e.

$$\Delta v^i = \frac{d}{dt}(x^i + \xi^i) - \frac{dx^i}{dt} = \frac{d\xi^i}{dt}. \tag{1.32}$$

1.4 Elasticity

In constrast to a fluid, an elastic solid can sustain a shear stress. A perfectly elastic solid will recover its original shape after *any* small stress, including a shear stress, is removed. This will be very important in our modelling of the solid crust of a neutron star, and so we will develop the equations of motion for an elastic solid below.

1.4.1 The strain tensor

We can measure the deformation of an elastic body that undergoes a displacement ξ^i by taking the gradient $S_{ij} = \nabla_j \xi_i$ of the displacement vector. This second rank tensor can be split into three irreducible parts [18]:

$$S_{ij} = \frac{1}{3}\Theta g_{ij} + \Sigma_{ij} + R_{ij}, \tag{1.33}$$

where $\Theta = S_{ii}$ is the *expansion*, $\Sigma_{ij} = \frac{1}{2}(\nabla_j \xi_i + \nabla_i \xi_j) - \frac{1}{3}\Theta g_{ij}$ is the *shear*, $R_{ij} = \frac{1}{2}(\nabla_j \xi_i - \nabla_i \xi_j)$ is the *rotation*, and g_{ij} is the metric tensor. We ignore R_{ij}, because a local rotation of a volume element produces no corresponding stress force, and take

$$u_{ij} = \frac{1}{3}\Theta g_{ij} + \Sigma_{ij} = \frac{1}{2}(\nabla_j \xi_i + \nabla_i \xi_j) \tag{1.34}$$

as our definition of the *strain tensor*.

1.4.2 The stress tensor

The forces acting in an isotropic elastic material can also be described by means of a second rank tensor. If we consider two small neighbouring regions of the solid, the first region exerts a force dF_i on the second through their surface of contact dS_j (defined with the positive sense pointing from the first to the second). As this force is linearly proportional to the contact area, we have a relationship

$$dF_i = T_i{}^j dS_j, \tag{1.35}$$

and the second order tensor T_{ij} relating dF_i and dS_j is the *stress tensor*. We can then compute the total elastic force acting on a volume V to be

$$F_i = -\int_{\partial V} T_i{}^j dS_j = -\int_V \nabla_j T_i{}^j dV. \tag{1.36}$$

This should be true for any volume, so we find that the elastic force density f_i is

$$f_i^{\text{elastic}} = -\nabla_j T_i{}^j. \tag{1.37}$$

As with the strain tensor, we can split the stress tensor into a pure trace and a symmetric trace-free part:

$$T_{ij} = P g_{ij} + T_{ij}^{\text{shear}}. \tag{1.38}$$

Here P can be identified with the pressure. As the shear part T_{ij}^{shear} is trace-free, we can write the pressure in terms of the stress tensor as

$$P = \frac{1}{3} T^i{}_i. \tag{1.39}$$

The stress tensor (1.38) for an elastic material can be compared with that for an ideal fluid, which can only sustain an isotropic stess $T_{ij}^{\text{fluid}} = P g_{ij}$.

In an elastic solid, we expect both the expansion and shear parts of the strain tensor to cause a corresponding stress in the star. We assume Hooke's Law, i.e. that this relationship is linear: $P = -K\Theta$ and $T_{ij}^{\text{shear}} = -2\mu\Sigma_{ij}$, where K and μ are constants [43]. These constants are called the *bulk modulus* and *shear modulus* respectively. This means that in linear elasticity, the stress tensor can be written in terms of the strain tensor as

$$T_{ij} = -K\Theta g_{ij} - 2\mu\Sigma_{ij}. \tag{1.40}$$

The elastic force density $f_i^{elastic}$ is then found to be

$$f_i^{elastic} = K\nabla_i\Theta + 2\mu\nabla_j\Sigma_i{}^j = \left(K + \frac{1}{3}\mu\right)\nabla_i(\nabla_j\xi^j) + \mu\nabla_j\nabla^j\xi_i. \tag{1.41}$$

In this thesis we will mainly be interested in the incompressible case, where $\Theta = 0$. In this case the stress tensor becomes

$$T_{ij} = -2\mu\Sigma_{ij}, \tag{1.42}$$

with

$$f_i^{elastic} = \mu\nabla_j\nabla^j\xi_i. \tag{1.43}$$

as the corresponding force density.

1.5 Plan of the thesis

The thesis starts with two introductory chapters, the first on general neutron star physics and the second focussed on neutron star glitches. In Chapter 3 we then move on to give some order-of-magnitude estimates of the energy made available by a starquake and the amplitude of the oscillations excited.

The next three chapters develop the background needed to make a more detailed physical model of a starquake. We start by studying equilibrium models of a rotating star in Chapter 4, finding analytic solutions for the case of an incompressible solid star. In Chapter 5 we discuss modes of oscillation of neutron stars. In particular we derive the mode spectrum for the same model of an incompressible solid star and investigate it numerically. Chapter 6 contains the mathematical background needed to show that we have an orthogonal set of oscillation modes to project against, and illustrates this with a series of toy models of mode excitation by initial data.

We are then in a position to use this work to produce a toy model of a starquake, in the special case where the star spins down to zero angular velocity before glitching. We carry this out in Chapter 7, constructing initial data for the glitch and projecting it against our basis of normal modes.

Chapters 8 and 9 deal with the extension of this model to include rotation. In Chapters 8 we investigate the change in the oscillation modes to first order in the rotation, while in Chapter 9 we extend the projection scheme to take into account the fact that the modes are no longer orthogonal, and discuss some preliminary results.

Chapter 2

Glitches

Pulsars normally rotate at an extremely regular rate, with most of the change over time attributable to the gradual slowdown from magnetic dipole radiation. Accounting for this steady change, pulsars keep time to an accuracy of one part in 10^{11} or more [54]. However, not all variations in pulse period can be explained in this way. There is a small contribution from 'timing noise', small random deviations in the pulse period. This is particularly pronounced in the youngest pulsars [51]. More dramatically, some pulsars have been observed to show a sudden speedup in rotation rate, known as a 'glitch'.

First observed in the Vela pulsar in 1969 [71], [73], the cause of glitches is still unknown and an active area of research. Two of the leading mechanisms advanced to explain glitches will be discussed in the chapter. We will also discuss one of these mechanisms, the starquake model, in more depth, and obtain some order-of-magnitude estimates for the energies released in a glitch.

2.1 Glitch observations

Glitches are known to occur in a significant fraction of pulsars – out of 700 pulsars monitored at Jodrell Bank, 128 have been observed to glitch [29].

Figure 2.1 shows the $P - \dot{P}$ diagram with those pulsars that have been known to glitch marked. It can be seen clearly that with the exception of one millisecond pulsar, the glitching pulsars fall into the top right portion of the diagram. This indicates that they are younger pulsars (characteristic ages of $10^3 - 10^6$ years) with reasonably strong magnetic fields (upwards of 10^{12} gauss). Within this population, the youngest pulsars glitch most often, with the rate falling off with age [29].

The size of a glitch can be characterised by the ratio $\frac{\Delta\nu}{\nu}$, where ν is the spin frequency of the pulsar, and $\Delta\nu$ is the change in spin frequency during the glitch. This size varies

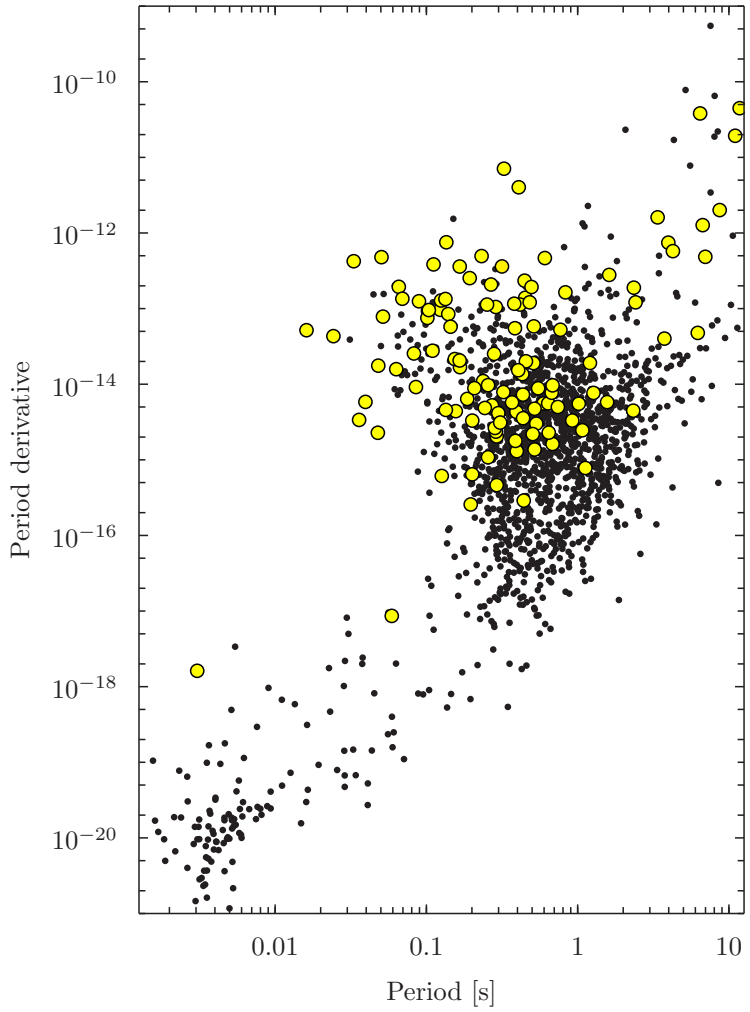

Figure 2.1: $P - \dot{P}$ diagram showing period of rotation of pulsars in seconds against dimensionless period derivative. Pulsars which have been seen to glitch at least once are marked with yellow circles.

widely, with glitches being measured across the range $\frac{\Delta\nu}{\nu} = 10^{-11} - 10^{-5}$. Different pulsars have characteristic glitching patterns. As examples, we can look at two of the best studied glitching pulsars, the Crab and Vela pulsars, which have both been under observation since 1968 [76]. The Crab is one of the youngest known pulsars, a remnant from the supernova recorded in the year 1054. It undergoes relatively small glitches of size $\frac{\Delta\nu}{\nu} \approx 10^{-8}$, and glitch sizes are distributed over a wide range [86]. The Vela pulsar is older, with characteristic age 11000 years. Vela glitches are larger, with a much more regular size of around $\frac{\Delta\nu}{\nu} = 10^{-7}$ [29].

After a glitch, many pulsars relax to close to their original spin rate: for example, this is the case in the Vela Pulsar [58]. However in some neutron stars, such as the Crab, the change in spin rate is permanent (or at least is retained until the next glitch) [55].

2.2 Overview of glitch models

2.2.1 Superfluid model

A connection between pulsar glitches and the superfluid core of the star was first proposed by Baym, Pethick and Pines [15]. A more detailed scenario was then suggested by Anderson and Itoh [9].

Superfluidity allows the neutron star to contain two components with differing rotation speeds. The rotation rate of the pulsar is determined by its radio beam from the magnetic poles, which are attached to the crust. The pulsar's magnetic field will then ensure that the electrons and protons in the fluid interior stay strongly coupled to this component. However, the superfluid neutrons in the interior form a separate component, parts of which may be more weakly coupled to the crust.

This happens because rotation in a superfluid is quantised, with each superfluid vortex carrying a fixed amount of angular momentum. The rotation of the whole component is then proportional to the area density of these vortices, and so it can only slow down if the vortices move outwards towards the crust.

This outward migration of the vortices should be able to occur in the liquid interior, but as they reach the solid crust they may become pinned to the nuclei in the crystal lattice. This fixes the angular momentum of this part of the superfluid, so that it is unaffected by the gradual slowdown of the neutron star through magnetic braking.

A glitch would then be triggered by an event that could suddenly increase the coupling between the two components by producing a sudden collective unpinning of these vortices. This would release large amounts of angular momentum to the crust, giving rise to the glitch event. Various mechanisms for this unpinning have been proposed [8], [32], [60].

The superfluid model has the ability to account for large glitches, and so is the leading candidate for explaining the behaviour of pulsars such as the Vela.

2.2.2 Starquake model

The idea of starquakes in the crust of a neutron star as a possible explanation for glitches was first advanced by Ruderman in 1969 [74], soon after the first glitch observations. This mechanism was later considered in more detail by Baym and Pines [16].

Figure 2.2 illustrates the main stages of the starquake model. At this point we will introduce some notation that we will use throughout the thesis, and refer to the four main stages of the starquake model as Stars A-D. The star starts in a relaxed configuration

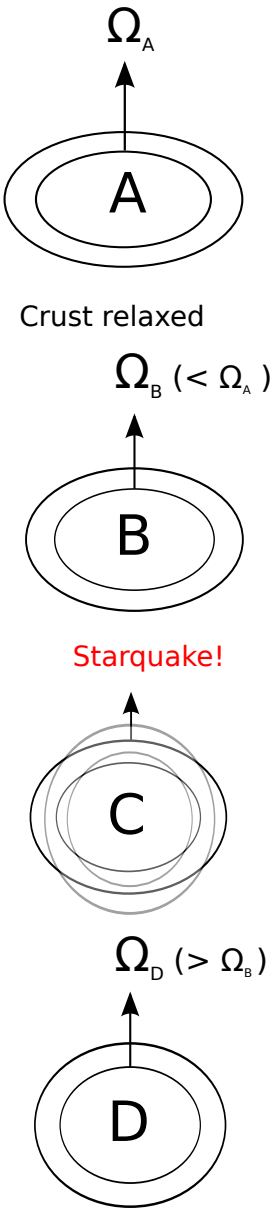

Figure 2.2: Schematic of the starquake model. As the star spins down from an initial, relaxed configuration (Star A), strain builds up in the crust. When this reaches a critical level (Star B), the crust cracks and strain is removed. Immediately after the starquake the star is out of equilibrium (Star C), and oscillates briefly before settling down to a new equilbrium state (Star D).

(Star A), with some initial angular velocity Ω_A. As the star loses energy and spins down, it becomes less oblate. While a fluid star would be able to freely adjust its shape to the new spin rate, the solid crust of a neutron star will resist the deformation from its relaxed state; consequently, it will stay more oblate than a fluid star would. It is this residual oblateness that is then removed by the starquake.

In the starquake model, there is some maximum level of strain that the crust can withstand. This occurs at some critical angular velocity Ω_B, which is shown in Star B of the figure. At this critical level, the crust cracks and relieves some of the strain.

This release of strain means that the star is now relaxed and loses its residual oblateness. The moment of inertia decreases, and so by conservation of angular momentum there must be a corresponding increase in the star's angular velocity. This is the glitch we observe.

Immediately after the glitch, the star will briefly be out of equilibrium – this is Star C of the figure. It is this stage of the model that we will be most interested in, as we expect oscillation modes of the star to be excited. These oscillations will then quickly damp down and the star will reach a new equilibrium state, Star D, which is spinning at the new, faster angular velocity Ω_D.

This model is unable to account for the largest glitches, as we shall see below. However, it is still of interest in describing the behaviour of the youngest pulsars, such as the Crab.

2.3 The Baym and Pines starquake model

Baym and Pines [16] developed an early model of a starquake, using an order-of-magnitude calculation of the ellipticity change in the star at the glitch to make estimates of the time between glitches. Later in the thesis we will build on this model, so we will discuss it in some detail here. The starquake model of Baym and Pines characterises the distortion of the rotating neutron star using a single parameter, the *oblateness parameter* ε. This is defined by

$$I = I_{\mathrm{S}}(1 + \varepsilon), \tag{2.1}$$

where I is the moment of inertia of the distorted star and I_{S} is that of the star while nonrotating and spherical. For the incompressible stellar models we will mainly be considering in this thesis, I_{S} would be that of a spherical star of the same volume.

The value of ε can be found by minimising the total energy of the star. For a rotating Newtonian neutron star this can be split into the parts

$$E = E_{\rm S} + E_{\rm rot} + E_{\rm grav} + E_{\rm strain}. \tag{2.2}$$

Here $E_{\rm S}$ is the energy the star would have if spherical, and $E_{\rm rot} = \frac{L^2}{2I}$ is the rotational kinetic energy. The last two terms are corrections due to the oblatenesss of the star arising from the gravitational and strain energy respectively. We now need to express these energies directly in terms of the oblateness ε. $E_{\rm grav}$ can be expanded to second order in ε as

$$E_{\rm grav} = E_{\rm grav,0} + A\varepsilon^2. \tag{2.3}$$

The term linear in ε vanishes because the spherical shape where $\varepsilon = 0$ minimises the gravitational energy. A is a constant proportional to M^2G/R, where M is the mass of the star, R is its radius and G is the gravitational constant.

We then assume that the crust is formed at an initial 'reference' value of the oblateness $\varepsilon_{\rm ref}$. As the star slows down and the oblateness decreases, the strain energy will increase as

$$E_{\rm strain} = B(\varepsilon - \varepsilon_{\rm ref})^2. \tag{2.4}$$

B is a constant that depends on the Coulomb energy of the crust, and generally $B \ll A$ (we will confirm this in the next section). The total energy can now be written as

$$E = E_S + \frac{L^2}{2I} + A\varepsilon^2 + B(\varepsilon - \varepsilon_{\rm ref})^2, \tag{2.5}$$

where E_S is the energy of the nonrotating star. The oblateness ε can then be found by minimising E with respect to ε, while keeping the angular momentum $L = I\Omega$ fixed:

$$\varepsilon = \frac{I_{\rm S}\Omega^2}{4(A+B)} + \frac{B}{A+B}\varepsilon_{\rm ref}. \tag{2.6}$$

Initially $\varepsilon = \varepsilon_{\rm ref}$, so by rearranging we find that the reference oblateness is

$$\varepsilon_{\rm ref} = \frac{I_{\rm S}\Omega_0^2}{4A}, \tag{2.7}$$

where Ω_0 is the initial angular velocity. We can then alternatively write ε as

$$\varepsilon = \frac{I_{\rm S}}{4(A+B)}\left(\Omega^2 + \frac{B}{A}\Omega_0^2\right). \tag{2.8}$$

2.3.1 Numerical estimates for a typical neutron star

At this point, it will be useful to get an idea of the relative sizes of these energies by putting in some typical numerical values for a neutron star. We can make an estimate for A using the exact value for a homogeneous incompressible star [16],

$$A = \frac{3}{25}\frac{M^2 G}{R}. \tag{2.9}$$

For a 10 km radius star with a mass of $1.4 M_\odot$, we have

$$A \sim 6 \times 10^{52} \text{ erg}. \tag{2.10}$$

As a rough estimate for the value of B, we can start by using our formula (2.4) for the strain energy to find the mean stress in the crust,

$$\sigma \equiv \left| \frac{1}{V_{\text{crust}}} \frac{\partial E_{\text{strain}}}{\partial \varepsilon} \right|, \tag{2.11}$$

where V_{crust} is the volume of the crust. In terms of E_{strain} this is

$$\sigma = \mu(\varepsilon - \varepsilon_{\text{ref}}), \tag{2.12}$$

with

$$\mu = \frac{2B}{V_{\text{crust}}} \tag{2.13}$$

as the mean shear modulus of the crust. Rearranging this expression, we have

$$B = \frac{1}{2}\mu V_{\text{crust}} = \frac{2\pi}{3}\mu \left(R^3 - R_{\text{inner}}^3\right), \tag{2.14}$$

where R and R_{inner} are the outer and inner radii of the crust. Using an estimate of 10^{30} erg cm^{-3} for the shear modulus of the crust [79], we find that

$$B \sim 6 \times 10^{47} \text{ erg} \tag{2.15}$$

assuming our 10 km radius star has a 1 km thick crust. This confirms that $B \ll A$.

We can also estimate the size of the kinetic energy contribution E_{rot}. For a homogeneous star, the moment of inertia I_{S} is

$$I_{\text{S}} = \frac{2}{5} M R^2. \tag{2.16}$$

Using the same values of mass and radius,

$$I_{\mathrm{S}} \sim 1 \times 10^{45}\ \mathrm{g\ cm^2}. \tag{2.17}$$

The kinetic energy is $T = \frac{1}{2} I_{\mathrm{S}} \Omega^2$ for uniform rotation; for our estimates we will just use the fact that it is of order

$$T = I_{\mathrm{S}} \Omega^2. \tag{2.18}$$

As an example, we will take the Crab pulsar, with an angular velocity $\Omega = 190\ \mathrm{s^{-1}}$. Then

$$T \sim 4 \times 10^{49}\ \mathrm{erg}, \tag{2.19}$$

again a few orders of magnitude smaller than the gravitational binding energy. As these energies will recur frequently throughout, we will define

$$b \equiv \frac{B}{A} \sim 9 \times 10^{-6}, \tag{2.20}$$

$$t \equiv \frac{T}{A} \sim 7 \times 10^{-7} \left(\frac{\Omega}{1\,\mathrm{Hz}} \right)^2. \tag{2.21}$$

For the Crab Pulsar, we have $t \sim 10^{-3}$. Looking back at our formula (2.8) for the oblateness of the star, we can now see that the first term of the right hand side dominates, assuming that the initial angular velocity Ω_0 is of the same order as the current angular velocity Ω.

2.3.2 The stress in the crust

We already have a formula for the mean stress σ in the crust, (2.12). Substituting in the oblateness of the star (2.6), this becomes

$$\sigma = \mu I_{\mathrm{S}} \frac{\Omega_0^2 - \Omega^2}{4(A+B)}. \tag{2.22}$$

A starquake occurs when the stress in the crust reaches some critical value, σ_c, and the crust cracks. This has the effect of 'resetting' the reference oblateness of the star to a new smaller value. This negative shift $\Delta\varepsilon_{\mathrm{ref}}$ will change the oblateness (2.6) of the star by

$$\Delta\varepsilon = \frac{B}{A+B} \Delta\varepsilon_{\mathrm{ref}}. \tag{2.23}$$

The angular momentum J must be conserved at the glitch, so

$$J = I_{\mathrm{S}}\,(1+\varepsilon)\,\Omega = I_{\mathrm{S}}\,(1+\varepsilon+\Delta\varepsilon)\,(\Omega+\Delta\Omega)\,, \tag{2.24}$$

where $\Delta\Omega$ is the change in angular velocity at the glitch. Keeping terms up to first order in the small quantities ε and $\Delta\Omega$ we have that

$$0 = \varepsilon\Delta\Omega + \Omega\Delta\varepsilon. \tag{2.25}$$

This relates the change in oblateness at the glitch $\Delta\varepsilon$ to an observable quantity, the fractional change in spin rate at the glitch:

$$\Delta\varepsilon = -\frac{\Delta\Omega}{\Omega}. \tag{2.26}$$

We can then use this to compare the model to glitch observations. In particular, we will look at what the model predicts for the time between starquakes.

2.3.3 Time between starquakes

Given the change in oblateness at the glitch (2.23), we can use our formula for the stress σ in the crust (2.12) to find the stress relieved in the quake:

$$\Delta\sigma = \mu(\Delta\varepsilon_{\mathrm{ref}} - \Delta\varepsilon) = \frac{A}{B}\,\mu\Delta\varepsilon. \tag{2.27}$$

We can then compare this with the rate at which stress is built up again after the quake to find the time between glitches. Making the approximation $\frac{B}{A} \ll 1$, the formula for the stress (2.22) becomes

$$\sigma = \mu I_{\mathrm{S}}\frac{\Omega_0^2 - \Omega^2}{4A}, \tag{2.28}$$

so that the rate of change of stress $\dot{\sigma}$ is

$$\dot{\sigma} \approx -\frac{\mu I_{\mathrm{S}}}{2A}\Omega\dot{\Omega}, \tag{2.29}$$

We label $\tau = -\frac{\Omega}{\dot{\Omega}}$ as the time characterising the rate at which the pulsar slows down. In terms of τ,

$$\dot{\sigma} \approx -\frac{\mu I_{\mathrm{S}}}{2A}\frac{\Omega^2}{\tau}. \tag{2.30}$$

The time t_q until the star reaches the critical strain level and quakes again is given by

$$t_q = \frac{|\Delta\sigma|}{\dot{\sigma}} = \frac{\omega_q^2}{\Omega^2}\tau\,|\Delta\varepsilon|\,, \tag{2.31}$$

where

$$\omega_q = \sqrt{\frac{2A^2}{BI_{\rm S}}}. \tag{2.32}$$

To get an idea of whether this model can account for glitches, we can compare the quake separation time t_q (2.31) with the observed time between glitches. We will do this for the Crab Pulsar, where glitches occur every few years.

Using these values of A, B and $I_{\rm S}$, we calculate ω_q^2 (2.32) to be

$$\omega_q^2 \sim 1.2 \times 10^{13}\ {\rm s}^{-1}. \tag{2.33}$$

We can now make estimates for the time between quakes. For the Crab, we have an angular velocity $\Omega = 190\ {\rm s}^{-1}$, characteristic time $T = 2260$ years and typical oblateness change $\Delta\epsilon = 0.9 \times 10^{-9}$ [76]. We then find that for our 10 km radius star with a 1 km crust, the time between quakes t_q is predicted to be

$$t_q({\rm Crab}) \sim 700\ {\rm years}, \tag{2.34}$$

two orders of magnitude higher than the observed time. The value of ω_q^2 depends sensitively on the radius of the star and thickness of the crust. Putting in upper estimates of $R = 13$ km, $R_{\rm inner} = 11$ km, we still find that the predicted time,

$$t_q({\rm Crab}) \sim 76\ {\rm years}, \tag{2.35}$$

is much too large. The parameters A, B, $I_{\rm S}$ have been calculated for more realistic equations of state by Pandharipande *et al.* [65]. These give lower values of t_q of down to around 10 years, but the model still has difficulties with accounting for the observed interval between glitches. The lowest values of t_q originally predicted by Baym and Pines were all for stars with properties now known to be unrealistic, including masses below $0.5\ M_\odot$.

It may be possible to obtain more realistic estimates of t_q by relaxing one of the idealisations in the Baym and Pines model. For example, the model assumes a 'steady state' model of starquakes, in which the stress always builds back up to the same critical level σ_c before cracking. In a realistic model, the critical stress level may change over time.

In any case, starquakes may still be expected to occur at some level in neutron stars. Given that the starquake model is arguably conceptually simpler that the superfluid model, it is worth modelling in more detail.

Chapter 3

Energy estimates for starquakes

Before making any detailed calculations, we can get more insight into the starquake mechanism for glitches by making some estimates for the energy released by the quake.

As an extremely rough estimate, we could take the rotational kinetic energy available to the star and multiply it by the fractional change in velocity characterising the glitch,

$$\Delta E \sim I\Omega \left(\frac{\Delta\Omega}{\Omega} \right). \tag{3.1}$$

This estimate can be found in the literature [3]. However, the actual value of the change in energy will depend strongly on the detailed physics of the glitch. This in turn depends on the mechanism that triggers the glitch. Estimates have been made based on different versions of the superfluid model [78], [84]. Here we will concentrate on the starquake model, and make some new estimates for the energy released in the glitch in this case.

To do this, we will start by building on the Baym and Pines model of Section 2.3. We will continue to use the language of Section 2.2 and Figure 2.2, in which Stars A to D represent the stages of the glitch model. After starting relaxed (Star A) at some initial angular velocity Ω_A, the glitch occurs when the star has slowed down to some velocity Ω_B where it has built up a critical level of strain (Star B).

To make these estimates, we will need to specify how the star changes at the glitch. At this point we would expect the crust to crack or otherwise deform to relieve some of this strain. We will consider the extreme case where *all* of the strain is lost. As this will be our model throughout the thesis, it is worth emphasising this point:

> Our model for the glitch is that all the strain is lost from the star. In terms of our model of Stars A–D, this means that the 'reference state' of the star (the state at which the star is relaxed) is reset at the glitch, so that the new reference state is that of Star B.

The strain energy released by the glitch then has to go somewhere. Later in the thesis, we will look at a specific toy mechanism for the glitch, in which the strain energy is simply lost from the system that we model – we can think of this as putting it all into heating the star. In this case, the shape of the star is unchanged immediately after the glitch, so that there is no difference in shape between Star B and the out-of-equilibrium, unstrained Star C. Star C will then settle to a new equilibrium state, Star D, with a faster spin rate.

In this case, with the strain energy lost from the system, the energy available to go into oscillations comes only from the change in the star's gravitational and kinetic energy as it settles to a new equilibrium state. This is the energy difference between Stars C and D, $\Delta E_{CD} = E_D - E_C$.

Although this is perhaps the simplest option to model, it is not necessarily the most realistic. We can also imagine taking the strain energy of the star before the glitch and putting it into, for example, the kinetic energy of the star after the quake (if the crust cracks or otherwise moves about).

The upper bound on this would be to put *all* the strain energy made available into gravitational or kinetic energy. This would correspond to the total energy immediately after the glitch being that of Star B. This gives us an upper limit on the energy available to go into oscillations at the glitch, $\Delta E_{BD} = E_B - E_D$.

In this chapter, for the purposes of making upper estimates on the amplitude of oscillations we will take ΔE_{BD} as the change in energy at the glitch . In the first section, we will use an argument based on the Baym and Pines energy model to calculate ΔE_{BD}. We will then use this to make an estimate for the maximum amplitude of the oscillations of the star after the glitch, and investigate the implications of this for gravitational wave emission.

3.1 The energy made available at a starquake

To start with, we will briefly restate a few of the main results of the Baym and Pines starquake model. For each equilibrium configuration A, B and D we can write the energy in the form

$$E = E_{\mathrm{S}} + \frac{1}{2} I_S (1+\varepsilon)\Omega^2 + A\varepsilon^2 + B(\varepsilon - \varepsilon_{\mathrm{ref}})^2, \tag{3.2}$$

where E_{S} is the energy of the spherical star and the three corrections are kinetic, gravitational and strain energy respectively. By minimising with respect to the ellipticity ε at fixed angular momentum J, we find that

$$\varepsilon = \frac{I_S \Omega^2}{4(A+B)} + \frac{B}{A+B}\varepsilon_{\text{ref}}. \tag{3.3}$$

We will make the $B \ll A$ assumption throughout this section, so that

$$\varepsilon = \frac{I_S \Omega^2}{4A}(1-b) + b\,\varepsilon_{\text{ref}} + O(b^2), \tag{3.4}$$

where $b \equiv \frac{B}{A}$. We can then apply this to the stages of our starquake model. Star A is unstrained, so that $\varepsilon_A = \varepsilon_{\text{ref}}$. This yields an ellipticity of

$$\varepsilon_A = \frac{I_S \Omega_A^2}{4A}. \tag{3.5}$$

The star then spins down to angular velocity Ω_B, still relaxed at ε_A so that

$$\varepsilon_B = \frac{I_S \Omega_B^2}{4A}(1-b) + b\,\varepsilon_A \tag{3.6}$$

to first order. We will now introduce the variables

$$t = \frac{I_S \Omega_B^2}{A}, \tag{3.7}$$

$$X = \frac{\Omega_A^2 - \Omega_B^2}{\Omega_B^2}, \tag{3.8}$$

so that the ellipticities of Stars A and B become

$$\varepsilon_A = \frac{t}{4}(1+X), \tag{3.9}$$

$$\varepsilon_B = \frac{t}{4}(1+bX). \tag{3.10}$$

As we saw in Section 2.3, t is generally a small parameter (2.21). We will use this fact to simplify later equations. We would also expect X, which is related to the difference in angular velocity between Star A and Star B, to be small.

Next we consider what happens after the starquake. At the glitch, all strain is lost, so that the reference ellipticity is set to that of Star B. This removal of strain will cause the star to be temporarily out of equilibrium (Star C). It will then oscillate before damping down to the new equilibrium state Star D.

We can calculate the ellipticity of this star again by using our general expression (3.3). Star D is rotating with angular velocity Ω_D and unstrained at ellipticity ε_B, so that

$$\varepsilon_D = \frac{I_S \Omega_D^2}{4(A+B)} + \frac{B}{A+B}\varepsilon_B. \tag{3.11}$$

We can rewrite this as

$$\varepsilon_D = \frac{t}{4}\left[\left(\frac{\Omega_D}{\Omega_B}\right)^2\left(\frac{1}{1+b}\right) + \frac{b(1+bX)}{1+b}\right] \tag{3.12}$$

To first order in b, this becomes

$$\varepsilon_D = \frac{t}{4}\left[\left(\frac{\Omega_D}{\Omega_B}\right)^2 + b\left(1-\left(\frac{\Omega_D}{\Omega_B}\right)^2\right)\right], \tag{3.13}$$

where we have written this in terms of the still unknown angular velocity Ω_D of Star D. Next we will show that we can find Ω_D, given the fact that angular momentum is conserved at the glitch.

3.1.1 Conservation of angular momentum

Conservation of angular momentum means that

$$\Omega_B(1+\varepsilon_B) = \Omega_D(1+\varepsilon_D). \tag{3.14}$$

Substituting in the expressions for ε_B (3.10) and ε_D (3.13), we obtain

$$1+\frac{t}{4}(1+bX) = \frac{\Omega_D}{\Omega_B}\left[1+\frac{t}{4}\left(\left(\frac{\Omega_D}{\Omega_B}\right)^2 + b\left(1-\left(\frac{\Omega_D}{\Omega_B}\right)^2\right)\right)\right]. \tag{3.15}$$

The right hand side has a term of order Ω_D^3, but we can simplify this by making one final approximation, which is that we know the fractional change in angular velocity at the glitch is small. Defining this as

$$z \equiv \frac{\Omega_D - \Omega_B}{\Omega_B} \tag{3.16}$$

we have that

$$1+\frac{t}{4}(1+bX) = \left[1+z+\frac{t}{4}\left((1+z)^3 + b\left(1-(1+z)^3\right)\right)\right]. \tag{3.17}$$

Since $z \ll 1$, to first order in z we can write this

$$1+\frac{t}{4}(1+bX) = 1+z+\frac{t}{4}(1+3z-3bz). \tag{3.18}$$

Solving for z,

$$z = \frac{btX}{4 + 3t(1-b)}. \tag{3.19}$$

As a check, we see that if $b = 0$ (zero strain energy) this reduces to $z = 0$, as expected. We will keep only terms up to second order in either b or t, so that

$$z = \frac{1}{4}btX. \tag{3.20}$$

Putting the angular velocities back into this,

$$\frac{\Omega_D - \Omega_B}{\Omega_B} = \frac{1}{4}bt\left(\frac{\Omega_A^2 - \Omega_B^2}{\Omega_B^2}\right). \tag{3.21}$$

We would expect the change in angular velocity between the unstrained state, Star A, and the state at the glitch, Star B, to be relatively small, given the observed time between glitches, so that $X = \left(\frac{\Omega_A^2}{\Omega_B^2} - 1\right)$ is small. This gives us a consistency constraint for the model: we can only use it for a change in spin at the glitch $\frac{\Delta\Omega_{BD}}{\Omega_B}$ that give a sensible result for X. This is equivalent to specifying that

$$\frac{4}{bt}\frac{\Delta\Omega_{BD}}{\Omega_B} \ll 1. \tag{3.22}$$

The constraint on the spin-up at the glitch is then

$$\frac{\Delta\Omega_{BD}}{\Omega_B} \lesssim 10^{-8}\left(\frac{b}{10^{-5}}\right)\left(\frac{t}{10^{-3}}\right). \tag{3.23}$$

This means that the model only works for the smaller glitches such as those of the Crab.

We can then substitute our result for z back into the elllipticity ε_D (3.13). If we keep only terms up to first order in either b or t, no terms depending on z remain and we are left with just

$$\varepsilon_D = \frac{t}{4}. \tag{3.24}$$

3.1.2 The change in energy at the glitch

Now we have the ellipticities of stars B and D, we can find their energy and hence the change in energy at the glitch. Star B has energy

$$E_B = E_S + \frac{1}{2}I_S(1+\varepsilon_B)\Omega_B^2 + A\varepsilon_B^2 + B(\varepsilon_B - \varepsilon_A)^2, \tag{3.25}$$

which we can rewrite in terms of b and t as

$$E_B = E_{\rm S} + A\left[\frac{1}{2}t(1+\varepsilon_B) + \varepsilon_B^2 + b(\varepsilon_B - \varepsilon_A)^2\right]. \tag{3.26}$$

To be consistent with our approximation for ε_D, we will keep terms up to fourth order in either b or t, so that

$$E_B = E_S + A\left[\frac{t}{2} + \frac{3t^2}{16} + \left(\left(\frac{X}{4} + \frac{X^2}{16}\right)t^2\right)b - \frac{1}{16}X^2t^2b^2\right] \tag{3.27}$$

After the glitch, Star D has energy

$$E_D = E_{\rm S} + \frac{1}{2}I_S(1+\varepsilon_D)\Omega_D^2 + A\varepsilon_D^2 + B(\varepsilon_D - \varepsilon_B)^2, \tag{3.28}$$

which can be rewritten as

$$E_D = E_{\rm S} + A\left[\frac{1}{2}t(1+\varepsilon_D) + \varepsilon_D^2 + b(\varepsilon_D - \varepsilon_B)^2\right], \tag{3.29}$$

or, again keeping terms up to fourth order,

$$E_D = E_S + A\left[\frac{t}{2} + \frac{3t^2}{16} + \left(\left(\frac{X}{4} + \frac{Xt}{16}\right)t^2\right)b\right]. \tag{3.30}$$

We can now calculate the maximum energy available to go into oscillations, $\Delta E_{BD} = E_B - E_D$. The lowest order term of this is

$$\Delta E_{BD} = \frac{1}{16}AX^2t^2b, \tag{3.31}$$

i.e.

$$\Delta E_{BD} = \frac{1}{16}B\left(\frac{\Omega_A^2}{\Omega_B^2} - 1\right)^2\left(\frac{I_S\Omega_B^2}{A}\right)^2. \tag{3.32}$$

3.2 Amplitude of the oscillations

We now want to find the maximum amplitude of the oscillation modes excited, by equating this change in energy ΔE_{BD} with the kinetic energy of oscillations $(E_{\rm mode})_{BD}$. This energy has the form

$$(E_{\rm mode})_{BD} = I_S\omega^2\alpha_{BD}^2 \tag{3.33}$$

where ω is the frequency of the oscillations and α_{BD} is a dimensionless number characterising their amplitude. Then

$$\alpha_{BD} \sim \frac{1}{\omega}\sqrt{\frac{\Delta E_{BD}}{I_S}}, \tag{3.34}$$

i.e.

$$\alpha_{BD} \sim \left(\frac{1}{\omega}\right)\sqrt{\frac{B}{I_S}}Xt. \tag{3.35}$$

3.2.1 Numerical estimates for the amplitude

We can now make a rough upper estimate of the amplitude of these oscillations, given an estimate of the maximum breaking strain of the crust, $u_{\rm break}$. The strain in the star must be less than this, so that

$$\varepsilon_A - \varepsilon_B \lesssim u_{\rm break}. \tag{3.36}$$

To lowest order in t and b we have

$$\varepsilon_A - \varepsilon_B \sim \frac{tX}{4}, \tag{3.37}$$

so

$$\alpha_{BD} \lesssim 4u_{\rm break}\left(\frac{1}{\omega}\right)\sqrt{\frac{B}{I_S}}\,. \tag{3.38}$$

The frequency ω depends on what type of mode is excited. We will make an estimate assuming that the energy goes into a fundamental fluid mode ('f-mode'). We will discuss this mode in more detail in Chapter 5; for now, we just need the approximate frequency $\omega \sim 2000$ Hz. Putting in an upper estimate of $u_{\rm break} = 0.1$ [38] and using our previous estimates of A (2.10), B (2.19) and I_S (2.17), we have

$$\alpha_{BD} \lesssim 8 \times 10^{-4}\left(\frac{u_{\rm break}}{0.1}\right). \tag{3.39}$$

However, we also have the constraint of the observed fractional change in spin at the glitch z. Given this, our model actually specifies the amplitude of oscillations: we have found the parameter X in our amplitude estimate (3.35) in terms of z (3.20). For consistency, we should expect this amplitude to be smaller than the upper limit based on $u_{\rm break}$.

To calculate this, we will rewrite (3.35) in terms of z as

$$\alpha_{BD} \sim \frac{4}{\sqrt{b}} \sqrt{\frac{A}{I_S}} \left(\frac{1}{\omega}\right) z. \tag{3.40}$$

Note that this is independent of the rotation rate Ω_B. We have previously seen that our model only makes sense for smaller glitches of amplitude $z \leq 10^{-8}$, typical of Crab glitches. Putting this and again using our previous estimates of A and I_S in we have

$$\alpha_{BD} \sim 2 \times 10^{-6} \left(\frac{b}{10^{-5}}\right)^{-\frac{1}{2}} \left(\frac{\omega/2\pi}{2000\,\mathrm{Hz}}\right)^{-1} \left(\frac{z}{10^{-8}}\right), \tag{3.41}$$

which is smaller than our upper estimate (3.39).

This dimensionless amplitude estimate α_{BD} for a star of radius R corresponds to displacements at the surface of the order $\delta r \sim \alpha_{BD} R$, i.e. surface oscillations of around 1 cm. This could be of interest in terms of electromagnetic radiation from the shaking of field lines at the surface.

3.3 Gravitational wave estimates

Next we will use this calculated maximum amplitude to make some estimates for the gravitational wave emission. In this section we will assume that an $l = 2$, $m = 0$ spheroidal oscillation mode has been excited, with the amplitude $\alpha_{BD} \sim 2 \times 10^{-6}$ just calculated.

We will discuss oscillation modes in more detail in Chapter 5; for now, we just need the fact that with this type of stellar oscillation, the pulsating stellar surface can be described by the polar equation

$$r(\theta, t) = R(1 + \alpha_{BD} e^{-i\omega t} P_2(\cos\theta)). \tag{3.42}$$

In Section 4.3 we will show that for any given time t this is the equation of an ellipsoid

$$\frac{x^2}{(1 - \frac{\alpha_{BD}}{2}\cos(\omega t))^2} + \frac{y^2}{(1 - \frac{\alpha_{BD}}{2}\cos(\omega t))^2} + \frac{z^2}{(1 + \alpha_{BD}\cos(\omega t))^2} = R^2 \tag{3.43}$$

to first order in α_{BD}. This is a reasonable choice of oscillation mode given that the rotating star also has this shape (we will show this explicitly in Chapter 4), and that the starquake produces a change in ellipticity of the star. In Chapter 7 we will construct a specific starquake toy model that has this $l = 2$, $m = 0$ character.

For the purposes of making an estimate of gravitational wave emission, we will also make the assumption that the star has a constant density throughout. In this case the corresponding eigenfunction for this mode has the form

$$\xi^i(r,\theta,\phi) = \alpha_{BD} r \left(2P_2(\cos\theta)\hat{r} + \frac{dP_2(\cos\theta)}{d\theta}\hat{\theta} \right). \tag{3.44}$$

Again, we will show this in Chapter 4.

3.3.1 The gravitational wave field of the star

To find the gravitational wave field, we first need to calculate the quadrupole moment tensor (1.14). Integrating over the volume of the ellipsoid, we find that the nonzero components of this tensor are

$$I_{xx} = I_{yy} = \frac{MR^2}{5}\left(1 - \alpha_{BD}e^{-i\omega t}\right), \tag{3.45}$$

$$I_{zz} = \frac{MR^2}{5}\left(1 + 2\alpha_{BD}e^{-i\omega t}\right), \tag{3.46}$$

The quadrupole gravitational wave field (1.13) for outgoing spherical radiation is then

$$\bar{h}_{jk}(t,x^i) = -\frac{2\omega^2}{r} I_{jk}(r-\omega t). \tag{3.47}$$

We can choose a TT gauge transverse to the direction of the motion of the wave by using a projection (1.16). For waves travelling at an angle θ to the z-axis and with $y = 0$, the normal vector to the direction of motion is $n_i = (\sin\theta, 0, \cos\theta)$, and so the projection tensor (1.15) is

$$P_{ij} = \begin{pmatrix} \cos^2\theta & 0 & -\sin\theta\cos\theta \\ 0 & 1 & 0 \\ -\sin\theta\cos\theta & 0 & \sin^2\theta \end{pmatrix}. \tag{3.48}$$

Using this projection, we find that in TT gauge the wavefield is

$$\bar{h}^{\mathrm{TT}} = -3\omega^2\alpha_{BD}\sin^2\theta\frac{MR^2}{5}\frac{e^{i\omega(r-t)}}{r}\begin{pmatrix} \cos^2\theta & 0 & -\sin\theta\cos\theta \\ 0 & -1 & 0 \\ -\sin\theta\cos\theta & 0 & \sin^2\theta \end{pmatrix}. \tag{3.49}$$

This gives us the waveform as seen by an observer with spatial axes (x,y,z) aligned with those of the star. A final simplification can be made by rotating to a new set of observer axes $(\hat{x},\hat{y},\hat{z})$ where the $\hat{z}$-axis points along the direction of propagation of the wave:

$$\begin{pmatrix} \hat{x} \\ \hat{y} \\ \hat{z} \end{pmatrix} = \begin{pmatrix} \cos\theta & 0 & -\sin\theta \\ 0 & 1 & 0 \\ \sin\theta & 0 & \cos\theta \end{pmatrix} \begin{pmatrix} x \\ y \\ z \end{pmatrix}. \tag{3.50}$$

Calling the rotation matrix R_{ij}, the wave field in the new coordinate system is

$$\bar{h}_{ij}^{\text{new}} = R^k{}_i R^l{}_j \bar{h}_{kl}^{\text{TT}} = -3\omega^2 \alpha_{BD} \sin^2\theta \frac{MR^2}{5} \frac{e^{i\omega(r-t)}}{r} \begin{pmatrix} 1 & 0 & 0 \\ 0 & 1 & 0 \\ 0 & 0 & 0 \end{pmatrix}. \tag{3.51}$$

From this, we can see that the wave is purely in the 'plus' polarisation, with

$$h_+ = -3\omega^2 \alpha_{BD} \sin^2\theta \frac{MR^2}{5} \frac{e^{i\omega(r-t)}}{r}. \tag{3.52}$$

3.3.2 Gravitational wave luminosity of the star

We can calculate the rate energy is carried away from the star by gravitational waves using the energy flux formula (1.22) developed in Section 1.2. With our form (3.51) for the gravitational wave field this becomes

$$F = \frac{\omega^2}{32\pi} \langle 2h_+^2 \rangle = \frac{1}{32\pi} \frac{9}{25} \alpha_{BD}^2 \omega^6 M^2 R^4 \frac{\sin^4\theta}{r^2}. \tag{3.53}$$

This can then be integrated over a sphere of radius r to get the total luminosity,

$$L = -\frac{dE}{dt} = \frac{3G}{125c^5} \alpha_{BD}^2 \omega^6 M^2 R^4. \tag{3.54}$$

Here we have switched to working explicitly in terms of G and c using the conversion factor $\frac{G}{c^5}$. This is in agreement with the results of Chau [23].

To find the damping timescale of the wave, we need to know how much energy is stored in the oscillations of the star. We can find this by calculating the energy at the point in the oscillation cycle where the star is spherical. This means that there is no gravitational energy perturbation, so we only need to calculate the kinetic energy of the pulsation mode. For a mode with eigenfunction ξ^i, we have

$$E = \frac{1}{2}\rho\omega^2 \int_V |\xi^2| dV. \tag{3.55}$$

Substituting in our mode eigenfunction (3.44), we find that the initial energy E_0 in the star's oscillation is

$$E_0 = -\frac{1}{5}\rho\,\alpha_{BD}^2\,\omega^2\pi R^5. \tag{3.56}$$

This can then be compared with the luminosity (3.54), to find that the energy as a function of time satisfies

$$E(t) = E_0 e^{-\frac{t}{2\tau}}, \tag{3.57}$$

where τ is the *damping timescale*

$$\tau = \frac{25c^5}{2GMR^2\omega^4}\,. \tag{3.58}$$

The energy $E \propto h_+^2$, and so the wavefield decays as

$$h_+(t) = -\frac{3G}{5c^4}\omega^2\alpha_{BD}\sin^2\theta MR^2\frac{e^{i\omega(r-t)}}{r}e^{-\frac{t}{\tau}}. \tag{3.59}$$

3.3.3 Numerical estimates

We now make estimates for a homogeneous fluid star with a mass of $1.4M_\odot$ and a radius of 10 km. We will again put in an estimate of 2000 Hz for the excited mode, appropriate for an f-mode. The damping timescale (3.58) is then

$$\tau \sim 0.07 \text{ s}. \tag{3.60}$$

Taking the Crab's rotation rate of 30Hz as a typical example, we can put in our value of $\alpha_{BD} \sim 2\times10^{-6}$. For a source at a distance of 1 kiloparsec, the strain h_+ is then

$$h_+ \sim 1\times10^{-23}\left(\frac{\omega/2\pi}{2000\,\text{Hz}}\right)\left(\frac{r}{1\,\text{kpc}}\right)^{-1}\left(\frac{b}{10^{-5}}\right)^{-\frac{1}{2}}\left(\frac{z}{10^{-8}}\right), \tag{3.61}$$

where we have used our value for the amplitude α_{BD} (3.41). For the purposes of comparing to a detector sensitivity curve, we are more interested in the *characteristic strain*,

$$h_+\sqrt{\tau} \sim 4\times10^{-24}\ \text{Hz}^{\frac{1}{2}}. \tag{3.62}$$

This level of strain should be detectable with third generation detectors. Figure 3.1 shows a preliminary sensitivity curve for the Einstein telescope [70]. Our upper estimate is plotted for a star oscillating at an f-mode frequency 2000Hz and lies above the curve.

The figure also shows the planned Advanced LIGO sensitivity curve for a representative choice of detector configuration (the Zero Det, High Power configuration) [77]. Our upper estimate on the strain level is below this curve.

3.4 Estimates for solid quark stars

The estimates given so far have been for a normal neutron star with a crust around 1 km thick. More exotic models have however been proposed, including quark stars with a large solid core [33, 87]. These models are of interest in terms of gravitational wave emission as they are expected to be able to sustain a larger maximum ellipticity [63, 36]. More relevant to us here is the possibility that a solid star of this type could be expected to undergo a much larger quake.

In this section we will make some estimates for this scenario, based on a solid star with a shear modulus of $\mu_{\rm solid} \sim 4 \times 10^{32}$ erg cm^{-3} [87].

For a completely solid star, our formula for B (2.19) becomes

$$B_{\rm solid} = \frac{2\pi}{3}\mu R^3, \tag{3.63}$$

which for a 10 km radius star becomes

$$B_{\rm solid} \sim 8 \times 10^{50}, \tag{3.64}$$

so that

$$b_{\rm solid} \equiv \frac{B_{\rm solid}}{A} \sim 1 \times 10^{-2}, \tag{3.65}$$

a much larger value than our previous estimate of $b \sim 10^{-5}$ for a star with a fluid core. This means that the star in our model can sustain larger glitches: our criterion (3.21) that the difference in angular velocity between Stars A and B is small yields

$$\frac{4}{b_{\rm solid} t}\frac{\Delta\Omega_{BD}}{\Omega_B} \lesssim 1, \tag{3.66}$$

so that

$$z_{\rm solid} \equiv \frac{\Delta\Omega_{BD}}{\Omega_B} \lesssim 2 \times 10^{-6}. \tag{3.67}$$

We are thus able to use this model for glitches of around a factor of 100 larger than for a normal neutron star model.

Using our new values of $z_{\rm solid}$ and $b_{\rm solid}$, the amplitude of the oscillations in our model (3.40) is

$$(\alpha_{BD})_{\rm solid} \sim 1 \times 10^{-2} \left(\frac{b_{\rm solid}}{10^{-5}}\right)^{-\frac{1}{2}} \left(\frac{\omega/2\pi}{2000\,{\rm Hz}}\right)^{-1} \left(\frac{z_{\rm solid}}{10^{-6}}\right), \tag{3.68}$$

and the corresponding value of the characteristic strain is

$$\left(h_+\sqrt{\tau}\right) \sim 5 \times 10^{-22}\ \mathrm{Hz}^{-\frac{1}{2}}, \tag{3.69}$$

a factor of 100 larger. This is plotted on the sensitivity curve in Figure 3.1, again for an oscillation at 2000 Hz, and this time is above the projected sensitivity curves for both ET and Advanced LIGO.

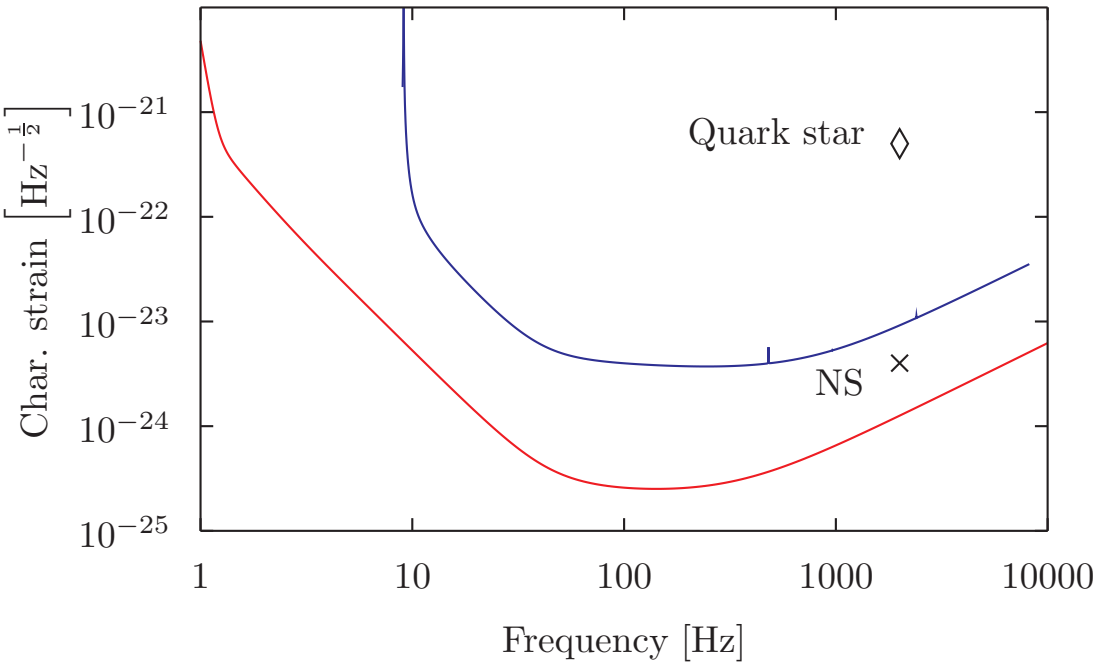

Figure 3.1: A plot of the proposed Advanced LIGO (*blue*) and Einstein Telescope (*red*) sensitivity curves, with our upper estimates for the characteristic strain produced by a normal neutron star with a fluid core (marked by a cross) and by a solid quark star (marked by a diamond). Both of these are plotted for a typical f-mode frequency of 2000 Hz.

Chapter 4

Equilibria of rotating stars

4.1 Overview

To be able to model the way the neutron star changes at the starquake, we need to be able to construct equilibrium models of the star before and after the glitch. We will do this analytically for the case of a completely solid, incompressible elastic star.

To describe rotation we will use a perturbative approach, where the centrifugal force is treated as a small perturbation to a non-rotating, spherical background model. This is a reasonable assumption in the *slow rotation* limit, where the centrifugal force is small compared to the gravitational force at the surface of the star [80]. To do this we will use the Lagrangian and Eulerian perturbation schemes described in Section 1.3.3.

The aim is to calculate how the star is deformed by rotation, in terms of a displacement field mapping the positions of particles in the nonrotating background star to their new positions under rotation. This will form the basis of our initial data for the starquake toy model we develop in later chapters.

In the next section we will start by finding the structure of the background, spherical star. We will then look at the simpler case of a rotating fluid star. This will also be useful in understanding the full elastic calculation, which we carry out in the final section of the chapter.

4.2 The background model: a spherical fluid star

Our background model is a spherical star in hydrostatic equilibrium, so that the background pressure p and gravitational potential Φ satisfy

$$-\nabla_i p - \rho \nabla_i \Phi = 0. \tag{4.1}$$

We will look for radially symmetric solutions $p = p(r)$, $\Phi = \Phi(r)$. The gravitational potential Φ is governed by Poisson's equation

$$\frac{d^2\Phi}{dr^2} + \frac{2}{r}\frac{d\Phi}{dr} = 4\pi G\rho. \tag{4.2}$$

We try a solution of the form $\Phi = Ar^2 + B$ and find that $A = \frac{2\pi}{3}G\rho$. To fix B, we use the fact that Φ is continuous at the surface $r = R$ of the star. This can be seen by integrating Poisson's equation (4.2) above over a small cube of volume V on the surface of the sphere. This means that we can match Φ^{int} to the exterior gravitational field $\Phi^{\text{ext}} = -\frac{MG}{r}$, where M is the mass of the star. We find that $B = -2\pi GR^2\rho$, and so the gravitational potential inside the star is

$$\Phi(r) = \frac{2\pi}{3}G\rho r^2 - 2\pi GR^2\rho. \tag{4.3}$$

We can then substitute Φ back into the equation of hydrostatic equilibrium (4.1) and integrate to find p:

$$p(r) = \frac{2\pi}{3}G\rho^2(R^2 - r^2). \tag{4.4}$$

The constant of integration has been fixed by using the defining property of the surface, $p(R) = 0$.

4.3 Rotation of an incompressible fluid star

We now perturb the spherical background star by adding a centrifugal force governed by the potential

$$\phi^c = \Omega^2 r^2 \sin^2\theta, \tag{4.5}$$

where Ω is the angular velocity of the perturbed, rotating star. It will later be useful if we rewrite this as

$$\phi^c = \frac{\Omega^2 r^2}{3}\left(1 - P_2(\cos\theta)\right), \tag{4.6}$$

where $P_2(\cos\theta) = \frac{1}{2}(3\cos^2\theta - 1)$ is the second Legendre polynomial. Properties of the Legendre polynomials are discussed in, for example, Arfken and Weber [11]. The centrifugal force will induce perturbations in the pressure and gravitational potential of the star. We will use the Eulerian description of the perturbations (see Section 1.3.3). These perturbations δp and $\delta\Phi$ will satisfy the force equation

$$-\rho\nabla_i\phi^c = -\nabla_i\delta p - \rho\nabla_i(\delta\Phi). \tag{4.7}$$

Making perturbations to the density of an incompressible star is slightly more subtle. Incompressibility means that the Lagrangian perturbation of the density $\Delta\rho = 0$, and we will use this to find the Eulerian perturbation $\delta\rho = \Delta\rho - \eta^i\nabla_i\rho$. Here η^i is the Lagrangian perturbation field mapping particles to their new configurations in the rotating star. The background density of the star ρ is constant inside the star and zero outside. Formally we can write

$$\rho(r) = \rho(1 - H(r - R)), \tag{4.8}$$

where $H(x)$ is the Heaviside step function

$$H(x) = \begin{cases} 0 & x < 0 \\ \frac{1}{2} & x = 0 \\ 1 & x > 0 \end{cases}. \tag{4.9}$$

The derivative of the density is then

$$\frac{d\rho}{dr} = -\rho\delta(r - R), \tag{4.10}$$

where $\delta(x)$ is the Dirac delta function, $\frac{d}{dx}[H(x)] = \delta(x)$. Using this, the Eulerian perturbation $\delta\rho$ becomes

$$\delta\rho = \rho\delta(r - R)\eta^r, \tag{4.11}$$

where η^r is the radial component of η^i. We can see that this vanishes everywhere except at the surface. This means that $\delta\rho = 0$ inside the star, but we must take care with the boundary conditions.

4.3.1 The perturbed gravitational potential

The perturbed gravitational potential $\delta\Phi$ also satisfies Poisson's equation,

$$\nabla^2\delta\Phi = 4\pi G\delta\rho. \tag{4.12}$$

Away from the surface we have $\delta\rho = 0$, and so this is just Laplace's equation. The general solution regular inside the star is then

$$\delta\Phi^{\rm int}(r,\theta,\phi) = \sum_{l=0}^{\infty}\sum_{m=-l}^{l} B_{lm}\, r^l Y_{lm}(\theta,\phi), \tag{4.13}$$

where the Y_{lm}s are spherical harmonics [11]. Outside the star we need regular solutions of the form

$$\delta\Phi^{\rm ext}(r,\theta,\phi) = \sum_{l=0}^{\infty}\sum_{m=-l}^{l} C_{lm}\, \frac{1}{r^{l+1}} Y_{lm}(\theta,\phi), \tag{4.14}$$

for arbitrary constants B_{lm} and C_{lm}.

From the form of the centrifugal potential we can guess that we will only need to consider solutions with $m = 0$ and $l = 2$, so that

$$\delta\Phi(r,\theta) = B_2 r^2 P_2(\cos\theta) \tag{4.15}$$

inside the star, where $P_2(\cos\theta)$ is a Legendre polynomial. However, in considering how to match these solutions at the surface we will stick with the general case – it will be useful for reference in later chapters.

We obtain our first matching condition by integrating Poisson's equation (4.12) for $\delta\Phi$ over a small volume V on the surface. Applying Stokes' theorem,

$$\int_{\partial V} \nabla_i \delta\Phi dS^i = 4\pi G\rho\eta^r(R,\theta,\phi). \tag{4.16}$$

On the left hand side, only the top and bottom sides of V contribute to the integral, so we have

$$\frac{\partial(\delta\Phi)^{\rm ext}}{\partial r} - \frac{\partial(\delta\Phi)^{\rm int}}{\partial r} = 4\pi G\rho\eta^r(R,\theta,\phi). \tag{4.17}$$

Integrating once more, we find a second condition, which is that $\delta\Phi$ is continuous at the surface. We can combine these two conditions to eliminate C_{lm} and show that

$$-\sum_{l=0}^{\infty}\sum_{m=-l}^{l} (2l+1) B_{lm} R^{l-1} Y_{lm} = 4\pi G\rho\eta^r(R,\theta,\phi). \tag{4.18}$$

For our current problem, where the gravitational potential takes the simplified form (4.15) above, this condition becomes

$$4\pi G\rho\eta^r(R,\theta,\phi) = -5B_2 R P_2(\cos\theta). \tag{4.19}$$

4.3.2 Finding the rotation shape

We can now return to the force equation (4.7), which can be integrated to find that

$$\rho\phi^c - \delta p - \rho\delta\Phi = C, \tag{4.20}$$

where C is a constant. Substituting in the centrifugal potential ϕ^c and the form of the gravitational perturbation (4.15), we see that the pressure perturbation δp must have the form

$$\delta p(r,\theta) = C + \frac{\Omega^2 r^2}{3} - \rho\left(B_2 + \frac{\Omega^2}{3}\right) r^2 P_2(\cos\theta). \tag{4.21}$$

To find the two unknown constants B_2 and C, we can use the fact that the pressure of the star vanishes at the surface. This means that the Lagrangian perturbation of the pressure Δp will be zero at $r = R$, so that

$$\delta p(R,\theta) = \frac{4\pi G\rho^2 R}{3}\eta^r(R,\theta). \tag{4.22}$$

Substituting in the boundary condition (4.19) for the gravitational potential, we have that

$$\delta p(R,\theta) = -\frac{5}{3}B_2\rho R^2 P_2(\cos\theta). \tag{4.23}$$

This can then be compared to our previous expression (4.21) for δp, to find the constants $B_2 = \frac{\Omega^2}{2}$, $C = -\frac{\Omega^2 R^2}{3}$, so that the final forms of the pressure and gravitational perturbations are

$$\delta p(r,\theta) = \frac{\Omega^2}{3}(r^2 - R^2) - \frac{5}{6}\rho\Omega^2 r^2 P_2(\cos\theta). \tag{4.24}$$

and

$$\delta\Phi = \frac{\Omega^2}{2}r^2 P_2(\cos\theta). \tag{4.25}$$

We also find the radial displacement at the surface to be

$$\eta^r(R,\theta) = -\frac{5\Omega^2 R}{8\pi G\rho}P_2(\cos\theta). \tag{4.26}$$

This is the only part of the displacement field η^i of the rotating fluid star that we can find unambiguously. We will discuss the reasons for this in Chapter 6. However, the radial displacement at the surface is enough to give us the surface shape of the star. This can be described by the polar equation

$$r(\theta) = R(1 + a_2 P_2(\cos\theta)), \tag{4.27}$$

where $a_2 = -\frac{5\Omega^2}{8\pi G\rho}$. We will now describe this shape in more detail. It will be helpful to introduce Cartesian coordinates, with the z-axis pointing along the axis of rotation. By axisymmetry it is sufficient to consider the star's shape in the $x - z$ plane. First we show that the polar equation (4.27) above is the equation of an ellipse

$$\frac{x^2}{a^2} + \frac{z^2}{c^2} = 1, \tag{4.28}$$

accurate to first order in $\varepsilon = a - c$ (i.e. valid for small differences in the major and minor axes of the ellipse). To show this, we can first write the ellipse equation (4.28) in spherical coordinates $x = r\sin\theta, z = r\cos\theta$:

$$\frac{r^2\sin^2\theta}{a^2} + \frac{r^2\cos^2\theta}{(a-\varepsilon)^2} = 1. \tag{4.29}$$

We then expand to first order in ε, finding that

$$r(\theta) = c\left[1 + \frac{\varepsilon}{c}(\cos^2\theta - 1)\right]. \tag{4.30}$$

To compare with our equation for the surface of the star (4.27), we need to find ε in terms of the unperturbed radius R. We know that the radial displacement η^r is zero when $P_2(\cos\theta) = 0$, i.e. when $\cos^2\theta = \frac{2}{3}$. At this point $r(\theta) = R$, i.e.

$$R = c - \frac{2\varepsilon}{3}. \tag{4.31}$$

Using this, we can then show that

$$r(\theta) = R\left[1 + \frac{c-a}{3c}(3\cos^2 - 1)\right] = R\left[1 + \frac{2(c-a)}{3c}P_2(\cos\theta)\right]. \tag{4.32}$$

Finally, we can rewrite this using

$$a = R + \eta^r_{\text{initial}}\left(R, \frac{\pi}{2}\right) = R - \frac{a_2}{2}, \tag{4.33}$$

$$c = R + \eta^r_{\text{initial}}(R, 0) = R + a_2 \tag{4.34}$$

to show that $\frac{2(c-a)}{3c} = a_2$ to first order, giving us the stellar surface as in (4.27).

4.4 Rotating elastic star

We now turn to the case where the star is a completely solid elastic body currently rotating at angular velocity Ω. As before, we will assume that the star is incompressible. The elastic star will have some 'reference' angular velocity, Ω_A, at which the star is unstrained. At this angular velocity, the star will have a shape equivalent to that of a completely fluid star.

Figure 4.1 sketches this situation. We wish to find the displacement field, which we have labelled ξ^{AB}, connecting particles of the star in its current state – labelled Star B – with their position in its unstrained reference state, Star A. To find this, we will need to also use maps between the background, nonrotating star, labelled Star S, and A and B. We will call these maps η^{SA} and η^{SB}.

The special case where Star A is spherical and nonrotating is discussed in Love's 'Theory of Elasticity' [52]. Baym and Pines [16] quote results for the displacement and strain fields in the general case. In this section we give details of how to calculate these, following a similar method to that used by Franco, Link and Epstein [30] for a two-component rotating star.

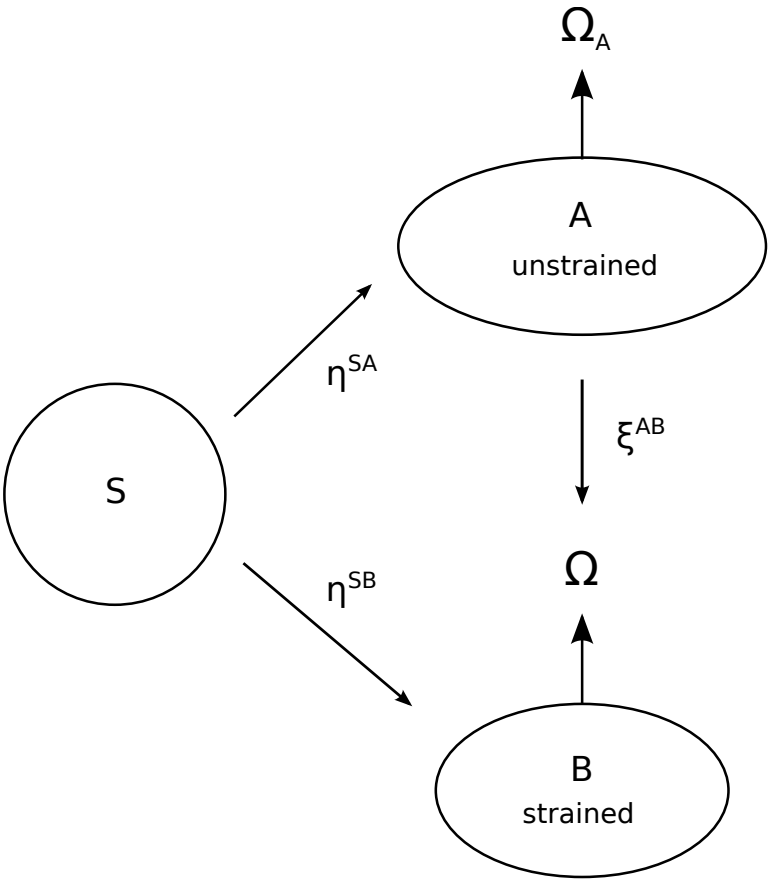

Figure 4.1: Schematic describing the perturbation method for calculating the equilibrium state of a rotating elastic star

We already know that to first order the shape of Star A can be found as a perturbation about a spherical, nonrotating background (Star S in the figure), by the same method used for a fluid star in Section 4.3. The rotation at angular velocity Ω_A will induce a centrifugal force governed by the potential $(\phi^c)^{\mathrm{SA}} = \Omega_A^2 r^2 \left(\frac{1}{3} - \frac{1}{3}P_2(\cos\theta)\right)$, producing pressure and gravitational perturbations δp^{SA} (4.24) and $\delta\Phi^{\mathrm{SA}}$ (4.24) in the star. We can also find the radial displacement at the surface $(\eta^r)^{\mathrm{SA}}(R)$

Next, we perturb the star again so that it rotates at a different angular velocity Ω, introducing a further centrifugal potential $(\phi^c)^{\mathrm{AB}} = (\Omega^2 - \Omega_A^2) r^2 \left(\frac{1}{3} - \frac{1}{3}P_2(\cos\theta)\right)$, and new perturbations $\delta p^{\mathrm{AB}}, \delta\Phi^{\mathrm{AB}}$ to the pressure and gravitational perturbations. This perturbation of the star will induce a strain field that can be calculated from the displacement field $(\xi^i)^{\mathrm{AB}}$ mapping the relaxed star A to the new strained configuration, Star B.

We can write the total pressure perturbation taking us from S to B as the sum $\delta p^{SB} = \delta p^{\mathrm{SA}} + \delta p^{\mathrm{AB}}$, and similarly for $\delta\Phi^{\mathrm{SB}} = \delta\Phi^{\mathrm{SA}} + \delta\Phi^{\mathrm{AB}}$ and $(\eta^i)^{\mathrm{SB}} = (\eta^i)^{\mathrm{SA}} + (\xi^i)^{\mathrm{AB}}$. We also have a total centrifugal potential

$$(\phi^c)^{\mathrm{SB}} = (\phi^c)^{\mathrm{SA}} + (\phi^c)^{\mathrm{AB}} = \frac{\Omega^2 r^2}{3}\left(1 - P_2(\cos\theta)\right). \tag{4.35}$$

Using these quantities allows us to keep working in terms of perturbations about a spherical background, which will be easier when imposing boundary conditions.

4.4.1 Equations of motion

The background, Star S, still has an isotropic stress tensor

$$T_{ij} = -p\delta_{ij} \tag{4.36}$$

identical to that of the fluid star, and we can write the background equation of hydrostatic equilibrium (4.1) as

$$\nabla_j T_i{}^j - \rho\nabla_i\Phi = 0. \tag{4.37}$$

We then perturb the background star by adding a centrifugal force governed by the potential $(\phi^c)^{\mathrm{SB}}$. This will induce Lagrangian perturbations Δp^{SB}, $\Delta\Phi^{\mathrm{SB}}$ in the pressure and gravitational perturbations. There will also be an induced strain field, which depends only on the displacement field $(\xi^{\mathrm{AB}})^i$. The Lagrangian perturbations satisfy

$$-\nabla_i(\phi^c)^{\mathrm{SB}} = \Delta^{\mathrm{SB}}\left[\nabla_j T_i{}^j - \rho\nabla_i\Phi\right]. \tag{4.38}$$

We can use the commutation relation (see e.g. Shapiro and Teukolsky [76]),

$$\Delta\nabla_j T_{ij} = \nabla_j \Delta T_i{}^j - \nabla_j(\xi^k \nabla_k) T_{ij}, \tag{4.39}$$

so that the perturbed equation of motion is

$$-\nabla_i(\phi^c)^{\mathrm{SB}} = \nabla_j(\Delta T^{\mathrm{SB}})_i{}^j - \rho\nabla_i\Delta\Phi^{\mathrm{SB}}, \tag{4.40}$$

where we have used the background equation (4.37) to cancel terms.

The perturbed stress tensor $\Delta T_{ij}^{\mathrm{SB}}$ is made up of an isotropic pressure contribution from the perturbation from S to the unstrained state A,

$$\Delta T_{ij}^{\mathrm{SA}} = (\delta p)^{\mathrm{SA}}\delta_{ij}, \tag{4.41}$$

plus the perturbation from A to B, which picks up an extra shear strain term characteristic of incompressible elastic material (1.42),

$$\Delta T_{ij}^{\mathrm{AB}} = (\delta p)^{\mathrm{AB}}\delta_{ij} + 2\mu u_{ij}^{\mathrm{AB}}. \tag{4.42}$$

Taking the divergence gives

$$\nabla_j(\Delta T^{\mathrm{SB}})^i{}_j = \nabla_j \Delta p^{\mathrm{SB}} + \nabla_j(2\mu(u^{\mathrm{AB}})^i{}_j), \tag{4.43}$$

and for an incompressible star we have (1.43)

$$2\mu\nabla_j(u_{ij}^{\mathrm{AB}}) = \mu\nabla^2(\xi^{\mathrm{AB}})^i. \tag{4.44}$$

Putting this back into the perturbed equation of motion (4.40) we finally obtain

$$-\nabla_i(\phi^c)^{\mathrm{SB}} = -\nabla_i\Delta p^{\mathrm{SB}} + \mu\nabla^2(\xi^{\mathrm{AB}})_i - \rho\nabla_i\Delta\Phi^{\mathrm{SB}}. \tag{4.45}$$

Along with the perturbed equation of motion, we also have Poisson's equation for the perturbed gravitational potential:

$$\nabla^2\Delta\Phi^{\mathrm{SB}} = 4\pi G\delta\rho^{\mathrm{SB}}. \tag{4.46}$$

As with the fluid case (4.11), the continuity equation for incompressible perturbations gives an expression for the perturbed density,

$$\delta\rho^{\mathrm{SB}} = \rho\delta(r - R)(\xi^{\mathrm{SB}})^r. \tag{4.47}$$

4.4.2 Boundary conditions

Before solving for the displacement field $\xi^{\rm AB}$, it will be helpful to collect together all the boundary conditions for the problem. The conditions on the perturbed gravitational potential can be found from Poisson's equation (4.46) in the same way as for the fluid case (4.16). We find that $\delta\Phi^{\rm SB}$ must be continuous at the surface but that the derivative $\frac{\partial(\delta\Phi^{\rm SB})}{\partial r}$ has a discontinuity. Combining these conditions, we have

$$\delta\Phi^{\rm SB} = -\frac{4\pi G\rho}{5R}(\eta_r')^{\rm SB}(R)\, r^2 P_2(\cos\theta), \tag{4.48}$$

where we have written $\eta^{\rm SB} = (\eta')^{\rm SB}P_2(\cos\theta)$. From this we can also find the Lagrangian perturbation $\Delta\Phi^{\rm SB}$ to be

$$\Delta\Phi^{\rm SB} = \left[\frac{4\pi G\rho r}{3} - \frac{4\pi G\rho r^2}{5R}\right](\eta_r')^{\rm SB}(R)P_2(\cos\theta). \tag{4.49}$$

We also have conditions on the displacement field at the surface. As with the fluid problem, particles on the surface of the background star where $T_{ij} = 0$ should still have a zero stress tensor at the perturbed surface, so that

$$-(\Delta p^{\rm SB}(R))\delta_{ir} + 2\mu u_{ir}^{\rm AB}(R) = 0. \tag{4.50}$$

In spherical coordinates, the relevant components of the strain tensor are [43]

$$u_{rr}^{\rm AB} = \frac{\partial\xi_r^{\rm AB}}{\partial r}, \tag{4.51}$$

$$2u_{r\theta}^{\rm AB} = \frac{\partial\xi_\theta^{\rm AB}}{\partial r} - \frac{\xi_\theta^{\rm AB}}{r} + \frac{1}{r}\frac{\partial\xi_r^{\rm AB}}{\partial r}. \tag{4.52}$$

Substituting these in to the boundary condition (4.50) gives

$$-(\Delta p^{\rm SB}(R)) + 2\mu\frac{\partial\xi_r}{\partial r}^{\rm AB}(R) = 0, \tag{4.53}$$

for the rr component, while the $r\theta$ component becomes

$$\frac{\partial\xi_\theta}{\partial r}^{\rm AB} - \frac{\xi_\theta}{r}^{\rm AB} + \frac{1}{r}\frac{\partial\xi_r}{\partial\theta}^{\rm AB} = 0. \tag{4.54}$$

4.4.3 Solving for the displacement field

It will be useful to write

$$\mu h^{\mathrm{SB}} = -\Delta p^{\mathrm{SB}} - \rho \Delta \Phi^{\mathrm{SB}} + \rho (\phi^c)^{\mathrm{SB}}, \tag{4.55}$$

so that our equation of motion (4.45) becomes

$$\nabla_i h^{\mathrm{SB}} + \nabla^j \nabla_j (\xi_i)^{\mathrm{AB}} = 0. \tag{4.56}$$

Taking the divergence, we find that

$$\nabla^2 h^{\mathrm{SB}} = 0, \tag{4.57}$$

so h^{SB} must satisfy Laplace's equation, and the general solution regular at $r = 0$ and with the same symmetries as the centrifugal potential is

$$h^{\mathrm{SB}} = H_2 r^2 P_2(\cos\theta) + H_0. \tag{4.58}$$

We also need to find the form of the displacement field $(\xi^i)^{\mathrm{AB}}$. To do this, we will need to go back to the force equation (4.45), and decompose the displacement vector $\boldsymbol{\xi}^{\mathrm{AB}}$ into radial and tangential parts:

$$\boldsymbol{\xi}^{\mathrm{AB}} = U^{\mathrm{AB}}(r) P_2(\cos\theta) \boldsymbol{e}_r + V^{\mathrm{AB}}(r) \boldsymbol{\nabla} P_2(\cos\theta). \tag{4.59}$$

where $\boldsymbol{e}_r$ is a radial unit vector. As the divergence of $\boldsymbol{\xi}^{\mathrm{AB}}$ is zero, the vector Laplacian term of the equation of motion (4.56) is just $\boldsymbol{\nabla}^2 \boldsymbol{\xi}^{\mathrm{AB}} = -\boldsymbol{\nabla} \times \boldsymbol{\nabla} \times \boldsymbol{\xi}^{\mathrm{AB}}$. In terms of our decomposition this is

$$\begin{aligned} \boldsymbol{\nabla}^2 \boldsymbol{\xi}^{\mathrm{AB}} = -\boldsymbol{\nabla} \times \boldsymbol{\nabla} \times \boldsymbol{\xi}^{\mathrm{AB}} = &-\frac{6}{r^2} \left(U^{\mathrm{AB}} - (V^{\mathrm{AB}})' \right) P_2(\cos\theta) \boldsymbol{e}_r \\ &- \left((U^{\mathrm{AB}})' - (V^{\mathrm{AB}})'' \right) \boldsymbol{\nabla} P_2(\cos\theta). \end{aligned} \tag{4.60}$$

Inserting this back into the force equation (4.56), we find that the $\boldsymbol{e}_r$ component becomes

$$r H_2 = \frac{3}{r^2} \left(U^{\mathrm{AB}} - (V^{\mathrm{AB}})' \right), \tag{4.61}$$

while the $\boldsymbol{\nabla} P_2$ component is

$$r^2 H_2 = \left((V^{\mathrm{AB}})'' - (U^{\mathrm{AB}})' \right). \tag{4.62}$$

We can also rewrite the incompressibility condition $\nabla_i (\xi^{\mathrm{AB}})^i = 0$ using this decomposition, obtaining

$$6V^{\mathrm{AB}} = 2rU^{\mathrm{AB}} + r^2(U^{\mathrm{AB}})'. \tag{4.63}$$

Eliminating H_2 and V^{AB} from these three equations, we can obtain a third order equation in U^{AB}

$$r^3(U^{\mathrm{AB}})''' + 3r^2(U^{\mathrm{AB}})'' - 12r(U^{\mathrm{AB}})' + 12U^{\mathrm{AB}} = 0. \tag{4.64}$$

The general solution finite at the origin is

$$U^{\mathrm{AB}}(r) = Dr + Er^3, \tag{4.65}$$
$$V^{\mathrm{AB}}(r) = \frac{1}{2}Dr^2 + \frac{5}{6}Er^4, \tag{4.66}$$

D and E constants. By substitution back into the radial component of the force equation (4.45), we find that $H_2 = -7E$, so that

$$U^{\mathrm{AB}}(r) = Dr - \frac{1}{7}H_2r^3, \tag{4.67}$$
$$V^{\mathrm{AB}}(r) = \frac{1}{2}Dr^2 - \frac{5}{42}H_2r^4. \tag{4.68}$$

At this point, we need to refer back to the boundary conditions.

First we have the $(r\theta)$ component (4.54) of the traction condition at the surface, which can be written in terms of U^{AB} and V^{AB} as

$$R(V^{\mathrm{AB}})'(R) - 2V^{\mathrm{AB}}(R) + RU^{\mathrm{AB}}(R) = 0. \tag{4.69}$$

From this we find that $D = \frac{8H_2R^2}{21}$, so that

$$U^{\mathrm{AB}}(r) = H_2\left(-\frac{r^3}{7} + \frac{8}{21}R^2r\right), \tag{4.70}$$
$$V^{\mathrm{AB}}(r) = H_2\left(\frac{8R^2}{42}r^2 - \frac{5}{42}r^4\right). \tag{4.71}$$

To fix H_2 we can then use the (rr) component (4.53), which becomes

$$-\Delta p^{\mathrm{SB}}(R) + 2\mu(U^{\mathrm{AB}})'(R)P_2(\cos\theta) = 0. \tag{4.72}$$

We can write Δp^{SB} in terms of h^{SB} as

$$-\Delta p^{\mathrm{SB}} = \mu h^{\mathrm{SB}} + \rho\Delta\Phi^{\mathrm{SB}} - \rho(\phi^c)^{\mathrm{SB}}, \tag{4.73}$$

and from the boundary condition for the perturbed gravitational potential (4.49) we find that at the surface,

$$\Delta\Phi^{\mathrm{SB}}(R) = \frac{8\pi G\rho R}{15}((\eta_r')^{\mathrm{SA}}(R) + U(R))P_2(\cos\theta), \tag{4.74}$$

where we have made the split $\eta'^{\mathrm{SB}} = \eta'^{\mathrm{SA}} + \xi'^{\mathrm{AB}}$. The first term $(\eta_r')^{\mathrm{SA}}(R)$ is just the radial displacement at the surface of a completely fluid star, which we have already found in Section 4.3 to be

$$(\eta_r')^{\mathrm{SA}}(R) = -\frac{5\Omega_A^2 R}{8\pi G\rho}. \tag{4.75}$$

Substituting this in along with the form of U^{AB} at the surface (4.70) gives

$$\Delta\Phi^{\mathrm{SB}}(R) = \left(\frac{8\pi G\rho R^4}{63}H_2 - \frac{\Omega_A^2 R^2}{3}\right)P_2(\cos\theta). \tag{4.76}$$

Inserting this and the centrifugal potential $(\phi^c)^{\mathrm{SB}}$ (4.35) back into our expression for Δp^{SB} (4.73), we have

$$\begin{aligned}-\Delta p(R) = \left[\mu H_2 R^2 + \left(\frac{8\pi G\rho R^4}{63}H_2 - \frac{\Omega_A^2 R^2}{3}\right)P_2(\cos\theta) + \frac{\rho\Omega^2 R^2}{3}\right]P_2(\cos\theta)\\ +\mu H_0 - \frac{\rho\Omega^2 R^2}{3}.\end{aligned} \tag{4.77}$$

Finally, we can then put this back into the rr condition (4.53). Comparing constant terms, we have

$$\mu H_0 = \frac{\rho\Omega^2 R^2}{3}, \tag{4.78}$$

while comparing terms proportional to $P_2(\cos\theta)$ gives

$$\frac{19\mu H_2}{21}R^2 + \frac{8\pi G\rho R^4}{63}H_2 - \frac{\Omega_A^2 R^2}{3} + \frac{\rho\Omega^2 R^2}{3} = 0. \tag{4.79}$$

Rearranging,

$$H_2 = \frac{21\rho(\Omega_A^2 - \Omega^2)}{57\mu + 8\pi G\rho^2 R^2}. \tag{4.80}$$

4.4.4 Results

At this point, it will be helpful to simplify our expressions by introducing some more concise notation, writing

$$\lambda = \frac{5}{8\pi G\rho} \tag{4.81}$$

and

$$b = \frac{57\mu}{8\pi G\rho^2 R^2}. \tag{4.82}$$

The parameter b gives the ratio of the strain energy to the gravitational energy of the star [16]. This is $b = \frac{B}{A}$ in the notation we have used in Chapter 3. In terms of these parameters H_2 (4.80) is

$$H_2 = -\frac{21}{5R^2}\frac{\lambda}{1+b}(\Omega^2 - \Omega_A^2). \tag{4.83}$$

4.4.4.1 Displacement field and surface shape of the star

We can now find the displacement field: U^{AB} (4.70) and V^{AB} (4.71) become

$$U^{\mathrm{AB}}(r) = \frac{1}{5R^2}\frac{\lambda}{1+b}(\Omega^2 - \Omega_A^2)\left(3r^3 - 8R^2 r\right), \tag{4.84}$$

$$V^{\mathrm{AB}}(r) = \frac{1}{5R^2}\frac{\lambda}{1+b}(\Omega^2 - \Omega_A^2)\left(\frac{5}{2}r^4 - 4R^2 r^2\right). \tag{4.85}$$

At the surface

$$U_r^{\mathrm{AB}}(R) = -\lambda R\frac{\Omega^2 - \Omega_A^2}{1+b}. \tag{4.86}$$

To find the surface shape of Star B we can then add this surface displacement to that already calculated for the fluid star, (4.26):

$$\left(\eta^{\mathrm{SB}}\right)^r(R) = \left(\eta^r\right)^{\mathrm{SA}}(R) + \left(\eta^{\mathrm{AB}}\right)^r(R). \tag{4.87}$$

Rewriting the fluid star displacement as

$$\left(\eta^r\right)^{\mathrm{SA}}(R) = -\lambda R\Omega_A^2 P_2(\cos\theta), \tag{4.88}$$

we find that that the surface shape of the strained star is

$$(\eta^r)^{\mathrm{SB}}(R) = -\lambda R \frac{\Omega^2 + b\Omega_A^2}{1+b} P_2(\cos\theta). \tag{4.89}$$

If we take the special case where the elastic star is relaxed at zero spin and currently spinning at angular velocity Ω, it will have surface shape

$$\eta^r_{\mathrm{el}}(R) = -\lambda R \frac{\Omega^2}{1+b} P_2(\cos\theta). \tag{4.90}$$

Comparing with a fluid star also spinning at Ω using (4.88), the ratio of surface displacements is

$$\frac{\eta^r_{\mathrm{el}}(R)}{\eta^r_{\mathrm{fluid}}(R)} = \frac{1}{1+b}, \tag{4.91}$$

which can be written as

$$\frac{\eta^r_{\mathrm{el}}}{\eta^r_{\mathrm{fluid}}} = \frac{1}{1+\frac{19\mu}{2\rho g R}}, \tag{4.92}$$

where $g = \left[\frac{d\Phi}{dr}\right]_{r=R} = \frac{4}{3}G\rho R$. This result is quoted in Love [52]. This is a smaller deformation than for a fluid star, as expected given that the elastic star will resist a deformation of its shape from its relaxed state.

4.4.4.2 The perturbed gravitational potential

We can also find the scalar quantities associated with the displacement field ξ^{AB}: the perturbed gravitational potential $\delta\Phi^{\mathrm{AB}}$ and the perturbed pressure p^{AB}. Starting with $\delta\Phi^{\mathrm{AB}}$, we have already found $\delta\Phi^{\mathrm{SB}}$ in terms of η'^{SB} (4.48):

$$\delta\Phi^{\mathrm{SB}} = -\frac{4\pi G\rho}{5R}((\eta'_r)^{\mathrm{SA}}(R) + U^{\mathrm{AB}}(R))r^2 P_2(\cos\theta) \tag{4.93}$$

Substituting in $(\eta'_r)^{\mathrm{SA}}(R)$ (4.88) and U^{AB} (4.86) we get

$$\delta\Phi^{\mathrm{SB}} = -\frac{4\pi G\rho}{5}\lambda \frac{\Omega^2 + b\Omega_A^2}{1+b} r^2 P_2(\cos\theta), \tag{4.94}$$

which using the definition of λ (4.81) becomes

$$\delta\Phi^{\mathrm{SB}} = \frac{1}{2}\frac{\Omega^2 + b\Omega_A^2}{1+b} r^2 P_2(\cos\theta). \tag{4.95}$$

We can then find $\delta\Phi^{\mathrm{AB}} = \delta\Phi^{\mathrm{SB}} - \delta\Phi^{\mathrm{SA}}$. Here $\delta\Phi^{\mathrm{SA}}$ is the perturbation for a fluid star (4.25), so that

$$\delta\Phi^{\mathrm{AB}} = \frac{1}{2}\frac{\Omega_A^2 - \Omega^2}{1+b} r^2 P_2(\cos\theta). \tag{4.96}$$

4.4.4.3 The perturbed pressure

Next we find the pressure perturbations δp^{SB} and δp^{AB}. Starting from our expression for h^{SB} (4.55), we know that

$$\delta p^{\mathrm{SB}} = -\mu(H_0 + H_2 r^2 P_2(\cos\theta)) - \rho\delta\Phi^{\mathrm{SB}} + \rho(\phi^c)^{\mathrm{SB}}. \tag{4.97}$$

Inserting in H_0 (4.78), H_2 (4.83), and $(\phi^c)^{\mathrm{SB}}$ (4.35),

$$\delta p^{\mathrm{SB}} = -\frac{\rho\Omega^2 R^2}{3} + \mu\frac{21}{5R^2}\frac{\lambda}{1+b}(\Omega^2 - \Omega_A^2) r^2 P_2(\cos\theta)) - \rho\delta\Phi^{\mathrm{SB}} + \rho\frac{\Omega^2 r^2}{3}\left(1 - P_2(\cos\theta)\right). \tag{4.98}$$

Finally, substituting in $\delta\Phi^{\mathrm{SB}}$ (4.95) and rearranging we have

$$\delta p^{\mathrm{SB}} = \left[\mu\frac{21}{5R^2}\frac{\lambda}{1+b}(\Omega^2 - \Omega_A^2) - \rho\frac{1}{2}\frac{\Omega^2 + b\Omega_A^2}{1+b} - \rho\frac{\Omega^2}{3}\right] r^2 P_2(\cos\theta) + \frac{\rho\Omega^2}{3}(r^2 - R^2). \tag{4.99}$$

Finally we can find δp^{AB} by subtracting the value δp^{SA} (4.24):

$$\delta p^{\mathrm{AB}} = \left[\frac{21\mu}{5R^2}\frac{\lambda}{1+b}(\Omega^2 - \Omega_A^2) + \frac{\rho}{2}\frac{\Omega^2 + b\Omega_A^2}{1+b} - \frac{\rho\Omega^2}{3} - \frac{5\rho\Omega_A^2}{6}\right] r^2 P_2(\cos\theta) + \frac{\rho\Omega^2 - \Omega_A^2}{3}(r^2 - R^2). \tag{4.100}$$

4.4.4.4 Summary

These results will be used to find initial data for our starquake toy model, so we will collect together the most important ones here. The initial data will consist of a displacement field between the star immediately after the glitch and the new equilibrium state after the glitch. This will be built using the displacement field

$$\xi^{\mathrm{AB}} = U^{\mathrm{AB}} P_2(\cos\theta)\boldsymbol{e}_r + V^{\mathrm{AB}}\boldsymbol{\nabla} P_2, \tag{4.101}$$

where

$$U^{\mathrm{AB}}(r) = \frac{1}{5R^2}\frac{\lambda}{1+b}(\Omega^2 - \Omega_A^2)\left(3r^3 - 8R^2 r\right), \tag{4.102}$$

$$V^{\mathrm{AB}}(r) = \frac{1}{5R^2}\frac{\lambda}{1+b}(\Omega^2 - \Omega_A^2)\left(\frac{5}{2}r^4 - 4R^2 r^2\right). \tag{4.103}$$

The corresponding scalar perturbations are

$$\delta\Phi^{\mathrm{AB}} = \frac{1}{2}\frac{\Omega_A^2 - \Omega^2}{1+b} r^2 P_2(\cos\theta), \tag{4.104}$$

$$\begin{aligned}\delta p^{\mathrm{AB}} = \left[\frac{21\mu}{5R^2}\frac{\lambda}{1+b}(\Omega^2 - \Omega_A^2) + \frac{\rho}{2}\frac{\Omega^2 + b\Omega_A^2}{1+b} - \frac{\rho\Omega^2}{3} - \frac{5\rho\Omega_A^2}{6}\right] r^2 P_2(\cos\theta) \\ + \frac{\rho\Omega^2 - \Omega_A^2}{3}(r^2 - R^2).\end{aligned} \tag{4.105}$$

We also have the surface shape of the star,

$$(\eta^r)^{\mathrm{SB}}(R) = -\lambda R\frac{\Omega^2 + b\Omega_A^2}{1+b} P_2(\cos\theta). \tag{4.106}$$

Chapter 5

Oscillation modes of fluid and elastic stars

To find out which oscillation modes are excited in our glitch model, we will first have to calculate the full spectrum of modes of our star after the glitch. This is Star D of the model, a solid, rotating, incompressible elastic star.

In this chapter, we will neglect rotation, returning to consider its effects in Chapter 8, and concentrate on calculating the influence of elasticity on the mode spectrum.

After giving a brief introduction to oscillation modes, we will give a general discussion of radial modes in a fluid star, along with an analytic example of this type of mode. As a build-up to the elastic problem, we will then discuss the oscillations of an incompressible fluid star. These have one type of mode, the 'Kelvin mode', which corresponds to the f-mode of a more general fluid model. Finally, we will study the oscillations of a completely solid, elastic incompressible star. This problem was first studied analytically in 1898 by Bromwich [19]; we will follow this analysis and then investigate further numerically in the case of the $l = 2$ eigenfunctions, the ones most interesting for our glitch model. This will allow us to understand the spectrum of eigenvalues in more depth and to calculate the corresponding eigenfunctions.

5.1 Introduction

A star that is briefly disturbed from equilibrium will oscillate with a characteristic set of vibration patterns, analogous to those produced by hitting a drum. The wave pattern and frequency of these oscillations depends sensitively on the force that is working to restore the displaced elements of the star to their equilibrium positions. This means that stellar oscillations can be an extremely useful probe of the physics of the interior of a star.

The simplest types of oscillation are the purely radial pulsation modes. The more complicated nonradial modes are classified by the main type of restoring force acting on the star. In a system as complex as a neutron star, there are many possible restoring forces, leading to a rich spectrum of oscillation modes.

In a non-rotating fluid star, the restoring forces arise from the fluid pressure and from the gravitational field. Cowling [24] classified the nonradial oscillations of a polytropic fluid star into high-frequency, predominantly radial *p-modes* sourced mainly by the pressure force, and lower frequency, predominantly tangential *g-modes* sourced by the gravitational field. The fundamental mode, known as the *f-mode*, has a frequency intermediate between these two classes. Cowling's classification has been retained for more general stellar models with similar qualitative features [26].

An elastic material like the neutron star crust can support new classes of modes restored by shearing forces. A arbitrary displacement vector $\boldsymbol{\xi}$ can be decomposed into a part of the form $U(r)\boldsymbol{e}_r + V(r)\boldsymbol{\nabla} Y_{lm}$ and a second part of the form $W(r)(\boldsymbol{e}_r \times \boldsymbol{\nabla} Y_{lm})$, where the Y_{lm} are spherical harmonics. Oscillation modes with eigenfunctions of the first type are known as *spheroidal* (or *polar*) modes, and those of the second type are *toroidal* (or *axial* or *torsional*) modes [83].

Toroidal modes produce a 'twisting' motion confined to concentric spheres of the star; this kind of pure shearing motion cannot be supported by a non-rotating fluid star. The fluid p-, g- and f-modes all belong to the category of spheroidal modes. In the elastic crust there can also be new classes of spheroidal modes, which have been labelled *s-modes* and *i-modes* [59]. The s-modes are shear-dominated and affect the whole crust, while i-modes are interfacial modes concentrated mainly at the fluid-elastic boundary.

We will discuss oscillations of fluid and elastic stars further in this chapter, using simplified analytic models as illustration. Neutron stars can also support several other types of oscillations. For us, the most important will be those produced by rotation of the star, which are restored by the Coriolis force. These *inertial modes* include a purely toroidal subclass which have been labelled *r-modes* [66], in analogy with the Rossby ocean waves produced by the Earth's rotation. We will discuss modes of a rotating star further in Chapter 8, when we introduce rotation into our glitch model.

5.2 Oscillation modes in a fluid star

We will start by deriving the equations for small perturbations of a background fluid star. The background star will be assumed to be in hydrostatic equilibrium with pressure P, density ρ and gravitational potential Φ:

$$\nabla_i P + \rho \nabla_i \Phi = 0. \tag{5.1}$$

We assume that the star has a barotropic equation of state

$$P = P(\rho). \tag{5.2}$$

Following the method of the discussion in Shapiro and Teukolsky [76], we will make Lagrangian perturbations to the background quantities, obtaining

$$\Delta\left(\rho\frac{dv^i}{dt} + \nabla_i P + \rho\nabla_i\Phi\right) = 0. \tag{5.3}$$

The perturbed equation of state will be

$$\frac{\Delta P}{P} = \Gamma_1\frac{\Delta\rho}{\rho}, \tag{5.4}$$

where

$$\Gamma_1 = \frac{d(\log P)}{d(\log\rho)} \tag{5.5}$$

is the adiabatic index for the perturbations. This may be different to the adiabatic index Γ of the background star. To find oscillation modes we will assume a time dependence $\xi(r,t) = \xi(r)\cos(\omega t + \theta)$ in our force equation, and also use the relation $\Delta\frac{dv^i}{dt} = \frac{d^2\xi^i}{dt^2}$, so that

$$-\omega^2\rho\xi_i = -\Delta\left(\nabla_i P + \rho\nabla_i\Phi\right). \tag{5.6}$$

The right hand side can be expanded with the commutation relation

$$\Delta\nabla_i = \nabla_i\Delta - (\nabla_i\xi^j)\nabla_j. \tag{5.7}$$

Using this, and simplifying the result with the hydrostatic equilibrium equation (5.1), we obtain

$$-\omega^2\rho\xi_i = -\nabla_i\Delta P + \frac{\Delta\rho}{\rho}\nabla_i P - \rho\nabla_i\Delta\Phi. \tag{5.8}$$

It will be useful for us to rewrite this equation so that all terms are expressed only in terms of the unperturbed variables P and Φ, and the displacement ξ_i. From conservation of mass we have that $\frac{\Delta\rho}{\rho} = -\nabla_i\xi^i$, and by using this along with the equation of state (5.4) for the perturbations we can rewrite ΔP and $\Delta\rho$ in terms of the displacement ξ^i. Finally, we can expand the last term in terms of the Eulerian perturbation $\delta\Phi$. Putting these together we have

$$-\omega^2\rho\xi_i = \nabla_i\left(\Gamma_1 P\nabla_j\xi^j\right) - (\nabla_j\xi^j)\nabla_i P + (\nabla_i\xi^j)\nabla_j P - \rho\nabla_i\delta\Phi - \rho\xi^j(\nabla_i\nabla_j\Phi). \quad (5.9)$$

The gravitational perturbation $\delta\Phi$ can also be written in terms of ξ^i if required, as a solution of Poisson's equation

$$\delta\Phi = -G\int\frac{\nabla'_i(\rho'\xi'^i)}{|x^i - x'^i|}d^3x'. \quad (5.10)$$

5.3 Radial perturbations

In this section we will concentrate on purely radial perturbations $\xi(r)$. Although not directly useful for the case of gravitational wave emission, this simpler case will be useful for later reference, in particular for understanding how to project initial data against our mode spectrum. For these radial perturbations our equation (5.9) above simplifies to become

$$-\omega^2\rho\xi = \frac{d}{dr}\left(\Gamma_1 P\frac{1}{r^2}\frac{d}{dr}(r^2\xi)\right) - \frac{4}{r}\frac{dP}{dr}\xi - \rho\frac{d\Phi}{dr} - \rho\xi(\nabla^2\Phi). \quad (5.11)$$

In this section, we will again follow the method of Shapiro and Teukolsky [76]. The last term can be rewritten using Poisson's equation $\nabla^2\Phi = 4\pi G\rho$. We can also integrate Poisson's equation for the perturbations, $\nabla^2\delta\Phi = -4\pi G\rho\nabla_i\xi^i$, to find that the last two terms cancel, leaving

$$\frac{d}{dr}\left(\Gamma_1 P\frac{1}{r^2}\frac{d}{dr}(r^2\xi)\right) - \frac{4}{r}\frac{dP}{dr}\xi + \omega^2\rho\xi = 0. \quad (5.12)$$

The boundary conditions for this system are

1. $\xi = 0$ at the centre $r = 0$,
2. $\Delta P = 0$ at the surface, i.e. fluid elements at the surface of the unperturbed star stay at the surface. We can see from our equation of state (5.4) for the perturbations that $\Delta P = -\Gamma_1\xi^i\,\nabla_i P$. Since P also vanishes at the surface, it is sufficient to demand that ξ is finite at $r = R$.

5.3.1 The homogeneous background star

A useful special case that can be solved analytically is when the background star is homogeneous (the density ρ is constant). We have already used this as a background

model in Chapter 4, where we found the pressure P (4.4) and gravitational potential Φ (4.3).

5.3.1.1 Perturbing the background

To find the eigenfunctions $\xi(r)$ of this system, we can substitute the background pressure (4.4) back into the radial perturbation equation (5.12) that we derived earlier. Following [76], we will then change variables in our radial equation (5.12), so that

$$\left(1-x^2\right)\xi'' + \left(\frac{2}{x} - 4x\right)\xi' + \left(A - \frac{2}{x^2}\right)\xi = 0, \tag{5.13}$$

with $x = \frac{r}{R}$, $' = \frac{d}{dx}$, $A = \frac{3\omega^2}{2\pi G\rho\Gamma_1} + \frac{8}{\Gamma_1} - 2$. Our boundary conditions then become

$$\xi(0) = 0, \tag{5.14}$$

$$\xi(1) \text{ finite.} \tag{5.15}$$

We look for a series solution and find that the acceptable solutions finite at the centre are polynomials of the form

$$\xi_n = \sum_{i=0}^{n} c_i x^{i+1}, \tag{5.16}$$

with odd coefficients zero, and even coefficients satisfying

$$\frac{c_{i+2}}{c_i} = \frac{i^2+5i+4-A}{i^2+7i+10}. \tag{5.17}$$

To satisfy the second boundary condition this series must terminate, so

$$A = n^2 + 5n + 4, \quad n = 0, 2, 4\ldots \tag{5.18}$$

Eigenfrequencies ω can then be calculated from A. The first five eigenfunctions ξ_n are plotted in Figure 5.1, with normalisation chosen so that $\xi(1) = 1$.

We will use these eigenfunctions again for a simple model of mode excitation in Section 6.3.

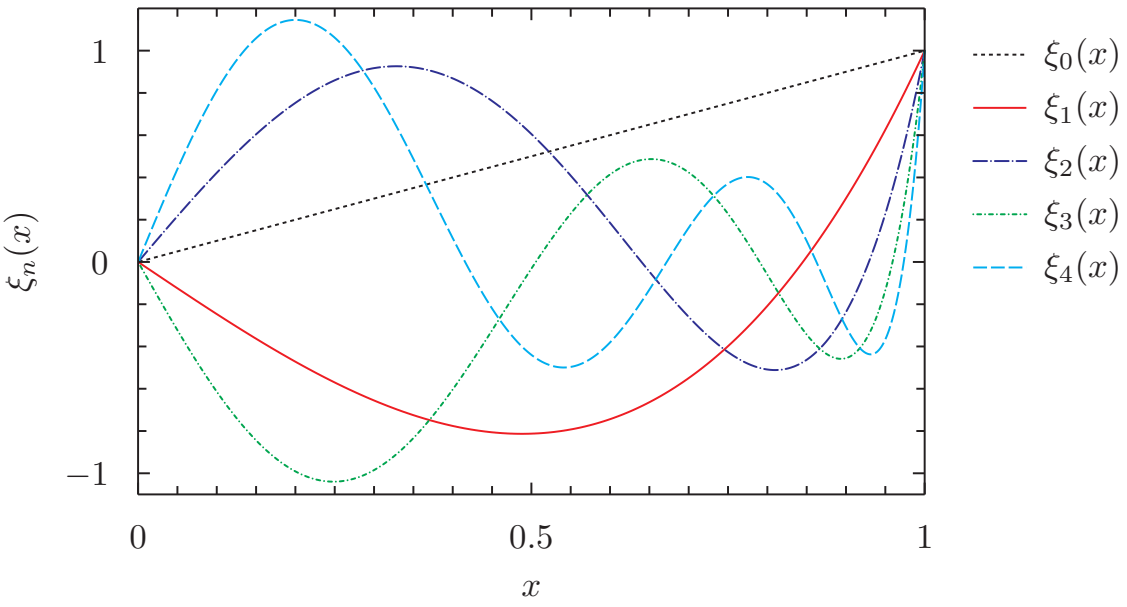

Figure 5.1: The first five eigenfunctions for the compressible radial perturbations of a homogeneous star. The amplitude of each eigenfunction is plotted against the normalised radial coordinate $x = \frac{r}{R}$.

5.4 Nonradial modes for an incompressible fluid star

The oscillation modes of a homogeneous, incompressible fluid star were first found by Kelvin in 1863 [82]. Although this is not a very realistic stellar model, it is of interest because the frequencies and associated eigenfunctions can be calculated analytically. This will make it a good testbed for many of the problems we will want to investigate in later chapters, including working out which modes are excited by glitch initial data, and studying the possibilities for gravitational wave emission.

We have already found the pressure p (4.4) and gravitational potential Φ (4.3) of an incompressible fluid star. We will now make *incompressible* perturbations to this background configuration, rather than the compressible radial perturbations of the last section. These incompressible perturbations will have to be non-radial.

As in Chapter (4), we will make Eulerian perturbations δp, $\delta\Phi$, $\delta\rho$ to the background quantities. We have already found the form (4.13) of the perturbed gravitational potential, as well as the boundary conditions (4.18) it satisfies at the surface. For convenience we repeat them here:

$$\delta\Phi^{\text{int}}(r,\theta,\phi) = \sum_{l=0}^{\infty}\sum_{m=-l}^{l} B_{lm}\, r^l Y_{lm}(\theta,\phi), \tag{5.19}$$

$$-\sum_{l=0}^{\infty}\sum_{m=-l}^{l}(2l+1)B_{lm}R^{l-1}Y_{lm} = 4\pi G\rho\xi_r(R,\theta,\phi). \tag{5.20}$$

We also know the form (4.11) taken by the density perturbation $\delta\rho$:

$$\delta\rho = \rho\delta(r-R)\xi^r. \tag{5.21}$$

Making Eulerian perturbations to the background equations of hydrostatic equilibrium yields the force equation

$$\frac{d^2\xi_i}{dt^2} = -\frac{1}{\rho}\nabla_i(\delta p) - \nabla_i\delta\Phi. \tag{5.22}$$

To find the allowable modes we again look for displacements with time-dependence $\xi^i(r,\theta,\phi,t) = \xi^i(r,\theta,\phi)e^{-i\omega t}$, so that $\frac{d^2\xi^i}{dt^2} = -\omega^2\xi^i$. We then take the divergence of our force equation (5.22), remembering that for an incompressible fluid $\nabla_i\xi^i = 0$ so that

$$\nabla^2\delta p = 0 \tag{5.23}$$

inside the star. This has solutions

$$\delta p(r,\theta,\phi) = \sum_{l=0}^{\infty}\sum_{m=-l}^{l}A_{lm}r^lY_{lm}(\theta,\phi), \tag{5.24}$$

where the A_{lm} are arbitrary constants representing the amplitudes of the perturbations, and the Y_{lm} are the normalised spherical harmonic functions as defined in, for example, Arfken [11].

We also have a boundary condition for the pressure perturbation, which is that the Lagrangian perturbation vanishes at the surface. Substituting in the Eulerian pressure perturbation δp (5.24) and the background pressure p (4.4) gives

$$A_{lm}R^lY_{lm} - \frac{4\pi}{3}G\rho^2R\xi^r(R,\theta,\phi) = 0. \tag{5.25}$$

Finally these last two equations give us a relation between the constants A_{lm} and B_{lm},

$$B_{lm} = -\frac{3}{\rho(2l+1)}A_{lm}, \tag{5.26}$$

and so $\delta\Phi^{\text{int}}$ can be written as

$$\delta\Phi^{\text{int}} = \sum_{l=0}^{\infty}\sum_{m=-l}^{l}-\frac{3A_{lm}}{\rho(2l+1)}r^lY_{lm}, \tag{5.27}$$

which is our final form for the perturbed gravitational potential.

5.4.0.2 Finding the oscillation modes

Now that we have the perturbed quantities δp (5.24) and $\delta\Phi$ (5.27) expressed in terms of the single set of coefficients A_{lm}, we can substitute them back into the force equation (5.22) to find that the displacement vector ξ^i satisfies

$$\xi_i = \sum_{l=0}^{\infty} \sum_{m=-l}^{l} \frac{2(l-1)}{2l+1} \frac{A_{lm}}{\rho\omega^2} \nabla_i (r^l Y_{lm}). \tag{5.28}$$

Finally, we can cancel factors of A_{lm} in our force equation finding that the only allowable oscillation modes ω satisfy

$$\omega^2 = \frac{8\pi G\rho}{3} \frac{l(l-1)}{2l+1}. \tag{5.29}$$

This is the result that Kelvin derived in 1863. In the cases $l = 0$ and $l = 1$ we can see that the frequency is zero.

We can also show that the Lagrangian perturbation of the pressure as well as the density is zero for this class of modes. We assumed that this was the case at the surface, but by substituting the displacement vector (5.28) and pressure perturbation (5.24) into $\Delta p = \delta p + \xi^i \nabla_i p$, we can see that

$$\Delta p = 0 \tag{5.30}$$

holds throughout the star.

For representative neutron star parameters (mass $1.4 M_\odot$, radius 10 km) the lowest, $l = 2$ mode has a frequency of around 2kHz.

5.5 Oscillations of an incompressible elastic star: analytic work

We will now introduce elasticity to the problem, and calculate the oscillation modes of a solid, incompressible elastic star, following the method of Bromwich [19]. In this case our force equation (5.22) has an extra elastic force term $f_i^{elastic} = \mu \nabla_j \nabla_j \xi_i$ (see the discussion of the rotating elastic star in Section 4.4), so that

$$-\rho\omega^2 \xi_i = -\nabla_i(\delta p) + \mu \nabla_j \nabla_j \xi_i - \rho \nabla_i(\delta\Phi). \tag{5.31}$$

This can be rearranged and written in vector form as

$$(\boldsymbol{\nabla}^2 + k^2)\boldsymbol{\xi} = \frac{1}{\mu}\boldsymbol{\nabla}(\delta p + \rho\delta\Phi), \tag{5.32}$$

where

$$k^2 = \omega^2\frac{\rho}{\mu}. \tag{5.33}$$

This is an inhomogeneous vector Helmholtz equation, and we will start by solving this to find the form of the eigenfunctions $\boldsymbol{\xi}$. Later we will impose boundary conditions to find the allowable modes of oscillation.

The background solution is that of the previous fluid problem, with isotropic pressure p and gravitational potential Φ as derived in (4.4) and (4.3) respectively. As with the fluid star, the gravitational potential perturbation $\delta\Phi$ satisfies Laplace's equation. We will specialise to axisymmetric solutions here, because the rotation shape of the star is axisymmetric, and so

$$\delta\Phi = \sum_{l=0}^{\infty} B_l r^l P_l(\cos\theta), \tag{5.34}$$

inside the star, where B_l are constants. To simplify expressions, summation over l will be implied in the rest of this section.

5.5.1 Finding the eigenfunctions

The solution to the Helmholtz equation (5.32) will have the form $\boldsymbol{\xi} = \boldsymbol{\xi}_c + \boldsymbol{\xi}_p$, where $\boldsymbol{\xi}_c$ is the complementary solution satisfying the homogeneous equation

$$(\boldsymbol{\nabla}^2 + k^2)\boldsymbol{\xi}_c = 0, \tag{5.35}$$

and $\boldsymbol{\xi}_p$ is the particular solution for the full inhomogeneous equation.

5.5.1.1 Complementary solution

The solution to the homogeneous equation can be split into three parts

$$\boldsymbol{\xi}_c = \boldsymbol{\xi}_1 + \boldsymbol{\xi}_2 + \boldsymbol{\xi}_3, \tag{5.36}$$

where

$$\boldsymbol{\xi}_1 = \boldsymbol{\nabla}\varphi, \tag{5.37}$$

$$\boldsymbol{\xi}_2 = \boldsymbol{\nabla} \times (\chi \mathbf{c}), \tag{5.38}$$

$$\boldsymbol{\xi}_3 = \frac{1}{k}\boldsymbol{\nabla} \times \boldsymbol{\xi}_2, \tag{5.39}$$

with φ and χ solutions of the scalar Helmholtz equation, and $\mathbf{c}$ a constant vector we will choose below to suit our problem [45].

In an incompressible star, these vectors $\boldsymbol{\xi}$ must be divergence free. This is satisfied automatically by $\boldsymbol{\xi}_2$ and $\boldsymbol{\xi}_3$, whereas $\boldsymbol{\xi}_1$ must obey $\boldsymbol{\nabla} \cdot \boldsymbol{\xi}_1 = \nabla^2\varphi = 0$. Substituting this into the Helmholtz equation, we see that $\boldsymbol{\xi}_1 = 0$.

To satisfy the scalar Helmholtz equation, we choose

$$\chi = D j_l(kr) P_l(\cos\theta), \tag{5.40}$$

where $j_l(x)$ is a spherical Bessel function and P_l is a Legendre polynomial as before. We can see that $\boldsymbol{\xi}_2$ is then a solution of the vector Helmholtz equation because

$$(\boldsymbol{\nabla}^2 + k^2)\boldsymbol{\xi}_2 = (\boldsymbol{\nabla}^2 + k^2)\boldsymbol{\nabla} \times (\chi\mathbf{c}) = \boldsymbol{\nabla} \times \left[\mathbf{c}(\nabla^2\chi + k^2\chi)\right], \tag{5.41}$$

and so $\boldsymbol{\xi}_2$ satisfies the vector Helmholtz equation if χ satisfies the scalar one. This can also be shown in a similar way for $\boldsymbol{\xi}_3$.

We will choose the constant $\mathbf{c}$ by looking at the surface boundary conditions. One of our conditions is that the tangential components of the surface strain vanish at $r = R$. It will be useful to pick $\mathbf{c}$ so that $\boldsymbol{\xi}_2$ and $\boldsymbol{\xi}_3$ are tangential to the surface, so we take $\mathbf{c} = r\mathbf{e}_r$.

We can now write $\boldsymbol{\xi}_2$ and $\boldsymbol{\xi}_3$ directly in terms of χ. We have

$$\boldsymbol{\xi}_2 = -Dr j_l(kr)(\mathbf{e}_r \times \boldsymbol{\nabla} P_l). \tag{5.42}$$

From this we can find that

$$\boldsymbol{\xi}_3 = \frac{l(l+1)}{r}\frac{1}{k} D j_l(kr) P_l \mathbf{e}_r + \left(\frac{1}{k} D j_l(kr) + D r j_l'(kr)\right)\boldsymbol{\nabla} P_l, \tag{5.43}$$

where we have used the identities

$$\mathbf{e}_r \times (\mathbf{e}_r \times \boldsymbol{\nabla} P_l) = -\boldsymbol{\nabla} P_l \tag{5.44}$$

and

$$\boldsymbol{\nabla} \times (\mathbf{e}_r \times \boldsymbol{\nabla} P_l) = -\frac{l(l+1)}{r^2} P_l \mathbf{e}_r. \tag{5.45}$$

5.5.1.2 Particular solution

We can show that the particular solution must have the form $\boldsymbol{\xi}_p = \boldsymbol{\nabla}\Psi$ for some scalar Ψ by taking the curl of the force equation (5.32). We find that

$$(\boldsymbol{\nabla}^2 + k^2)(\boldsymbol{\nabla} \times \boldsymbol{\xi}_p) = \frac{1}{\mu} \boldsymbol{\nabla} \times \boldsymbol{\nabla}(\delta p + \rho \delta \Phi) = 0, \tag{5.46}$$

so $\boldsymbol{\nabla} \times \boldsymbol{\xi}_p = 0$ and and $\boldsymbol{\xi}_p$ can be written as $\boldsymbol{\xi}_p = \boldsymbol{\nabla}\Psi$. This means that Ψ satisfies Laplace's equation $\nabla^2 \Psi = 0$, with general solution

$$\Psi = C r^l P_l(\cos\theta), \tag{5.47}$$

and so

$$\boldsymbol{\xi}_p = l C r^{l-1} P_l \mathbf{e}_r + C r^l \boldsymbol{\nabla} P_l. \tag{5.48}$$

We can also use this to find an expression for δp and $\delta\Phi$. Substituting the form of $\boldsymbol{\xi}_p$ back into the force equation (5.32), we then find that

$$\boldsymbol{\nabla}\Psi = \frac{1}{k^2 \mu} (\delta p + \rho \delta \Phi). \tag{5.49}$$

Integrating,

$$\frac{1}{\rho \omega^2} (\delta p + \rho \delta \Phi) = C r^l P_l(\cos\theta), \tag{5.50}$$

where the integration constant has been found to be zero by evaluating the expression at $r = 0$.

5.5.2 Finding the oscillation modes

We will search for spheroidal and toroidal modes separately, so before imposing boundary conditions it will be helpful to split $\boldsymbol{\xi}$ into these parts:

$$\boldsymbol{\xi}^{\text{spheroidal}} = U(r)\mathbf{e}_r + V(r)\boldsymbol{\nabla} P_l, \tag{5.51}$$

$$\boldsymbol{\xi}^{\text{toroidal}} = W(r)(\mathbf{e}_r \times \boldsymbol{\nabla} P_l). \tag{5.52}$$

Comparing with our previous expression for $\boldsymbol{\xi}_2$, $\boldsymbol{\xi}_3$ and $\boldsymbol{\xi}_p$ (5.37), we see that the toroidal part only requires $\boldsymbol{\xi}_2$, while the spheroidal part requires $\boldsymbol{\xi}_3 + \boldsymbol{\xi}_p$. Specifically, we have

$$U(r) = lCr^{l-1} + \frac{l(l+1)}{r}\frac{1}{k}Dj_l(kr), \tag{5.53}$$

$$V(r) = Cr^l + \frac{1}{k}Dj_l(kr) + Drj_l'(kr), \tag{5.54}$$

$$W(r) = -Drj_l(kr). \tag{5.55}$$

In spherical coordinate components,

$$\boldsymbol{\xi}^{\text{spheroidal}} = \left[lCr^{l-1} + \frac{l(l+1)}{r}\frac{D}{k}j_l(kr)\right]P_l\mathbf{e}_r + \left[Cr^{l-1} + \frac{D}{kr}j_l(kr) + Dj_l'(kr)\right]\frac{dP_l}{d\theta}\mathbf{e}_\theta. \tag{5.56}$$

and

$$\boldsymbol{\xi}^{\text{toroidal}} = -Dj_l(kr)\mathbf{e}_\phi. \tag{5.57}$$

5.5.2.1 Boundary conditions

We have already derived the necessary boundary conditions in previous sections, but for completeness we restate them here. As with the rotating elastic problem studied in Section 4.4, we have the surface boundary condition (4.72),

$$-\Delta p\delta_{ir} + 2\mu u_{ir} = 0. \tag{5.58}$$

We also have the boundary condition for the gravitational potential at the surface (4.18), derived for the rotating fluid star in Section 4.3:

$$-(2l+1)B_lR^{l-1}P_l = 4\pi G\rho\xi_r(R,\theta,\phi), \tag{5.59}$$

so that

$$\delta\Phi = -\frac{4\pi G\rho}{(2l+1)}\frac{r^l}{R^{l-1}}\xi_r(R). \tag{5.60}$$

5.5.2.2 Finding the toroidal modes

For the toroidal modes we only need the $\boldsymbol{\xi}_2$ vector, which in components is

$$\boldsymbol{\xi}^{\text{toroidal}} = \boldsymbol{\xi}_2 = \begin{pmatrix} 0 \\ 0 \\ -Dj_l(kr)\frac{dP_l}{d\theta} \end{pmatrix}. \tag{5.61}$$

Our boundary condition here reduces to just

$$u_{r\phi}(R) = 0. \tag{5.62}$$

In spherical coordinates,

$$2u_{r\phi} = \frac{1}{r\sin\theta}\frac{\partial \xi_r}{\partial \phi} + \frac{\partial \xi_\phi}{\partial r} - \frac{\xi_\phi}{r}, \tag{5.63}$$

so that at $r = R$,

$$-\frac{\partial}{\partial r}\left(Dj_l(kr)\frac{dP_l}{d\theta}\right) + \frac{1}{r}Dj_l(kr)\frac{dP_l}{d\theta} = 0, \tag{5.64}$$

leading to the boundary condition

$$kRj_l'(kR) - j_l(kR) = 0 \tag{5.65}$$

For any value of l, we can then find the eigenvalues ω_n numerically by finding the roots $K_n = \omega_n\sqrt{\frac{\rho}{\mu}}R$ of the function

$$f_{\text{toroidal}}(K, l) = Kj_l'(K) - j_l(K) = 0. \tag{5.66}$$

5.5.2.3 Finding the spheroidal modes

In constrast to the toroidal modes, where the displacement has no radial component, the spheroidal modes are affected by gravity, which makes them more complicated to analyse. This problem was first studied by Bromwich in 1898 [19], and we shall follow a similar method. In components, the spheroidal displacement field $\boldsymbol{\xi}^{\text{spheroidal}} = \boldsymbol{\xi}_p + \boldsymbol{\xi}_3$ is

$$\boldsymbol{\xi}^{\text{spheroidal}} = \begin{pmatrix} (lCr^{l-1} + \frac{Dl(l+1)}{kr}j_l(kr))P_l \\ (Cr^{l-1} + \frac{D}{kr}(j_l(kr) + krj_l'(kr)))\frac{dP_l}{d\theta} \\ 0 \end{pmatrix}. \tag{5.67}$$

The surface boundary conditions (5.58) are

$$-\Delta p + 2\mu\frac{\partial \xi_r}{\partial r} = 0, \tag{5.68}$$

for the rr component, and

$$r\frac{\partial}{\partial r}\left(\frac{\xi_\theta}{r}\right)+\frac{1}{r}\frac{\partial \xi_r}{\partial \theta}=0 \tag{5.69}$$

for the $r\theta$ condition. It will make the algebra slightly easier if we follow Bromwich in defining

$$\psi_l(x)=x^{-l}j_l(x), \tag{5.70}$$

so that the displacement field (5.67) becomes

$$\boldsymbol{\xi}=\begin{pmatrix} lr^{l-1}[C+D(l+1)\psi_l(kr)]P_l \\ r^{l-1}[C+(D\left(\psi_l(kr)+kr\psi_l'(kr)\right)]\frac{dP_l}{d\theta} \\ 0 \end{pmatrix}. \tag{5.71}$$

Substituting this into the two boundary conditions (5.68) and (5.69), we obtain

$$-\Delta p+2\mu\left[l(l+1)R^{l-2}\left(C+\frac{D}{k}(l+1)\psi_l(kR)\right)P_l+lR^{l-1}((l+1)D\psi_l'(kR))P_l\right]=0, \tag{5.72}$$

$$2C(l-1)+\frac{D}{k}\left[2\left(l^2-1\right)\psi_l(kR)-2kR\psi'(kR)-k^2R^2\psi_l(kR)\right]=0. \tag{5.73}$$

It is also possible to express Δp in terms of C and D, by using the relation between the Eulerian perturbations δp and $\delta\Phi$ (5.50) we obtained while finding the particular solution. Making use of the boundary condition for the gravitational potential (5.59), we find that

$$\Delta p(R,\theta)=-\frac{2l(l-1)}{2l+1}g\rho R^{l-1}\left[C+\frac{D}{k}(l+1)\psi_l(kR)\right]-\rho\omega^2CR^l, \tag{5.74}$$

where

$$g=\frac{4\pi G\rho R}{3}. \tag{5.75}$$

This can then be substituted back into the *(rr)* boundary condition (5.72), and combined with the *(rθ)* boundary condition (5.73) to yield

$$\begin{aligned} 2l(l-1)\left[1+\frac{g\rho R}{\mu(2l+1)}\right]\left(C+(l+1)\frac{D}{k}\psi_l(kR)\right) \\ -k^2R^2C+2Rl(l+1)D\psi'(kR)=0. \end{aligned} \tag{5.76}$$

Again following Bromwich, we simplify this by relabelling

$$Q = \frac{D}{k}\psi_l(kR), \tag{5.77}$$

$$K = kR, \tag{5.78}$$

$$X = \frac{\psi_l'(kR)}{\psi(kR)}, \tag{5.79}$$

$$\theta = \frac{lg\rho R}{\mu(2l+1)}, \tag{5.80}$$

so that the boundary conditions become

$$2(l-1)(l+\theta)\left[C+(l+1)Q\right] - CK^2 + 2l(l+1)XKQ = 0 \tag{5.81}$$

for the rr condition and

$$2(l-1)C + Q\left[2(l^2-1) - 2XK - K^2\right] = 0. \tag{5.82}$$

for the $r\theta$ one. We can then eliminate C and Q to find

$$(l+1)(K+2lX) + \left[l+\theta-\frac{K^2}{2(l-1)}\right](K+2X) = 0. \tag{5.83}$$

Substituting back the original variables, we find that for given l, the eigenvalues are the roots K_{ln} of the equation

$$\begin{aligned} f_{\text{spheroidal}}\left(K, l, \frac{\rho}{\mu}\right) = \left(l + \frac{lgR}{(2l+1)}\left(\frac{\rho}{\mu}\right) - \frac{K^2}{2(l-1)}\right)\left(K + 2\frac{\psi_l'(K)}{\psi_l(K)}\right) \\ +(l+1)\left(K + 2l\frac{\psi_l'(K)}{\psi_l(K)}\right). \end{aligned} \tag{5.84}$$

This can then be solved numerically to find the allowed frequencies $\omega_{ln} = \frac{K_{ln}}{R}\sqrt{\frac{\mu}{\rho}}$.

5.5.3 Finding the spheroidal eigenfunctions

We can also find the eigenfunctions corresponding to these frequencies. To do this, we can use the $r\theta$ condition (5.82) to find a relationship between C and D and so eliminate C from our form (5.87) for the eigenfunctions:

$$C = q_{ln}D, \tag{5.85}$$

where

$$q_{ln} = \frac{1}{2(l-1)R^{l-3}}\left[2j_l'(k_{ln}R) + \left(\frac{2(l^2+l-1)}{k_{ln}R} - k_{ln}R\right)\right] j_l(k_{ln}R). \tag{5.86}$$

Our spheroidal eigenfunctions then become

$$\boldsymbol{\xi}_l^{\text{spheroidal}} = D\left[lq_{ln}r^{l-1} + \frac{l(l+1)}{r}\frac{1}{k_{ln}}j_l(k_{ln}r)\right] P_l\,\mathbf{e}_r + D\left[q_{ln}r^{l-1} + \frac{1}{kr}j_l(k_{ln}r) + j_l'(k_{ln}r)\right]\frac{dP_l}{d\theta}\mathbf{e}_\theta, \tag{5.87}$$

where

$$U_{ln}(x) = D_{ln}\left[lq_{ln}r^{l-1} + \frac{l(l+1)}{r}\frac{1}{k_{ln}}j_l(k_{ln}r)\right] \tag{5.88}$$

$$V_{ln}(x) = D_{ln}\left[q_{ln}r^{l-1} + \frac{1}{kr}j_l(k_{ln}r) + j_l'(k_{ln}r)\right] \tag{5.89}$$

and the $k_{ln} = \sqrt{\frac{\rho}{\mu}}\omega_{ln}$ are the roots of the equation $f_{\text{spheroidal}}\left(x, l, \frac{B}{A}\right)$ (5.84) derived above.

5.5.4 Other perturbed quantities

Using our eigenfunctions $\boldsymbol{\xi}$, we can find the perturbed scalar quantities $\delta\Phi$ and δp. First, we can use the boundary condition on $\delta\Phi$, (5.20), to show that

$$\delta\Phi_{ln} = B_{ln}r^2 P_2(\cos\theta) \tag{5.90}$$

with

$$(2l+1)B_{ln}R^{l-1}P_l(\cos\theta) = 4\pi G\rho(\xi_r)_{ln}(R,\theta,\phi). \tag{5.91}$$

Substituting in the radial part of the spheroidal eigenfunctions (5.87),

$$\delta\Phi_{ln} = \frac{4\pi G\rho}{(2l+1)}D_{ln}\left[lq_{ln} + \frac{l(l+1)}{R^l}\frac{1}{k_{ln}}j_l(k_{ln}R)\right] r^2 P_2(\cos\theta) \tag{5.92}$$

We can also find δp using the relation (5.50) between δp and $\delta\Phi$

$$\delta p_{ln} = \rho\omega_{ln}^2 C r^l P_l(\cos\theta) - \rho\delta\Phi_{ln}, \tag{5.93}$$

so that

$$\delta p_{ln} = D_{ln}\left[\mu k_{ln}^2\, q_{ln} r^l - \frac{4\pi G\rho^2}{(2l+1)}\left(l q_{ln} + \frac{l(l+1)}{R^l}\frac{1}{k_{ln}} j_l(k_{ln}R)\right) r^2\right] P_2(\cos\theta). \quad (5.94)$$

5.6 Oscillations of an incompressible elastic star: numerical investigation

To further investigate the eigenvalue spectrum and associated eigenfunctions, we will need to carry out some of the work numerically. We will find toroidal and spheroidal eigenvalues by finding roots of the nonlinear equations (5.66) and (5.84) in Mathematica. We can then plot the corresponding eigenfunctions by using these eigenvalues in conjunction with the analytic eigenfunction forms (5.57) and (5.87).

For this work we will specialise to the case of $l = 2$, $m = 0$ modes, as these are the ones we find to be excited by our initial data for our first glitch model, where the glitch occurs at zero angular velocity. Obtaining this initial data will be discussed later in Chapter 7, but its $l = 2$ character should already seem plausible given that we will be constructing it using the rotating equililbrium solutions developed in Chapter 4. These have an angular $P_2(\cos\theta)$-dependence which matches that of the $l = 2$ eigenfunctions found in the previous section.

Other values of l become important for rotating stars, but as the $l = 2$ are the most important for our model we will restrict to looking at those here.

In general, we can parametrise our background stars by their radius, density and shear modulus (R, ρ, μ). We can make an arbitrary rescaling of the first two, as the only free parameter in determining the spacing of the eigenvalues (5.84) is the ratio $\frac{\mu}{\rho}$.

For our numerical work we first scale to unit radius, $R = 1$. Instead of rescaling the density ρ directly, we make the more useful physical choice of rescaling the frequencies against a typical mode frequency, the $l = 2$ fundamental Kelvin mode ω_K of a fluid star, which we calculated earlier in Section 5.4. Specialising the result (5.29) to $l = 2$, we have

$$\omega_K = \sqrt{\frac{16\pi}{15}}\sqrt{G\rho}\,. \quad (5.95)$$

We rescale so that $\omega_K = 1$, which is equivalent to fixing ρ. Finally, for comparison with our earlier energy results in Chapter 3, we switch from the ratio of shear modulus to density $\frac{\mu}{\rho}$ to the ratio of strain energy to gravitational energy (4.82),

$$\frac{B}{A} = \frac{57\mu}{8\pi G R^2 \rho^2}. \quad (5.96)$$

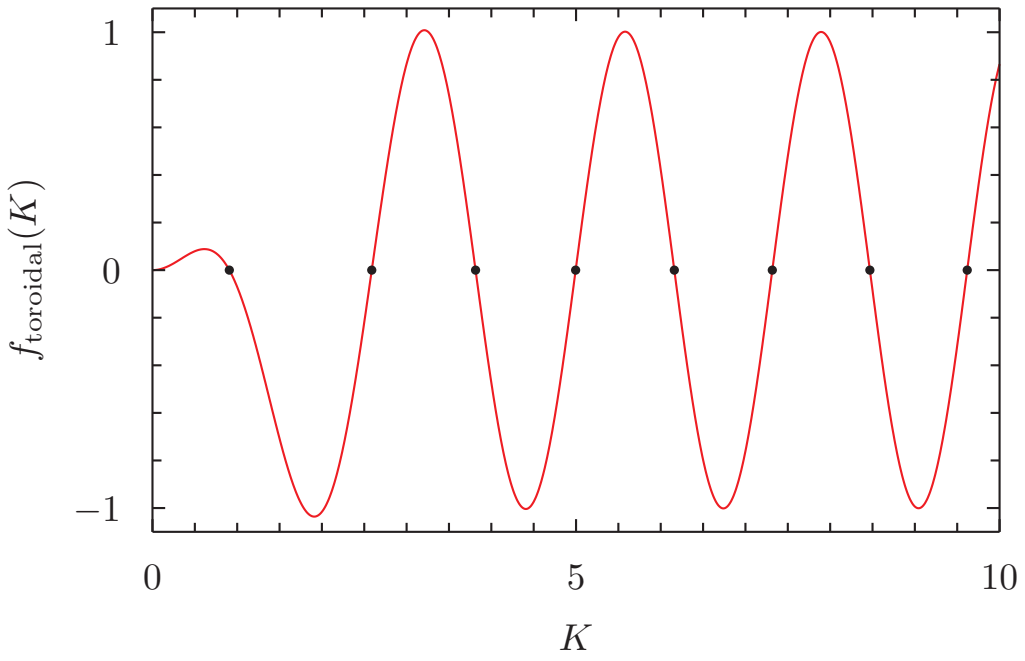

Figure 5.2: A plot of the function f_{toroidal}. The roots of this function (marked as black dots) are the toroidal eigenfrequencies.

Combining this with the scaling choices above, we obtain

$$\frac{\mu}{\rho} = \frac{5\left(\frac{B}{A}\right)}{38}. \tag{5.97}$$

5.6.1 Finding the eigenvalues

5.6.1.1 Toroidal eigenvalues

The toroidal eigenvalues are the roots of the function f_{toroidal} (5.66), which for $l = 2$ becomes

$$f_{\text{toroidal}}(K, 2) = Kj_2'(K) - j_2(K) = 0. \tag{5.98}$$

This function is shown in Figure 5.2. Toroidal modes will not be excited in our initial glitch model, where the star has zero angular velocity after the glitch. However, these will become important later once rotation is taken into consideration, and there is coupling between toroidal and spheroidal modes. The toroidal modes are also simpler to analyse because the roots of f_{toroidal} have no dependence on $\frac{B}{A}$, so they are worth considering first. However, the corresponding frequencies do depend on $\frac{B}{A}$: $\omega_n = K_n\sqrt{\frac{5}{38}\left(\frac{B}{A}\right)}$. We can see that in the fluid limit $B = 0$, these frequencies are zero as expected.

5.6.1.2 Spheroidal eigenvalues

In the $l = 2$ case, the equation we use to find the eigenvalues (5.84) becomes

$$f_{\text{spheroidal}}\left(x, 2, \frac{B}{A}\right) = \left(2 + \frac{4}{95\left(\frac{B}{A}\right)} - \frac{x^2}{2}\right)\left(x + 2\frac{\psi_2'(x)}{\psi_2(x)}\right) + 3\left(x + 4\frac{\psi_2'(x)}{\psi_2(x)}\right), \quad (5.99)$$

where we have scaled to unit radius $R = 1$. We find that the quantity $\frac{\psi_l'(x)}{\psi_l(x)}$ can be expressed in terms of cylindrical Bessel functions $J_l(x)$ as

$$\frac{\psi_l'(x)}{\psi_l(x)} = -\frac{J_{l+\frac{3}{2}}(x)}{J_{l+\frac{1}{2}}(x)}, \quad (5.100)$$

and so f diverges when x is a root of $J_{l+\frac{1}{2}}$. It is therefore easier numerically to find roots of

$$g\left(2, x, \frac{B}{A}\right) = J_{\frac{5}{2}}(x)\, f_{\text{spheroidal}}\left(2, x, \frac{B}{A}\right). \quad (5.101)$$

We carry this out in Mathematica using the external package RootSearch [28]; by plotting these functions in Mathematica we can also verify that finding the roots of g gives us all the roots of f. To interpret the results, we need to convert back from the roots x_n to the frequencies $(\omega_n)^2$. It will also be helpful to scale these to some typical mode frequency. In this case we will use the $l = 2$ fundamental Kelvin mode ω_K of a fluid star, which we calculated earlier in Section 5.4. Specialising the result (5.29) to $l = 2$, we have

$$\omega_K = \sqrt{\frac{16\pi}{15}}\sqrt{G\rho}\,. \quad (5.102)$$

We can then plot the scaled eigenvalues $\frac{\omega^2}{\omega_K^2}$ as a function of $\frac{B}{A}$; the first 30 of these are shown in Figure 5.3. Concentrating on a given value of $\frac{B}{A}$, we can see the start of an infinite set of eigenvalues. The squared frequency ω^2 scales linearly with $\frac{B}{A}$ and hence with the shear modulus μ: this is typical of modes of an elastic solid, which have frequency $\sim \sqrt{\frac{\mu}{\rho}}$.

The exception to this is the behaviour of the modes closest to the fluid Kelvin mode ω_K. Around this value, we see avoided crossings between modes. This is characteristic of systems where two different types of mode have a similar frequency [7]: in this case these are the single fluid-like mode close to the Kelvin mode frequency, and one of the elastic modes of the star.

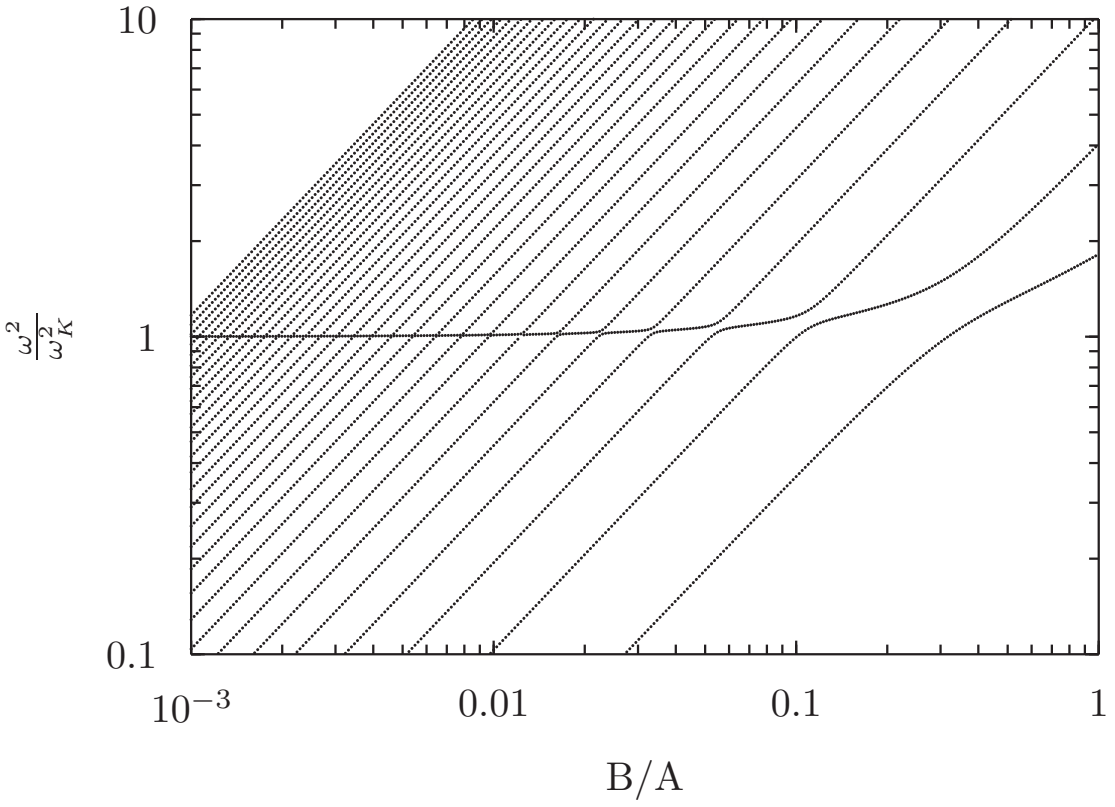

Figure 5.3: Plot showing how the $l = 2$ mode frequencies of an incompressible elastic star vary with the ratio of elastic to gravitational energy $\frac{B}{A}$. On the y-axis, frequencies are scaled by the fundamental $l = 2$ Kelvin mode of an incompressible fluid star, ω_K. For typical neutron star parameters, $\omega_K \sim 2000$ Hz.

5.6.2 Finding the eigenfunctions

5.6.2.1 Toroidal eigenfunctions

These functions have the form (5.52)

$$\boldsymbol{\xi}_{2n}^{\text{toroidal}}(x) = W(x)\left(\boldsymbol{e}_r \times \boldsymbol{\nabla} Y_{lm}\right), \tag{5.103}$$

where

$$W(x) = D_{2n} j_l\left(k_{2n} x\right). \tag{5.104}$$

and the eigenvalues $\omega_{2n} = k_{2n}\sqrt{\frac{\mu}{\rho}}$ are the roots of f_{toroidal} 5.57. As with the eigenvalues, we have scaled the equations so that the radius $R = 1$.

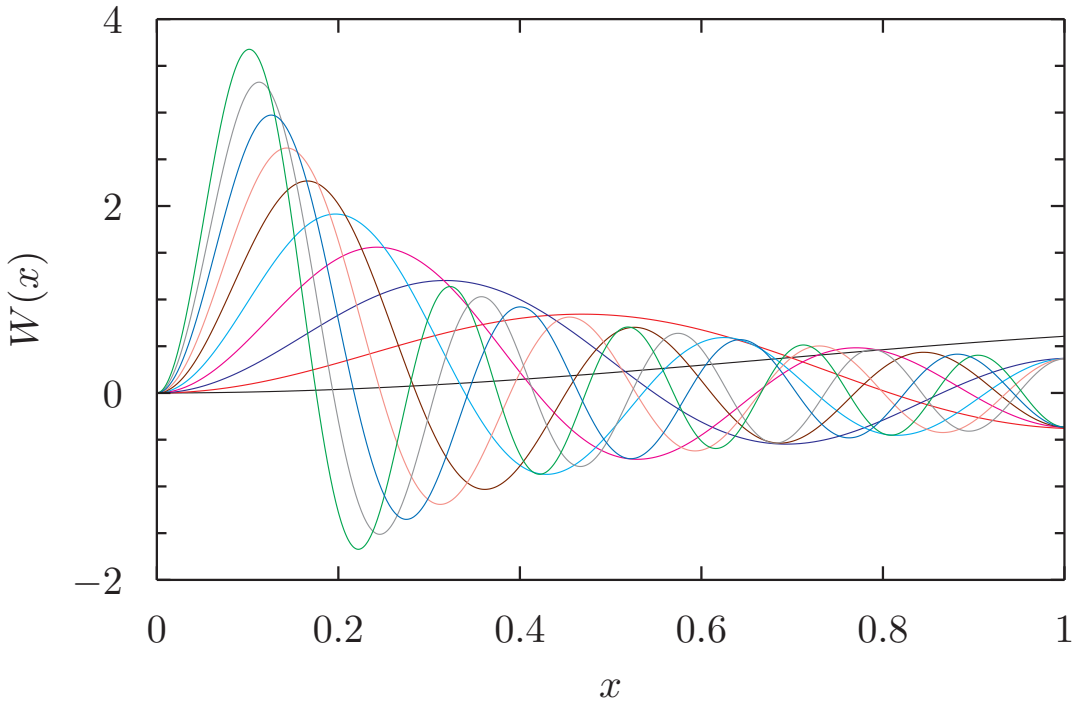

Figure 5.4: Plot of the W part of the first toroidal $l = 2$ eigenfunctions, as a function of the fractional radius $x = \frac{r}{R}$, for $\frac{B}{A} = 0.1$. The $n = 1$ eigenfunction is shown in black and the highest, $n = 10$ eigenfunction in green.

Figure 5.4 shows a plot of the first ten toroidal eigenfunctions for $\frac{B}{A} = 0.1$. The lowest, $n = 1$ eigenfunction is shown in black hand and has no nodes; each eigenfunction gains one more node with increasing n.

5.6.2.2 Spheroidal eigenfunctions

The form of the corresponding spheroidal eigenfunctions has been already been found analytically (5.87). For $l = 2$, this becomes

$$\boldsymbol{\xi}_{2n}^{\text{spheroidal}}(x) = U_{2n}(x)P_2\,\mathbf{e}_x + V_{2n}(x)\frac{dP_2}{d\theta}\mathbf{e}_\theta, \tag{5.105}$$

with

$$U_{2n}(x) = C_{2n}\left[2q_{2n}x + \frac{6}{k_{2n}x}j_2(k_{2n}x)\right], \tag{5.106}$$

$$V_{2n}(x) = C_{2n}\left[q_{2n}x + \frac{1}{k_{2n}x}j_2(k_{2n}x) + j_2'(k_{2n}x)\right] \tag{5.107}$$

where the C_{2n} are arbitrary constants and

$$q_{2n} = \frac{1}{2}\left[2j_2'(k_{2n}) + \left(\frac{10}{k_{2n}} - k_{2n}\right)\right] j_2(k_{2n}x). \tag{5.108}$$

As an example, Figure 5.5 shows the first ten eigenfunctions for $\frac{B}{A} = 0.01$. The majority of the eigenfunctions, shown in grey, are elastic modes. These form an ordered sequence with the lowest $n = 1$ mode having one stationary point, the $n = 2$ mode having two, etc. These modes also have a very small amplitude at the surface.

The eighth eigenfunction, marked in red, has a frequency just above ω_K and exhibits very different behaviour to the rest of the set. In particular, it has a much larger amplitude at the surface. This is consistent with this eigenfunction having a hybrid fluid-elastic character: the overall shape of the eigenfunction is similar to the linear $l = 2$ Kelvin mode eigenfunction 5.28 for a completely fluid star, while the elastic character of the mode is evident in the oscillations superimposed on this.

This behaviour is generic for all values of $\frac{B}{A}$ in the range $\frac{B}{A} = 10^{-6} - 1$ that we have studied. As $\frac{B}{A}$ gets smaller, the gap between mode frequencies gets smaller, so that the single hybrid mode is pushed to higher n. By $\frac{B}{A} = 10^{-6}$, the hybrid mode is at $n = 877$.

For lower values of $\frac{B}{A}$, where the star is closer to a fluid star, we should expect the linear, fluid-mode-like behaviour to be recovered. This is indeed what we see in Figure 5.6, where the hybrid mode is plotted for four different values of $\frac{B}{A}$.

Another way to obtain some insight into the behaviour of the eigenfunctions is to pick a value of n and track the variation of the eigenfunction with $\frac{B}{A}$. As an example, Figure 5.7 is a surface plot for $n = 3$, showing how the U part eigenfunction changes between $\frac{B}{A} = 10^{-3}$ and $\frac{B}{A} = 1$. We can see that the eigenfunction changes continuously, but goes through three distinct phases. For the smallest values of $\frac{B}{A}$ on the right, the three lowest eigenfunctions are all elastic-type eigenfunctions, and so the $n = 3$ eigenfunction is the third elastic eigenfunction with three stationary points. As $\frac{B}{A}$ gets larger there is a transitional area where the third mode has a hybrid character. For values of $\frac{B}{A}$ larger than around 0.1, the hybrid mode is found at $n = 1$ or 2, and so the $n = 3$ eigenfunction is again an elastic-type function, this time the second such function with two stationary points.

The contours projected onto the base of the graph show the how the zeroes of the eigenfunction vary with $\frac{B}{A}$. This makes it clear that the intermediate, hybrid eigenfunction has a very different character, with no zeroes.

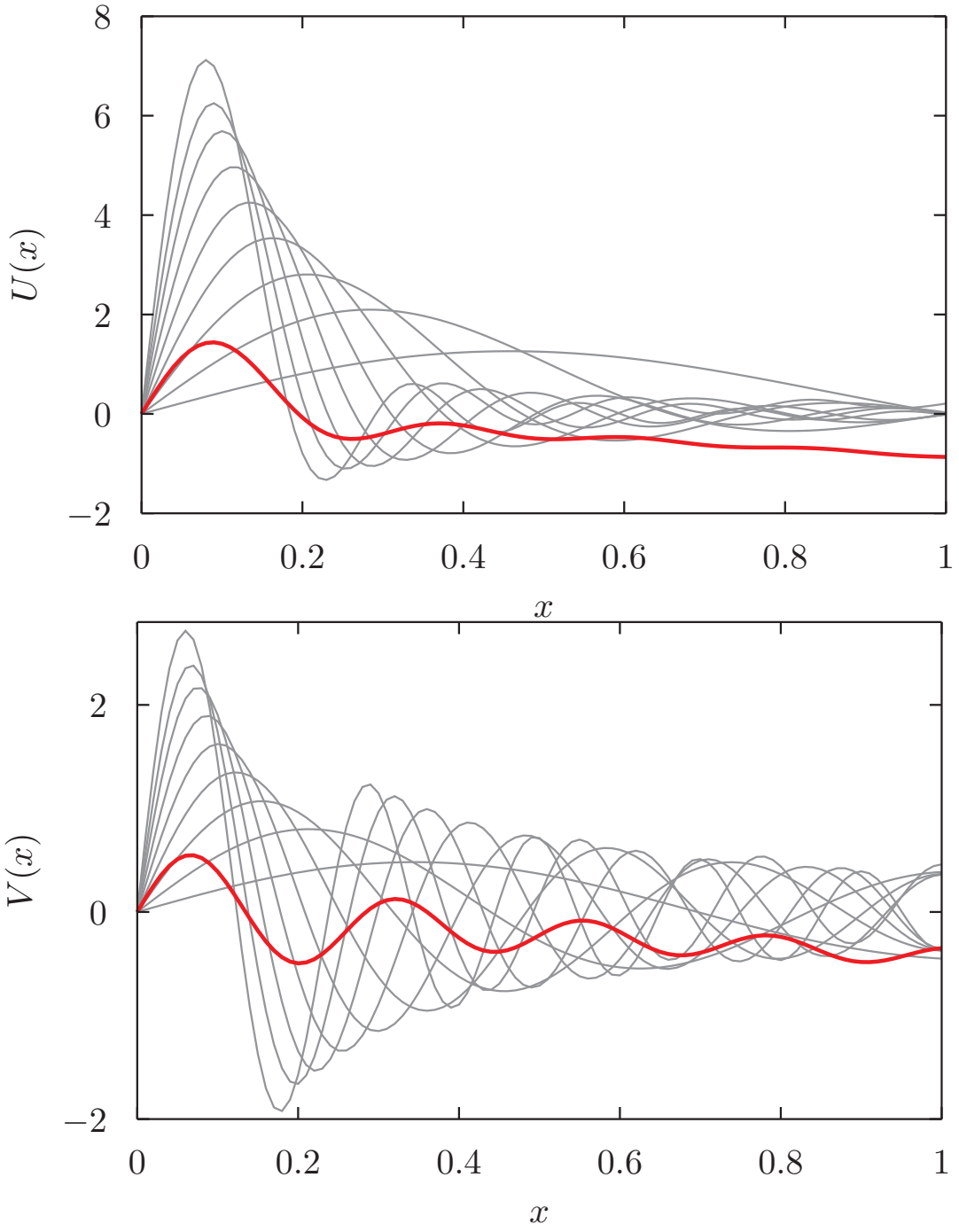

Figure 5.5: Plot of the U and V radial parts of the first ten eigenfunctions, as a function of the fractional radius $x = \frac{r}{R}$, for $\frac{B}{A} = 0.01$. The hybrid fluid-like mode is marked in red; the other modes have an elastic character.

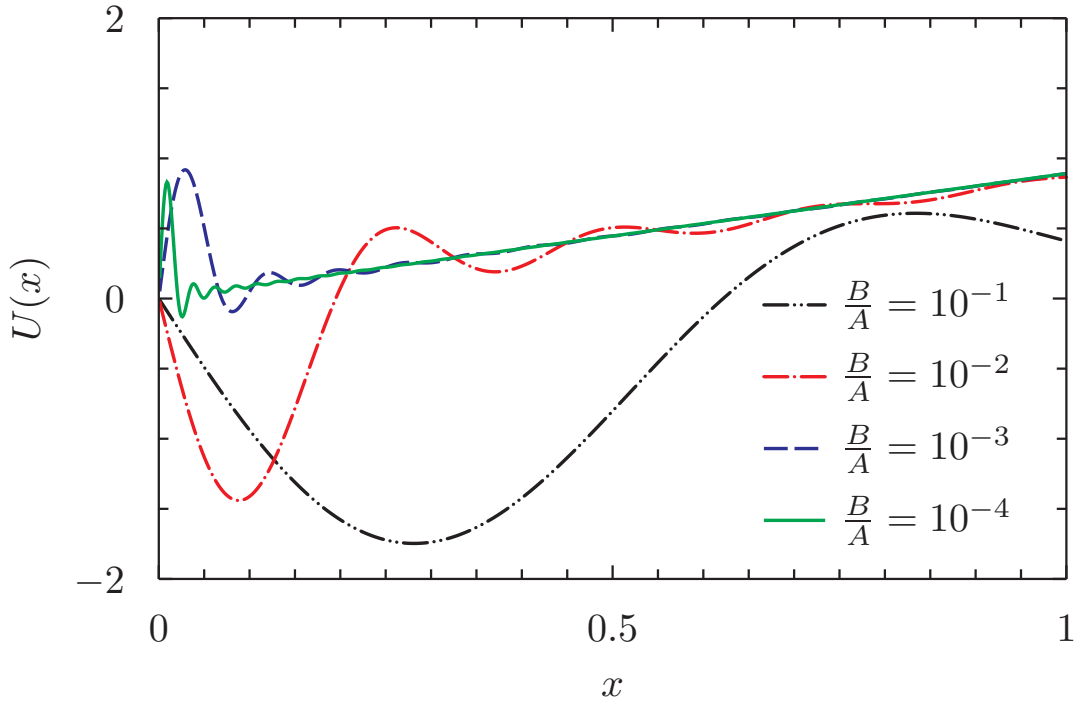

Figure 5.6: Plot showing the U radial part of the hybrid fluid-like mode for a range of values of $\frac{B}{A}$.

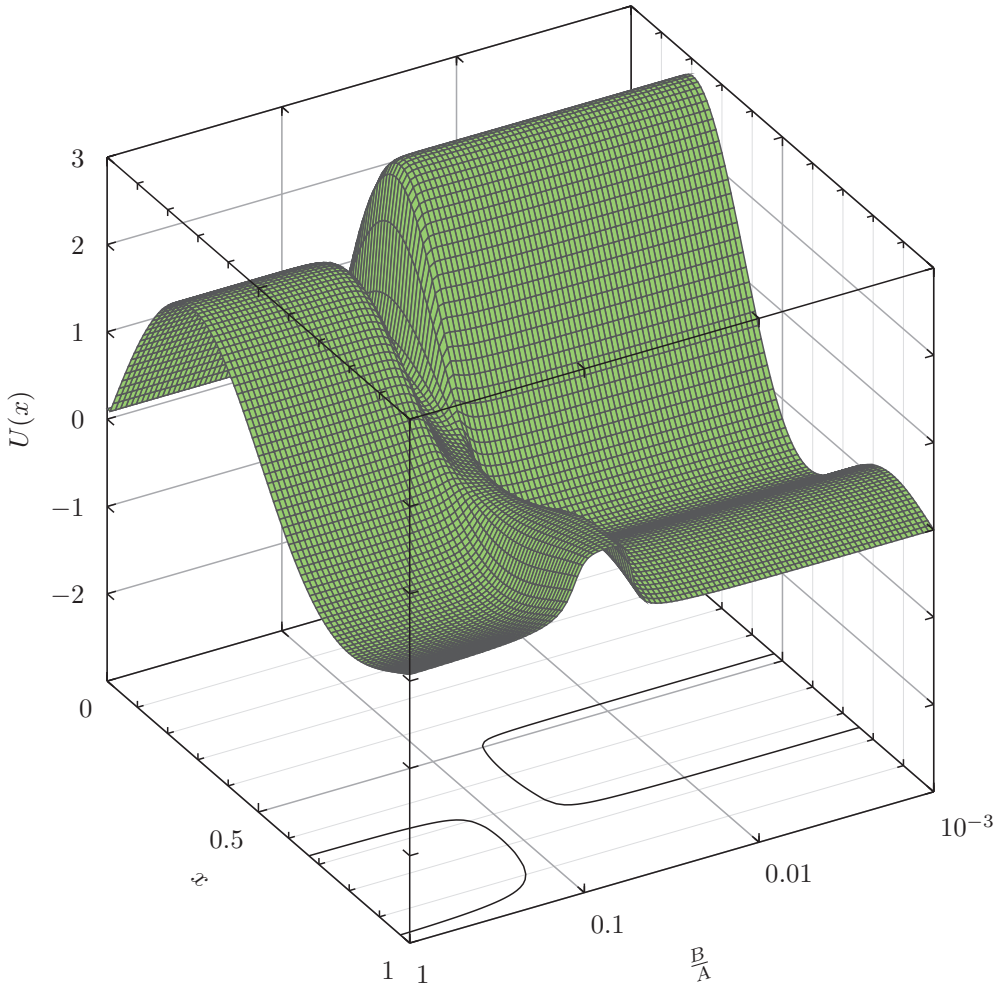

Figure 5.7: Surface plot showing how the U radial part of the $n = 3$ eigenfunction varies with $\frac{B}{A}$. The eigenfunction goes through three distinct phases: in the middle region around $\frac{B}{A} = 0.1$ there is a transitional area where this mode has a hybrid fluid-elastic character. The contours projected onto the base of the graph show the zeroes of the eigenfunction; there are none for the hybrid mode.

Chapter 6

Mode excitation by glitches

To find out which oscillation modes of the star are excited, we need to be able to project initial data against the basis of oscillation modes of our model. These are the modes of an incompressible, solid elastic star discussed in Chapter 5.

We will construct the initial data for our glitch model in Chapter 7, using the equilibrium solutions of Chapter 4. However, to carry out the projection we will also need to show that we have an orthogonal basis of eigenfunctions of the star after the glitch to project against.

In this chapter, we will build up to this projection problem by considering a series of three simpler models of mode excitation: one-dimensional motion in a fluid channel, radial oscillations of a fluid star and finally a simple nonradial oscillation problem, again for a fluid star. In the process, we will also develop the mathematical background required to show that the eigenfunctions are orthogonal, even for our case of an elastic star.

We will start with the fluid channel problem, where the eigenfunctions are trigonometric and the initial data can be written in terms of them as a simple Fourier series; this will help clarify the details of how we plan to carry out the projection.

For the more complicated stellar oscillation models, we will need to show that the eigenfunctions are orthogonal, so we next describe how to do this. We will show that it is sufficient to demonstrate that the operators in the equations governing the oscillation modes are Hermitian, given our boundary conditions. We then do this first for the simpler case of radial excitation and consider an example of radial mode excitation.

Finally, we will show that the eigenfunctions are orthogonal for the case of nonradial oscillations of an incompressible elastic star: this is the result we need for our glitch toy model. As preparation for this, we then discuss a very simple 'starquake' model where we excite a nonradial f-mode in an incompressible fluid star; the mode equation in this case is a special case of that for an incompressible elastic star in the limit of vanishing shear modulus μ, so we can use the result just derived.

6.1 A simple example: fluid in a channel

To clarify the projection problem, we will first discuss a very simple system consisting of one-dimensional motion of waves in a fluid channel with sides at $x = 0$ and $x = L$. We will assume that the unperturbed fluid is static, and that it obeys a polytropic equation of state $P = k\rho^{\Gamma}$.

We then disturb the fluid, introducing a horizontal displacement $\xi(x)$. This will produce corresponding changes δP, $\delta\rho$ in the pressure and density, and from the equation of state we see that

$$\frac{\delta P}{P} = \Gamma \frac{\delta \rho}{\rho}. \tag{6.1}$$

The Euler equation (1.28) for the fluid motion is

$$\frac{d^2\xi}{dt^2} = -\frac{1}{\rho}\frac{d(\delta P)}{dx}, \tag{6.2}$$

and by conservation of mass (1.25) we also have that

$$\delta\rho + \rho\frac{d\xi}{dx} = 0. \tag{6.3}$$

We can eliminate $\delta\rho$ from this using the equation of state (6.1), and by combining with conservation of mass we can obtain a wave equation in terms of ξ and the background quantities only:

$$\frac{d^2\xi}{dt^2} - a^2\frac{d^2\xi}{dx^2} = 0, \tag{6.4}$$

where $a = \sqrt{\frac{\Gamma P}{\rho}}$ is the sound speed of the fluid. We also make the assumption that the velocity perturbation has a time dependence $\delta v(x,t) = \delta v(x)\cos(\omega t + \theta)$, so that the general solution has the form

$$\xi = A\cos(\omega t + \theta)\sin\left(\frac{\omega x}{a} + \beta\right), \tag{6.5}$$

A and β constants.

6.1.1 Oscillation modes

To determine the oscillation modes of the fluid, we need to impose boundary conditions. We choose to require that the displacement $\xi(x)$ vanishes at the sides of the channel. The condition at $x = 0$ gives $\beta = 0$, while that at $x = L$ means that the frequency ω must satisfy

$$\omega = \frac{n\pi a}{L}, \tag{6.6}$$

where n is an integer. The corresponding eigenfunctions are

$$\xi_n(x,t) = A_n \cos(\omega t + \theta_n) \sin\left(\frac{n\omega}{a}x\right), \tag{6.7}$$

so that the most general solution can then be written as a sum of these eigenfunctions

$$\xi(x,t) = \sum_{n=1}^{\infty} A_n \cos(\omega t + \theta_n) \sin\left(\frac{n\omega}{a}x\right). \tag{6.8}$$

Substituting this back into the Euler equation (6.2) and integrating, we find that the pressure perturbation is

$$\delta P = \sum_{n=1}^{\infty} \frac{A_n n\pi a^2}{\rho L} \sin(\omega t + \theta_n) \cos\left(\frac{n\omega}{a}x\right); \tag{6.9}$$

this also fixes the density perturbation. (The constant of integration in both cases can be shown to be zero from the requirement that mass is conserved in the channel.)

6.1.2 Representing initial data as a sum of oscillation modes

We now wish to represent an arbitrary initial perturbation as a sum of the oscillation modes. First we note that our wave equation (6.4) is a second order differential equation in ξ, so initial conditions on the displacement and velocity

$$\xi(x,0) \equiv f(x), \tag{6.10}$$

$$\frac{d\xi}{dx}(x,0) \equiv g(x) \tag{6.11}$$

should fully determine the solution. We show explicitly below that the two undetermined sets of coefficients $\{A_n\}$ and $\{\theta_n\}$ do in fact give us this freedom to independently choose an arbitrary initial displacement and velocity.

For this simple example this can be done using ordinary Fourier analysis: we multiply our initial displacement by $\sin\left(\frac{n\omega}{a}x\right)$ and integrate between $x = 0$ and $x = L$ to find that

$$A_n \cos(\theta_n) = \frac{2}{L}\int_0^L f(x) \sin\left(\frac{n\omega}{a}x\right). \tag{6.12}$$

Similarly, we have that

$$A_n \sin(\theta_n) = -\frac{2}{\omega_n L}\int_0^L g(x)\sin\left(\frac{n\omega}{a}x\right), \tag{6.13}$$

and together these fully determine the solution. These results rely on the standard orthogonality relations of trigonometric functions. In the more complicated examples considered later, we will come across different sets of eigenfunctions. We need to show that we can still find an orthogonal basis to project against.

6.2 Orthogonality of eigenfunctions: general background

In this section, we will use the notation of Friedman and Schutz [31] and write our eigenvalue problems in the form

$$\omega^2 A\boldsymbol{\xi} + C\boldsymbol{\xi} = 0, \tag{6.14}$$

where A and C are operators. For example, for the incompressible elastic star of Chapter 5 we can rewrite the mode equation (5.31) so that the operators A and C would be

$$A\boldsymbol{\xi} \equiv \rho\boldsymbol{\xi}, \tag{6.15}$$

$$C\boldsymbol{\xi} \equiv -\boldsymbol{\nabla}(\delta p) + \mu\boldsymbol{\nabla}^2\boldsymbol{\xi}_i - \rho\boldsymbol{\nabla}(\delta\Phi) \tag{6.16}$$

We wish to show that the eigenfunctions of an incompressible elastic star are orthogonal with respect to the operator A, i.e. that for two eigenfunctions $\boldsymbol{\xi}$, $\boldsymbol{\eta}$ with different eigenvalues $\omega^\xi \neq \omega^\eta$, we have

$$\langle\boldsymbol{\eta}, A\boldsymbol{\xi}\rangle = 0. \tag{6.17}$$

Here the inner product is defined by an integral over the volume V of the star

$$\langle\boldsymbol{\eta}, \boldsymbol{\xi}\rangle = \int_V \boldsymbol{\eta}^* \cdot \boldsymbol{\xi}\, dV. \tag{6.18}$$

This will follow if the operators A, C are Hermitian (or self-adjoint), i.e. if

$$\langle\boldsymbol{\eta}, A\boldsymbol{\xi}\rangle = \langle\boldsymbol{\xi}, A\boldsymbol{\eta}\rangle^*, \tag{6.19}$$

$$\langle\boldsymbol{\eta}, C\boldsymbol{\xi}\rangle = \langle\boldsymbol{\xi}, C\boldsymbol{\eta}\rangle^*, \tag{6.20}$$

given the boundary conditions that we have. We start by showing this. In the process, we will also demonstrate that the eigenvalues ω^2 are always real. The argument is a standard one, very similar to that found in most quantum mechanics textbooks [72].

We start with the mode equation (6.14) for two eigenfunctions η, ξ:

$$(\omega^{\eta})^2 A\boldsymbol{\eta} = -C\boldsymbol{\eta}, \tag{6.21}$$
$$(\omega^{\xi})^2 A\boldsymbol{\xi} = -C\boldsymbol{\xi}. \tag{6.22}$$

Next we take the inner product of ξ with the first equation, and the inner product of η with the second:

$$(\omega^{\eta})^2 \langle \boldsymbol{\xi}, A\boldsymbol{\eta}\rangle = -\langle \boldsymbol{\xi}, C\boldsymbol{\eta}\rangle, \tag{6.23}$$
$$(\omega^{\xi})^2 \langle \boldsymbol{\eta}, A\boldsymbol{\xi}\rangle = -\langle \boldsymbol{\eta}, C\boldsymbol{\xi}\rangle. \tag{6.24}$$

Taking the complex conjugate of this last equation and using the fact that the operators A, C are Hermitian (6.19), (6.20) yields

$$\left[(\omega^{\xi})^2\right]^* \langle \boldsymbol{\xi}, A\boldsymbol{\eta}\rangle = -\langle \boldsymbol{\xi}, C\boldsymbol{\eta}\rangle. \tag{6.25}$$

The right hand side of this is now identical to that of our first inner product (6.23), so that

$$\left\{(\omega^{\eta})^2 - \left[(\omega^{\xi})^2\right]^*\right\} \langle \boldsymbol{\xi}, A\boldsymbol{\eta}\rangle = 0. \tag{6.26}$$

In the special case where $\boldsymbol{\xi} = \boldsymbol{\eta}$, we then have

$$(\omega^{\xi})^2 = \left[(\omega^{\xi})^2\right]^*, \tag{6.27}$$

showing that the eigenvalue $(\omega^{\xi})^2$ is real for every eigenfunction ξ. If $(\omega^{\xi})^2 > 0$, the frequency ω^{ξ} itself is real and the eigenfunction $\boldsymbol{\xi}(x,t) = e^{i\omega^{\xi} t}\boldsymbol{\xi}(x)$ is oscillatory in nature. If $(\omega^{\xi})^2 < 0$, the frequency is imaginary and the perturbation can grow exponentially (the system is dynamically unstable) [26]. In the systems we have analysed in Chapter 5, all the eigenvalues are positive.

For $\boldsymbol{\xi} \neq \boldsymbol{\eta}$ our equation (6.26) then becomes

$$\left\{(\omega^{\eta})^2 - (\omega^{\xi})^2\right\} \langle \boldsymbol{\xi}, A\boldsymbol{\eta}\rangle = 0. \tag{6.28}$$

If $(\omega^\xi)^2 \neq (\omega^\eta)^2$, by the definition of A (6.15) we have

$$\langle \boldsymbol{\xi}, \rho\boldsymbol{\eta} \rangle = 0, \tag{6.29}$$

i.e. the eigenfunctions are orthogonal with respect to this inner product.

We will now discuss two special cases in detail. One is that of purely radial oscillations, considered in Section 5.12; we will use this relatively straightforward example to demonstrate how to carry out projection of initial data against the basis of modes. The second is that of oscillations of the incompressible, self-gravitating elastic star of Section 5.5. This case is particularly important to us, as we will later be using this basis of modes in our starquake model. We will then illustrate how to use this in a toy model, for the special case of a purely fluid star.

6.3 Radial mode excitation for a fluid star

For our next illustrative example, we will consider the case of excitation of radial modes of a fluid star. This is not the stellar model we will be using in our glitch calculations, but it does allow us to test some of the projection theory in a simpler context. We found the general equation (5.12) governing these modes in Section 5.3. First we will need to show that this can be put into self-adjoint form.

6.3.1 Orthogonality of eigenfunctions for radial oscillations

To show orthogonality, we will start by writing our mode equation (5.12) in the form

$$\omega^2 a\xi + c\xi = 0, \tag{6.30}$$

where a and c are the operators

$$a\xi = \rho\xi, \tag{6.31}$$

$$c\xi = \Gamma_1 P\xi'' + \left(2\Gamma_1 \frac{P}{r} + \Gamma_1 P'\right)\xi' + \frac{1}{r^2}\left(-2\Gamma_1 P - 4rP + 2\Gamma_1 rP'\right)\xi. \tag{6.32}$$

The boundary conditions are

$$\xi = 0 \quad \text{at} \quad r = 0, \tag{6.33}$$

$$\xi \text{ finite} \quad \text{at} \quad r = R. \tag{6.34}$$

Currently, the operators a and c are not Hermitian. However, we can show that we can always put a second order linear equation with real coefficients into Hermitian form by multiplying by a suitable integrating factor. In general, this equation will have the form

$$L\xi = P(r)\xi'' + Q(r)\xi' + R(r)\xi = 0, \tag{6.35}$$

with P, Q and R real. Taking the inner product with another eigenfunction η, we have

$$\langle \eta, L\xi \rangle = \left\langle \eta, P(r)\xi'' \right\rangle + \left\langle \eta, Q(r)\xi' \right\rangle + \left\langle \eta, R(r)\xi \right\rangle, \tag{6.36}$$

which written out in full becomes

$$\langle \eta, L\xi \rangle = \int_0^R \eta^* \left[P(r)\frac{d^2\xi}{dr^2} + Q(r)\frac{d\xi}{dr} + R(r)\xi \right] dr \tag{6.37}$$

To see if this is Hermitian, we now want to compare this with

$$\langle \xi, L\eta \rangle^* = \int_0^R \xi \left[P(r)\frac{d^2\eta^*}{dr^2} + Q(r)\frac{d\eta^*}{dr} + R(r)\eta^* \right] dr, \tag{6.38}$$

where we have used the fact that P, Q and R are real. To make this comparison, we need to 'shift the operators across' from ξ to η. We can accomplish this by integrating by parts twice on the first term and once on the second, obtaining

$$\langle \eta, L\xi \rangle = \int_0^R \xi \left[\frac{d^2}{dr^2}(P(r)\eta^*) - \frac{d}{dr}(Q(r)\eta^*) + R(r)\eta^* \right] dr + \text{boundary term}. \tag{6.39}$$

We will deal with the boundary term later. Expanding the integral out, we get

$$\langle \eta, L\xi \rangle = \int_0^R \xi \left[P\frac{d^2\eta^*}{dr^2} + \left(2\frac{dP}{dr} - Q \right) \frac{d\eta^*}{dr} + \left(\frac{d^2P}{dr^2} - \frac{dQ}{dr} + R \right) \eta^* \right] dr. \tag{6.40}$$

Comparing this term-by-term with the previous equation, we find that for L to be Hermitian we need

$$Q = \frac{dP}{dr}, \tag{6.41}$$

i.e. our operator L needs to be of the form

$$L'\xi \equiv \frac{d}{dr}\left(p(r)\frac{d\xi}{dr} \right) + \rho(r)\xi. \tag{6.42}$$

This is know as *Sturm-Liouville form* [17]. We can transform any second order linear operator L (6.35) to this form by multiplying through by the *integrating factor*

$$h(r) = \frac{1}{P(r)} \exp\left[\int \left(\frac{Q(r)}{P(r)}\right) dx\right]. \tag{6.43}$$

We also need the boundary term of the inner product (6.39) to be zero. This term is

$$\text{boundary term} = \left[\eta^* P \frac{d\xi}{dr} - \frac{d}{dr}\left(\eta^* P\right)\xi + \eta^* Q \xi\right]_{r=a,b}, \tag{6.44}$$

so for a Hermitian operator we need

$$\left[p(x)\left(\eta^* \frac{d\xi}{dr} - \xi^* \frac{d\eta}{dr}\right)\right]_{r=a,b} = 0. \tag{6.45}$$

This can be satisfied for a wide range of boundary conditions [61]; we will show this just for our case of radial oscillations (6.30), where we have

$$P(r) = \Gamma_1 P, \tag{6.46}$$

$$Q(r) = \frac{1}{r^2}\left(\Gamma_1 P\right). \tag{6.47}$$

In this case the integrating factor is

$$h(r) = r^2. \tag{6.48}$$

Multiplying through by this, we get

$$\omega^2 A\xi + C\xi = 0, \tag{6.49}$$

with the Hermitian operators A and C defined by

$$A\xi = \omega^2 r^2 \rho, \tag{6.50}$$

$$C\xi = \frac{d}{dr}\left(\Gamma_1 P r^2\right) + \left(-2\Gamma_1 P - 4rP + 2\Gamma_1 r P' + \omega^2 r^2 \rho\right)\xi. \tag{6.51}$$

We also need to check that the constraint on the boundary conditions (6.52) is satisfied. In our case this becomes

$$\left[r^2 \Gamma_1 P\left(\eta^* \frac{d\xi}{dr} - \xi^* \frac{d\eta}{dr}\right)\right]_{r=0,R} = 0. \tag{6.52}$$

This is clearly satisfied at $r = 0$, and also at the surface $r = R$ where the pressure P vanishes. The eigenfunctions are then orthogonal with respect to the operator A:

$$\langle \eta, A\xi \rangle = 0 \tag{6.53}$$

for different eigenfunctions η, ξ with $\omega_\eta^2 \neq \omega_\xi^2$.

6.3.2 Using initial data to calculate mode excitation

To give an analytic example of mode excitation, we will now specialise to the case of compressible perturbations on a homogeneous background star, studied in Section 5.3. Our equation for the perturbations (5.13) can be put into the Sturm-Liouville form of the previous section as

$$\frac{d}{dx}\left((x^4 - x^2)\xi'\right) + (2 - Ax^2)\xi = 0. \tag{6.54}$$

We have seen that the eigenfunctions of this problem are polynomials

$$\xi_n = \sum_{i=0}^{n} c_i x^{i+1}, \tag{6.55}$$

with odd coefficients zero, and even coefficients satisfying

$$\frac{c_{i+2}}{c_i} = \frac{i^2 + 5i + 4 - A}{i^2 + 7i + 10}, \tag{6.56}$$

where

$$A = n^2 + 5n + 4, \quad n = 0, 2, 4 \ldots \tag{6.57}$$

The first two eigenfunctions are

$$\xi_0(x) = \sqrt{5}x, \tag{6.58}$$

$$\xi_1(x) = \frac{15}{2}\left(-\frac{7}{5}x^3 + x\right). \tag{6.59}$$

We now want to use our basis of orthonormal eigenfunctions to represent an arbitrary initial perturbation, with initial displacement and velocity

$$\xi(x, 0) = f(x), \tag{6.60}$$

$$\frac{d\xi}{dt}(x, 0) = g(x). \tag{6.61}$$

We know that a general perturbation ξ has the form

$$\xi(x,t) = \sum_{n=0}^{\infty} a_n \xi_n \cos(\omega_n t + \theta_n), \tag{6.62}$$

where a_n and θ_n are constant, so

$$f(x) = \sum_{n=0}^{\infty} a_n \xi_n \cos(\theta_n), \tag{6.63}$$

$$g(x) = -\sum_{n=0}^{\infty} a_n \omega_n \xi_n \sin(\theta_n). \tag{6.64}$$

Using our orthonormality condition, we can then multiply by $w(x)\xi_m$, where $w(x) = x^2$ is the weight function, and integrate over $[0,1]$ to find that

$$a_n \cos(\theta_n) = \int_0^1 f(x)\xi_n x^2 dx, \tag{6.65}$$

$$-a_n \omega_n \xi_n \sin(\theta_n) = \int_0^1 g(x)\xi_n x^2 dx. \tag{6.66}$$

We can then reconstruct the original functions $f(x)$ and $g(x)$ as a sum of these coefficients. To find the amplitude a_n of each excited mode, we can take

$$a_n = \left(\left(\int_0^1 f(x)\xi_n x^2 dx \right)^2 + \frac{1}{\omega_n^2} \left(\int_0^1 g(x)\xi_n x^2 dx \right)^2 \right)^{\frac{1}{2}}. \tag{6.67}$$

The phases θ_n can be found from

$$\tan(\theta_n) = -\frac{\omega_n \int_0^1 f(x)\xi_n x^2 dx}{\int_0^1 g(x)\xi_n x^2 dx}. \tag{6.68}$$

As an example, consider the initial data

$$\xi(x,0) = x^3, \tag{6.69}$$

$$\frac{d\xi}{dt}(x,0) = 0. \tag{6.70}$$

Using (6.65), we find

$$a_m \cos\theta_m = \int_0^1 \xi_m x^5 dx \tag{6.71}$$

and

$$a_m \sin\theta_m = 0. \tag{6.72}$$

The second condition fixes $\theta_n = 0$ for all values of n. We can then substitute the first two eigenfunctions (6.58) (6.59) into (6.71) to fix our amplitudes as

$$a_0 = \frac{\sqrt{5}}{7}, \tag{6.73}$$

$$a_1 = -\frac{2}{21}. \tag{6.74}$$

We can check these by reconstructing our original displacement in terms of our basis of normalised eigenfunctions

$$\xi_0 = \sqrt{5}x, \tag{6.75}$$

$$\xi_1 = \frac{15}{2}\left(-\frac{7}{5}x^3 + x\right). \tag{6.76}$$

We find that, as expected,

$$a_0\xi_0 + a_1\xi_1 = \frac{\sqrt{5}}{7}(\sqrt{5}x) - \frac{2}{21}\cdot\frac{15}{2}\left(-\frac{7}{5}x^3 + x\right) = x^3. \tag{6.77}$$

6.4 Orthogonality of eigenfunctions for oscillations of an incompressible elastic star

First, though, we will show that the eigenfunctions of the star in our glitch model are orthogonal. This is the case of a completely solid, elastic incompressible star, discussed in Section 5.5. In this case the mode equation (5.31) can again be written in the form

$$A_{ij}\omega^2\xi^j + C_{ij}\xi^j = 0, \tag{6.78}$$

where the operators A and C are defined by

$$A_{ij}\xi^j \equiv \rho\xi^j \tag{6.79}$$

$$C_{ij}\xi^j \equiv \nabla_j T_i{}^j - \rho\nabla_i\Phi. \tag{6.80}$$

Here T is the stress-energy tensor

$$T_{ij} = -\delta p\, \delta_{ij} + \mu(\nabla_i \xi_j + \nabla_j \xi_i). \tag{6.81}$$

The boundary condition (5.58) at the surface $r = R$ can then be written in terms of T_{ij} as

$$(T_{ij} - \xi^k \nabla_k p \delta_{ij})\hat{r}^i = 0. \tag{6.82}$$

The operator A is just multiplication by a scalar function, so it is Hermitian. We need to show that the operator C is also Hermitian. As we found in Chapter 5 that all the eigenfunctions and associated quantities δp, $\delta\Phi$ are all real, this just involves showing that C is symmetric,

$$\langle \eta, C\xi \rangle = \langle \xi, C\eta \rangle. \tag{6.83}$$

The symmetry of the operator C has been shown for the cases of nonradial oscillations of stationary, perfect fluid stars [21, 53, 31] and for the incompressible fluid star [22]. We will follow a similar method here.

Writing the inner product out in full,

$$\left\langle \eta^i, C_i{}^j \xi_j \right\rangle = \int_V \nabla_j T_i{}^j \eta^i dV + \int_V \rho(\nabla_i \delta\Phi)\eta^i dV. \tag{6.84}$$

It is then sufficient to show that each term of the right hand side is symmetric in ξ^i and η^i, given our boundary conditions. We will then have $\langle \eta, C\xi \rangle - \langle \xi, C\eta \rangle = 0$, and so C is symmetric.

To do this for the $T_i{}^j$ term, we first integrate by parts:

$$\int_V \nabla_j T_i{}^j \eta^i dV = -\int_V (\nabla_j \eta^i) T_i{}^j dV + \int_{\partial V} \eta^i T_i{}^j dS_j. \tag{6.85}$$

For the surface term, we can use the boundary conditions (6.82) to substitute in T_{ij}, so that

$$\int_{\partial V} \eta^i T_i{}^j dS_j = \int_{\partial V} \eta^r \xi^r \frac{dp}{dr}\, dS_r, \tag{6.86}$$

where we have used the spherical symmetry of the background star. This term is symmetric in ξ and η.

For the volume term, we expand out $T_i{}^j$ so that

$$-\int_V (\nabla_j \eta^i) T_i{}^j dV = -\int_V (\nabla_j \eta^i) \left(-\delta p \delta_i{}^j + \mu \nabla_i \xi^j + \mu \nabla^j \xi_i \right) dV \tag{6.87}$$

The first term of this is zero by incompressibility, while the third term is already symmetric. To deal with the second term, we will integrate half by parts with respect to ∇_i, and half with respect to ∇_j, so that

$$\begin{aligned} -\int_V \mu (\nabla_j \eta^i) \left(\nabla_i \xi^j \right) dV = \frac{1}{2} \Bigg[& \int_V \eta^i \nabla_j (\mu \nabla_i \xi^j) dV - \int_{\partial V} \mu \eta^i \nabla_i \xi^j dS_j \\ & + \int_V \xi^j \nabla_i (\mu \nabla_j \eta^i) dV - \int_{\partial V} \mu \xi^j \nabla_j \eta^i dS_i \Bigg] \end{aligned} \tag{6.88}$$

Using the product rule on the volume terms, this becomes

$$\begin{aligned} -\int_V \mu (\nabla_j \eta^i) \left(\nabla_i \xi^j \right) dV = \frac{1}{2} \Bigg[& \int_V (\nabla_j \mu) \eta^i (\nabla_i \xi^j) dV + \int_V \mu \eta^i \nabla_j \nabla_i \xi^j dV \\ & + \int_V (\nabla_i \mu) \xi^j (\nabla_j \eta^i) dV + \int_V \mu \xi^j \nabla_i \nabla_j \eta^i dV \\ & - \int_{\partial V} \mu \eta^i \nabla_i \xi^j dS_j - \int_{\partial V} \mu \xi^j \nabla_j \eta^i dS_i \Bigg]. \end{aligned} \tag{6.89}$$

The shear modulus μ is constant over the surface of the star, and so its derivative $\nabla_i \mu$ is non zero only at the surface,

$$\nabla_i \mu = -\mu \delta(r - R) \hat{r}_i. \tag{6.90}$$

The terms containing $\nabla_i \mu$ then cancel with the two surface terms to leave

$$-\int_V \mu (\nabla_j \eta^i) \left(\nabla_i \xi^j \right) dV = \int_V \mu \eta^i \nabla_j \nabla_i \xi^j dV + \int_V \mu \xi^j \nabla_i \nabla_j \eta^i. \tag{6.91}$$

These two terms are zero, as can be seen by commuting ∇_i and ∇_j and using the incompressibility condition so that finally we have

$$\int_V \nabla_j T_i{}^j \eta^i dV = \int_{\partial V} \eta^r \xi^r \frac{dp}{dr} dS_r - \int_V \mu (\nabla_j \eta^i)(\nabla^j \xi_i). \tag{6.92}$$

Returning to the $\delta\Phi$ term of (6.84), we can show that this is symmetric by again integrating by parts, so that

$$\int_V \rho \nabla_i \delta\Phi \eta^i dV = -\int_V \delta\Phi \nabla_i (\rho \eta^i) + \int_{\partial V} \rho \delta\Phi \eta^i dS_i. \tag{6.93}$$

Considering the volume integral first, we have

$$\nabla_i(\rho\eta^i) = \eta^i\nabla_i\rho = -\rho\delta(r-R)\eta^r, \tag{6.94}$$

so in fact the integrand is only nonzero at the surface. Rewriting it as a surface integral,

$$\int_V \rho\nabla_i\delta\Phi\eta^i dV = 2\int_{\partial V}\rho\delta\Phi\eta^i dS_i. \tag{6.95}$$

We can then use the fact that $\delta\Phi$ is a solution of Poisson's equation,

$$\delta\Phi = -G\int_{V'}\frac{\delta\rho'}{|x^i - x'^i|}d^3x'. \tag{6.96}$$

Using the continuity equation (4.11) to rewrite $\delta\rho$, we obtain

$$\int_V \rho\nabla_i\delta\Phi\eta^i dV = -2G\int_{\partial V}\int_{\partial V'}\frac{\rho^2\xi^r\eta^r}{|x^i - x'^i|}dS'_r dS_r. \tag{6.97}$$

which is symmetric in ξ and η.

We have now shown that C is a symmetric operator, and so the eigenvalues of a self-gravitating elastic incompressible star are orthogonal with respect to $A \equiv \rho$:

$$\langle\eta, A\xi\rangle = 0, \quad \omega_\eta^2 \neq \omega_\xi^2. \tag{6.98}$$

6.5 Nonradial mode excitation: a 'starquake' toy model

As an example of nonradial mode excitation, we will consider a toy model of a rotating incompressible star, in which a 'starquake' is produced by the sudden artificial removal of all angular momentum from the star. The star will then be out of equilibrium, and oscillate about its spherical equilibrium configuration. Although this is a highly unrealistic example, it is useful for understanding how to represent a given nonradial perturbation as a sum of oscillation modes, as we can already take advantage of the work done in Section 5.4 calculating the fundamental Kelvin mode of an incompressible fluid star, and of our calculations of rotation shapes in Chapter 4.

6.5.1 Initial data and trivial displacements

We now wish to find out which modes of the star are excited by given initial data for the displacement and velocity fields. For a nonradial problem these are now vector functions:

$$\xi_0^i(r^i) = \xi^i(r^i, 0), \tag{6.99}$$

$$\frac{d\xi_0^i}{dt}(r^i) = \frac{d\xi^i}{dt}(r^i, 0). \tag{6.100}$$

The initial data should describe the equilibrium state of the star before the 'starquake' as a perturbation of the star in the equilbrium state it settles down to afterwards. In this toy model, the equilibrium state after the starquake is a spherical star, so the displacement vector field ξ_0^i should connect points in the spherical star to the corresponding points in the rotating star.

In Section 4.3, we found that the only part of this we can calculate unambiguously for a fluid star is the radial displacement field at the surface of the star. We will now discuss this in more detail. The problem is related to the fact that an ideal fluid is insensitive to shear stresses, so that it is possible to reorder fluid elements without affecting the macroscopic properties of the fluid. This means that the Eulerian perturbations of the pressure and gravitational potential (4.24) and (4.25) are not enough to uniquely determine the displacement field of the star.

Different displacement fields that correspond to the same set of macroscopic properties are said to differ by a *trivial displacement* (see Friedman and Schutz [31]). For these trivials, the corresponding Eulerian perturbations all vanish.

We can make one obvious choice for the displacement field of the whole star by taking the $\mu \to 0$ limit of the displacement field of a rotating incompressible elastic star, which we calculated previously, eqs. (4.84) and (4.85). This is labelled in Figure 6.1 a) as ξ^i_{rot}:

$$\xi^i_{\text{rot}} = \frac{\rho\Omega^2}{8\pi G\rho^2 R^2}\left[(3r^3 - 8R^2 r)P_2(\cos\theta)\mathbf{e}_r + \left(\frac{5}{2}r^4 - 4R^2r^2\right)\boldsymbol{\nabla}P_2(\cos\theta)\right]. \tag{6.101}$$

However, this initial displacement is not a sum of the eigenfunctions of the background spherical star. We have already found the general form (5.28) of these eigenfunctions, rewritten here as

$$\xi^i_{\text{kelvin}} = \sum_{l=0}^{\infty}\sum_{m=-l}^{m=l}\left(lA_{lm}r^{l-1}Y_{lm}\mathbf{e}_r. + A_{lm}r^l\boldsymbol{\nabla}Y_{lm}\right), \tag{6.102}$$

and ξ^i_{rot} cannot be put into this form. Instead, we will try to match the radial component of ξ^i_{rot} at the surface to ξ^i_{kelvin}. This can be done, and we find that $A_{20} = -\frac{5\Omega^2}{16\pi G\rho}$ and all other coefficients are zero. This gives us a set of initial data

$$\xi^i_{\text{initial}} = -\frac{5\Omega^2}{16\pi G\rho}\left(2rY_{20}\mathbf{e}_r + r^2\boldsymbol{\nabla}Y_{20}\right), \tag{6.103}$$

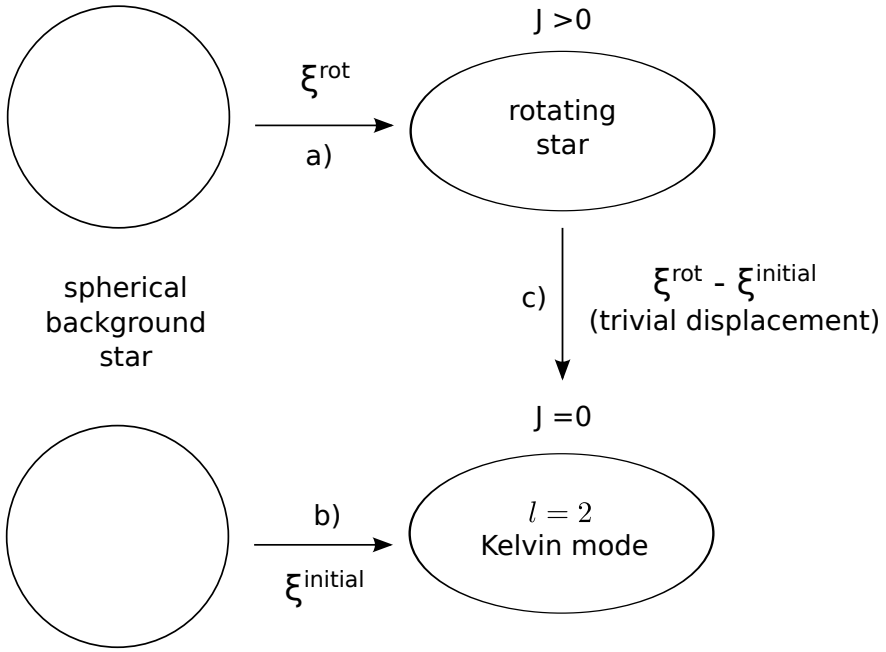

Figure 6.1: Diagram illustrating the difference between the displacement field of the rotating star $\xi^i_{\rm rot}$, found by taking the $\mu \to 0$ limit of the rotating elastic star, and the initial data $\xi^i_{\rm initial}$ we use for the starquake. a) $\xi^i_{\rm rot}$ maps the spherical, nonrotating background star to its rotating configuration. b) $\xi^i_{\rm initial}$ maps the background star to the $l = 2$ Kelvin mode of the star, with the amplitude chosen to match the surface shape of the rotating star. c) The difference between these, $\xi^i_{\rm rot} - \xi^i_{\rm initial}$, is a trivial displacement.

labelled in Figure 6.1 c). We can show that this is an acceptable substitute for $\xi^i_{\rm rot}$ by showing that the Eulerian perturbations of fluid quantities match in both cases, meaning that the difference $\xi^i_{\rm rot} - \xi^i_{\rm initial}$ is a trivial displacement (Figure 6.1 b)). This gives us confidence that the macroscopic properties of the star are the same in both cases.

We can expect issues of this kind to arise in any projection problem for a fluid star, so this analysis should provide useful insight for the more realistic case of a fluid star with a solid core. However, to construct our initial data for the glitch in later chapters we will be considering completely solid elastic stellar models, for which there is no ambiguity in finding the displacement field.

Chapter 7

The glitch toy model: glitch at zero spin

We are now in a position to bring in many of the elements developed in previous chapters, and construct our first full toy model of a starquake. In this initial toy model, we assume that the star spins down to *zero* angular velocity before 'glitching', which we model as a sudden loss of strain from the star.

This toy model may appear to be too much of a simplification, in that we have lost the key observational feature of the glitch, the sudden change in frequency of the star. However this model does give us considerable insight into constructing the initial data, and into the types of oscillation mode excited. In both cases there are enough new ideas to be introduced that it is worth discussing this model in detail, before adding in the extra complications of rotation in Chapter 9.

The basic idea of the model is to project initial data describing the starquake against the set of normal modes of the star after the glitch, in order to see which ones are excited. This process has three stages:

- First we construct the initial data, which will take the form of a displacement field describing how far particles in the star are displaced from equilibrium after the glitch. To do this, we will need to find the new equilibrium state of the star after the starquake. This will require the equilibrium models of a rotating star developed in Chapter 4.
- Next,we calculate the oscillation modes of this new equilibrium state. We will see that for this purpose we can approximate the star as spherical, so the oscillation modes are those of the elastic star found in Chapter 5.
- Finally, we can project the initial data against this set of modes. This relies on these eigenfunctions being an orthogonal set, which we have shown in Chapter 6.

We will start the chapter by giving an overview of our model for the glitch. We will then make some energy estimates to get an order-of-magnitude idea of the amplitudes of the modes that are likely to be excited in this model, as a check before we move on to a detailed construction of the initial data for the model. Finally, we will project this initial data against the normal modes of the star after the glitch and discuss the results.

7.1 Overview of the glitch model

In our toy model for a glitch, we assume that the star is completely solid and incompressible. As in Chapter 3, we will describe our model using our terminology of Stars A–D, first introduced in Section 2.2. The stages of the model are illustrated in Figure 7.1.

Star A is relaxed and spinning with angular velocity Ω_A. In its relaxed state, the star will have the same shape as a completely fluid star.

This star will then spin down as it loses energy. This will cause it to become less oblate, inducing a strain field in the star as it is deformed from its relaxed configuration. We expect the starquake to occur at the point where the strain has built up to some critical level where the crust can no longer support it.

We will model the special case where the starquake occurs when the star has reached zero angular velocity – this is **Star B** in the figure. This is now a strained configuration, and the strain field can be calculated from the displacement field $\xi^{\mathrm{AB}}(x^i)$ that connects particles in the unstrained Star A to their new positions in Star B.

We now need to specify our model of the glitch. We will use a special case of the model in Chapter 3:

> We again assume that all the strain is lost from the star at the glitch, so that the new, unstrained reference state of the star is that of Star B. Furthermore, we assume that this energy is just lost from the star (goes into heat), rather than going into kinetic or gravitational energy. This means that the mass distribution of the star will not be changed at the glitch: particles in Star C immediately after the glitch are not displaced from their positions in Star B.

After the glitch, the star will now be out of equilibrium (**Star C**), and so it will start to oscillate. These oscillations will be damped until the star finally reaches a new equilibrium configuration (**Star D**). This equilibrium state is deformed from its unstrained state, Star C, and so has some residual strain constructed from the displacement field ξ^{CD}. This means that although it has zero spin, it is not completely spherical.

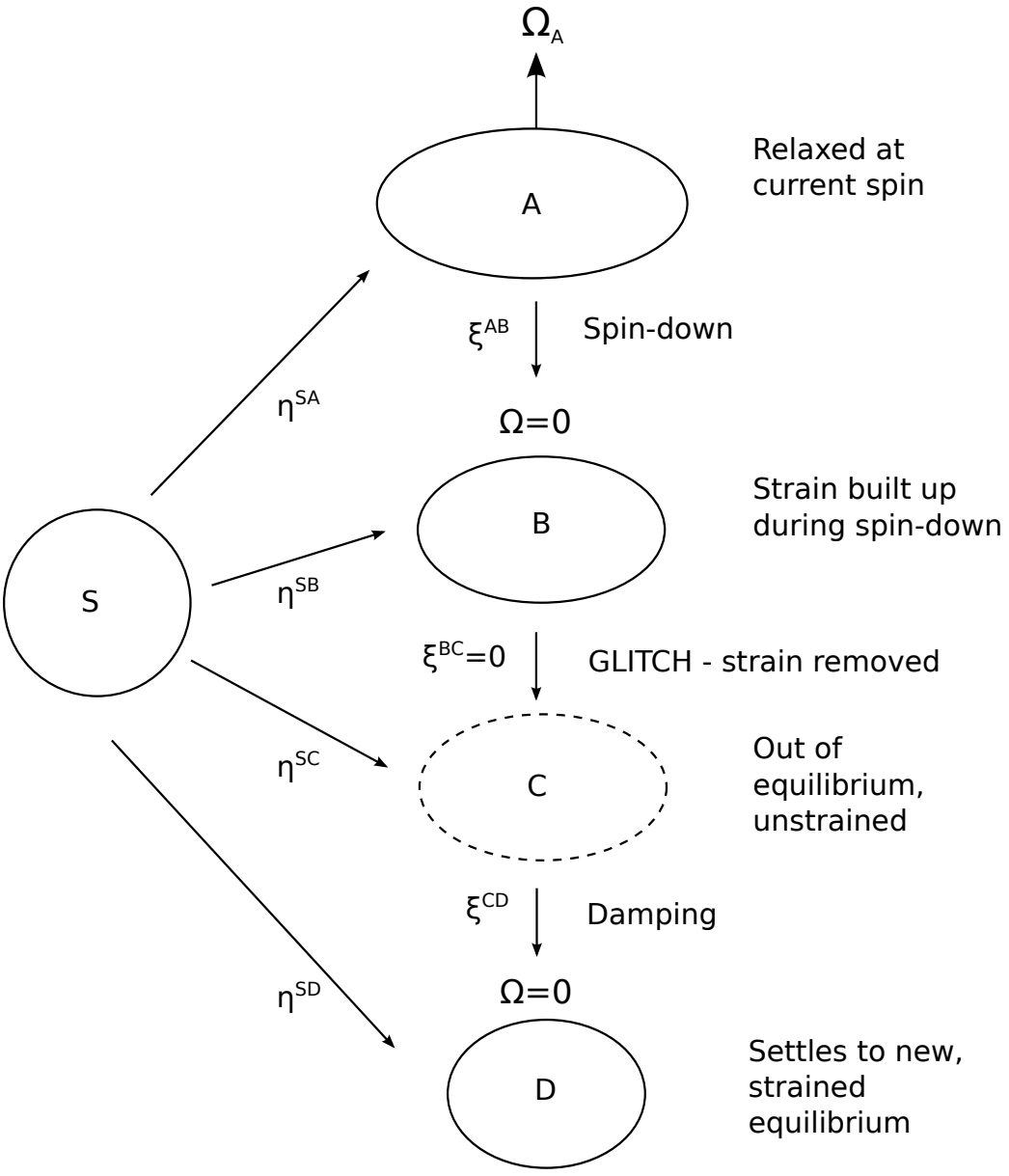

Figure 7.1: Diagram showing the main stages of the glitch model when the glitch occurs at zero spin. The star starts relaxed and spinning with initial velocity Ω_A. It then spins down to zero angular velocity, building up strain. The glitch is described by a sudden loss of strain, and the star then settles to a new equilibrium state. The equilibrium states A, B and D are found as perturbations about a spherical background, S. The maps η track the displacements of particles in S to their new positions in Stars A – D, while the ξ displacement fields map between A – D.

7.2 Energy estimates for the glitch model

In this section, we make some estimates of the energy released at the glitch, using the method of Chapter 3. This time, though we will be assuming that the glitch occurs at zero angular velocity, so that $\Omega_B = 0$. We will also be using our glitch model in which the strain is lost from the star at the glitch, so that the change in energy is the difference between the energies of Stars C and D (rather than that between B and D as in Chapter 3).

Specialising our results (3.5), (3.6) to $\Omega_B = 0$, we find that to first order in $b = \frac{B}{A}$, the ellipticities of Stars A and B are

$$\varepsilon_A = \frac{I_S \Omega_A^2}{4A}, \tag{7.1}$$

$$\varepsilon_B = b\,\varepsilon_A. \tag{7.2}$$

The energy of Star B in this case has no kinetic energy term:

$$E_B = E_S + A\varepsilon_B^2 + B\left(\varepsilon_A - \varepsilon_B\right)^2. \tag{7.3}$$

In our model, the star loses its strain energy at the glitch, so that immediately afterwards its energy is

$$E_C = E_S + A\varepsilon_B^2. \tag{7.4}$$

It then settles down to the new equilibrium state Star D, with $\Omega_D = 0$. Using our formula for the ellipticity of D (3.11) we have

$$\varepsilon_D = \frac{B}{A+B}\varepsilon_B, \tag{7.5}$$

This is $O(b^2)$, so that to the order we are working we can take the shape of Star D as spherical, and $\varepsilon_D = 0$. Its energy then only contains a strain contribution,

$$E_D = E_S + B\varepsilon_B^2, \tag{7.6}$$

and this is also $O(b^2)$, so that we can take its energy to be that of the spherical star, $E_D = E_S$. The energy available at the glitch is then the difference in energy between Stars C and D,

$$\Delta E_{CD} \equiv E_C - E_D = A\varepsilon_B^2. \tag{7.7}$$

We can write this as

$$\Delta E = \left(\frac{I_S \Omega_A^2}{4A}\right)^2 b^2. \tag{7.8}$$

This is the energy available to be converted into oscillations at the glitch. We expect the mode energy E_{mode} to have the form

$$E_{\text{mode}} \sim I_S \omega^2 \alpha_{CD}^2 \tag{7.9}$$

where ω is the frequency of the oscillations and α_{CD} is a dimensionless number characterising their amplitude. Equating this to the energy in the initial data ΔE (7.8), we find that for $b \ll 1$,

$$\alpha_{CD}^2 \sim \frac{1}{4}\left(\frac{\Omega_A}{\omega}\right)^2 b^2 \frac{I_S \Omega_A^2}{4A}\,. \tag{7.10}$$

For a star of density ρ and shear modulus μ we have the approximate scaling [16]

$$A \sim G\rho^2 R^5, \tag{7.11}$$

$$B \sim \mu R^3, \tag{7.12}$$

$$I_S \sim \rho R^5. \tag{7.13}$$

The oscillation mode frequency will depend on what kind of mode is excited. We have seen in Chapter 5 that our background star has two types of modes: elastic modes with a frequency $\omega \sim \sqrt{\frac{\mu}{\rho}}$, and a single mode similar to the f-mode of a fluid star. For these estimates we will use this fluid-type mode, which has scaling

$$\omega \sim \sqrt{G\rho}\,. \tag{7.14}$$

We will see later that this is a good choice for our particular initial data. Combining these, we get an estimate for the surface amplitude of the oscillations,

$$\alpha \sim \frac{\Omega_A^2}{G\rho}\left(\frac{B}{A}\right) = \frac{\mu \Omega_A^2}{G^2 R^2 \rho^3}\,. \tag{7.15}$$

We can use this as a consistency check for the scaling of the detailed amplitude calculations to follow.

7.3 Initial data for the glitch model

7.3.1 Plan of the calculation

Our initial data takes the form of a displacement and velocity field connecting the state of the star immediately after the glitch – Star C of our scheme – with the new equilibrium state, Star D.

We describe Stars A-D in terms of their deformation from the spherical background, Star S. This star has pressure p and gravitational potential Φ, and is in hydrostatic equilibrium

$$-\nabla_i p - \rho \nabla_i \Phi = 0. \tag{7.16}$$

The spherically symmetric solutions of this have pressure

$$p(r) = \frac{2\pi}{3} G\rho^2 (R^2 - r^2), \tag{7.17}$$

where R is the radius of the star.

To keep track of Lagrangian perturbations between different configurations, we label maps from the spherical background to Stars A-D with displacement fields η, and maps between Stars A-D with displacement fields ξ (see Figure 7.1). In this notation, the initial data we want to calculate is the displacement field ξ^{DC}.

We are also able to independently specify the initial velocity field, $\dot{\xi}^{\mathrm{DC}}$. In this toy model we take $\dot{\xi}^{\mathrm{DC}} = 0$, because we are assuming that the strain is suddenly removed from the star but the particles of the star remain at rest.

We find the initial data ξ^{DC} by constructing a sequence of equilibrium models to describe Stars A, B and D. Equilibria of this type were constructed in Chapter 4, so here we start by summarising the equations and boundary conditions that we need.

Each model obeys an equation of motion of the type

$$-\rho \nabla_i (\Omega^2 r^2 \cos^2\theta) = -\nabla_i \Delta p + \nabla_j T_{ij} - \rho \nabla_i \Delta\Phi, \tag{7.18}$$

where the centrifugal force is balanced by pressure, strain and gravitational potential perturbation terms.

Star C is out of equilibrium and so does not satisfy this equation of motion. However, we will see that in this case it is sufficient to specify the surface shape of Star C immediately after the glitch, which is the same as that of Star B.

For each equilibrium solution, we also have Poisson's equation for the gravitational perturbation (4.46)

$$\nabla^2 \delta\Phi = 4\pi G \delta\rho, \tag{7.19}$$

and the continuity equation (4.47)

$$\delta\rho + \nabla_i(\rho \xi^i) = 0. \tag{7.20}$$

The perturbations are also constrained to be incompressible,

$$\nabla_i \xi^i = 0. \tag{7.21}$$

At the surface, we have the traction boundary condition (4.50),

$$-(\Delta p(R))\delta_{ir} + 2\mu u_{ir}(R) = 0, \tag{7.22}$$

while the gravitational perturbation $\delta\Phi$ must satisfy the jump conditions (4.17)

$$[\delta\Phi]^{R+\epsilon}_{R-\epsilon} = 0, \tag{7.23}$$

$$\left[\frac{d}{dr}(\delta\Phi)\right]^{R+\epsilon}_{R-\epsilon} = 4\pi G\rho\xi_r(R,\theta,\phi). \tag{7.24}$$

7.3.2 Details of the calculation

Star A is an unstrained equilibrium configuration spinning at angular velocity Ω_A, and so satisfies the system of equations

$$-\rho\nabla_i(\Omega_A^2 r^2 \cos^2\theta) = -\nabla_i \Delta p^{\mathrm{SA}} - \rho\nabla_i \Delta\Phi^{\mathrm{SA}} \tag{7.25}$$

$$\nabla^2 \delta\Phi^{\mathrm{SA}} = 4\pi G\delta\rho^{\mathrm{SA}} \tag{7.26}$$

$$\delta\rho^{\mathrm{SA}} + \nabla_i(\rho(\xi^{\mathrm{SA}})^i) = 0, \tag{7.27}$$

along with the surface boundary condition

$$-(\Delta p^{\mathrm{SA}}(R))\delta_{ir} + 2\mu u^{\mathrm{SA}}_{ir}(R) = 0, \tag{7.28}$$

and the jump conditions (7.23), (7.24) on $\delta\Phi^{\mathrm{SA}}$. These are the same equations as a fluid star rotating at the same rate. In this case we are unable to fix the full displacement

field η^{SA}. However, we are able to find the radial component of η^{SA} evaluated at the surface,

$$(\eta^r)^{\mathrm{SA}}(R,\theta) = -\frac{5R\Omega_A^2}{8\pi G\rho}P_2(\cos\theta). \tag{7.29}$$

This is enough to find the surface shape of Star A, which we will find is all that is required for our model.

Star B is a strained, nonspinning equilibrium configuration which was relaxed when spinning at angular velocity Ω_A, and so satisfies

$$0 = -\nabla_i \Delta p^{\mathrm{SB}} - \nabla_j T_{ij}^{\mathrm{AB}} - \rho\nabla_i \Delta\Phi^{\mathrm{SB}}, \tag{7.30}$$

$$\nabla^2\delta\Phi^{\mathrm{SB}} = 4\pi G\delta\rho^{\mathrm{SB}}, \tag{7.31}$$

$$\delta\rho^{\mathrm{SB}} + \nabla_i(\rho(\xi^{\mathrm{SB}})^i) = 0 \tag{7.32}$$

along with the boundary condition

$$-(\Delta p^{\mathrm{SB}}(R))\delta_{ir} + 2\mu u_{ir}^{\mathrm{SB}}(R) = 0, \tag{7.33}$$

The pressure and gravitational potentials are perturbations about the spherical background S, while the strain force $\nabla_j T_{ij}^{\mathrm{AB}}$ is built from the displacement field ξ^{AB} between the unstrained Star A and the current configuration. This displacement field was calculated in Chapter 4 (4.84), (4.85); here we specialise to the case where the star was relaxed at Ω_A and is currently not spinning, $\Omega_B = 0$.

$$\boldsymbol{\xi}^{\mathrm{AB}}(r,\theta) = U^{\mathrm{AB}}(r)P_2(\cos\theta)\mathbf{e}_r + V^{\mathrm{AB}}(r)\boldsymbol{\nabla}P_2, \tag{7.34}$$

where $P_2(\cos\theta)$ are the $l=2$ Legendre polynomials, and the radial functions U^{AB} and V^{AB} are

$$U^{\mathrm{AB}}(r) = -\frac{1}{8\pi G\rho R^2}\frac{\Omega_A^2}{1+b}\left(3r^3 - 8R^2r\right), \tag{7.35}$$

$$V^{\mathrm{AB}}(r) = -\frac{1}{8\pi G\rho R^2}\frac{\Omega_A^2}{1+b}\left(\frac{5}{2}r^4 - 4R^2r^2\right). \tag{7.36}$$

Using this, we can also find the surface shape of Star B,

$$(\eta^r)^{\mathrm{SB}}(R,\theta) = -\frac{5R}{8\pi G\rho}\frac{b}{1+b}\Omega_A^2 P_2(\cos\theta). \tag{7.37}$$

Star C is out of equilibrium so we are unable to calculate maps between it and Star B in the same way. However, in our model it is sufficient to use the constraint that the surface shape is the same as that of Star B, $\eta_r^{\mathrm{SB}}(R) = \eta_r^{\mathrm{SC}}(R)$.

Star D is an equilibrium configuration, so we can again write the equations of motion for it as a perturbation about Star S:

$$0 = -\nabla_i \Delta p^{\mathrm{SD}} - \nabla_j T_{ij}^{\mathrm{CD}} - \rho \nabla_i \Delta \Phi^{\mathrm{SD}}, \tag{7.38}$$

$$\nabla^2 \delta\Phi^{\mathrm{SD}} = 4\pi G \delta\rho^{\mathrm{SD}}, \tag{7.39}$$

$$\delta\rho^{\mathrm{SD}} + \nabla_i(\rho(\xi^{\mathrm{SD}})^i) = 0 \tag{7.40}$$

Here the strain force term $\nabla_j T_{ij}^{\mathrm{CD}}$ depends on the deformation from the unstrained configuration C. As before we also have the surface boundary condition

$$-(\Delta p^{\mathrm{SD}}(R))\delta_{ir} + 2\mu u_{ir}^{\mathrm{CD}}(R) = 0, \tag{7.41}$$

To find the ξ^{CD} displacement field, we first write it in the form

$$\boldsymbol{\xi}^{\mathrm{CD}}(r,\theta) = U^{\mathrm{CD}}(r) P_2(\cos\theta)\mathbf{e}_r + V^{\mathrm{CD}}(r)\boldsymbol{\nabla} P_2, \tag{7.42}$$

as for ξ^{AB}. To fix U^{CD} and V^{CD}, we follow a similar method to that of Franco, Link and Epstein [30], defining h^{SD} such that

$$\mu h^{\mathrm{SD}} = -\Delta p^{\mathrm{SD}} - \rho \Delta \Phi^{\mathrm{SD}} \tag{7.43}$$

and using the mode equation (7.38) to find that

$$h^{\mathrm{SD}} = H_2 r^2 P_2(\cos\theta), \tag{7.44}$$

H_2 constant. Substituting this back into the mode equation and using the incompressibility condition (7.21), the displacement field is

$$U^{\mathrm{CD}}(r) = Cr - \frac{1}{7} H_2 r^3, \tag{7.45}$$

$$V^{\mathrm{CD}}(r) = \frac{1}{2} C r^2 - \frac{5}{42} H_2 r^4, \tag{7.46}$$

where C is another constant. This can be fixed along with H_2 by using the boundary conditions (7.41). From the $(r\theta)$ condition we get that $C = \frac{8}{21} H_2 R^2$, so that

$$U^{\mathrm{CD}}(r) = \frac{H_2}{21}\left(8R^2 r - 3r^3\right), \tag{7.47}$$

$$V^{\mathrm{CD}}(r) = \frac{H_2}{21}\left(4R^2 r^2 - \frac{5}{2}r^4\right). \tag{7.48}$$

For the (rr) condition, we can first write Δp^{SD} in terms of h^{SD} and $\Delta\Phi^{\mathrm{SD}}$ (7.43). To find $\Delta\Phi^{\mathrm{SD}}$, we use the jump conditions (7.23) and (7.24) on $\Delta\Phi$ to express it terms of the displacement field at the surface,

$$\Delta\Phi^{\mathrm{SD}} = \frac{8\pi G\rho}{15} r\left(\eta_r'^{\mathrm{SC}} + U^{\mathrm{CD}}(r)\right) P_2(\cos\theta). \tag{7.49}$$

We can then substitute in the form of U^{CD} (7.47), and the surface shape of Star C, $\eta_r'^{\mathrm{SC}}$. It is at this point that we use our model assumption that Star C has the same surface shape as Star B, (7.37).

Rearranging for H_2, we find

$$H_2 = \frac{21}{8\pi G\rho R^2}\frac{K\Omega_A^2}{(1+K)^2}, \tag{7.50}$$

and so the displacement field ξ^{CD} (7.42) is then given, with the radial functions

$$U^{\mathrm{CD}}(r) = \frac{1}{8\pi G\rho R^2}\frac{b}{(1+b)^2}\Omega_A^2\left(8R^2 r - 3r^3\right). \tag{7.51}$$

$$V^{\mathrm{CD}}(r) = \frac{1}{8\pi G\rho R^2}\frac{b}{(1+b)^2}\Omega_A^2\left(4R^2 r^2 - \frac{5}{2}r^4\right). \tag{7.52}$$

For $b \ll 1$ we find that at the surface

$$U^{\mathrm{CD}}(R) \sim -\frac{5R}{8\pi G\rho} b\Omega_A^2. \tag{7.53}$$

This shows the same scaling (7.15) as in our previous energy estimates in Section 7.2. We then find that the surface shape of Star D, $(\eta')^{\mathrm{SD}}(R)$, is

$$\eta^{\mathrm{SD}}(R,\theta) = -\lambda R\frac{K^2\Omega_A^2}{(1+K)^2}P_2(\cos\theta), \tag{7.54}$$

where we have also used the surface shape of Star C, (7.37).

In our model, we only determined the change in the displacement field at the star: we have not specified the pressure perturbation δp^{SD}. However, for a homogeneous star the shape of the star is enough to determine the gravitational potential perturbation, and we are able to calculate this. We have

$$\delta\Phi^{\mathrm{SD}} = B_2 r^2 P_2(\cos\theta), \tag{7.55}$$

with

$$B_2 = -\frac{4\pi G\rho}{5R}\eta_r'^{\mathrm{SD}}(R). \tag{7.56}$$

Inserting in the value of λ and rearranging, we get that

$$\delta\Phi^{\mathrm{SD}} = \frac{\Omega_A^2}{2}\frac{K^2}{(1+K)^2} r^2 P_2(\cos\theta). \tag{7.57}$$

To find $\delta\Phi^{\mathrm{CD}}$, we then need to subtract $\delta\Phi^{\mathrm{SC}}$, which is the same as $\delta\Phi^{\mathrm{SB}}$ (as the star's shape is unchanged immediately after the glitch). We derived this previously in Chapter 4 for arbitrary spin (4.95). Specialising to $\Omega = 0$ we get

$$\delta\Phi^{\mathrm{SC}} = \frac{1}{2}\frac{K\Omega_A^2}{1+K} r^2 P_2(\cos\theta) \tag{7.58}$$

so that

$$\delta\Phi^{\mathrm{CD}} = -\frac{1}{2}\frac{K\Omega_A^2}{(1+K)^2} r^2 P_2(\cos\theta). \tag{7.59}$$

7.3.3 Summary

For future reference, we collect together the main results of this section to obtain our initial data for the glitch model. This initial data takes the form of a map from the new equilibrium state Star D to Star C, so we will actually need the negative of the displacement field calculated here, $\xi^{\mathrm{DC}} = -\xi^{\mathrm{CD}}$. The initial displacement then takes the form

$$\boldsymbol{\xi}^{\mathrm{DC}}(r,\theta) = U^{\mathrm{DC}}(r) P_2(\cos\theta)\mathbf{e}_r + V^{\mathrm{DC}}(r)\boldsymbol{\nabla} P_2, \tag{7.60}$$

where

$$U^{\mathrm{DC}}(r) = -\frac{1}{8\pi G\rho R^2}\frac{b}{(1+b)^2}\Omega_A^2\left(8R^2 r - 3r^3\right). \tag{7.61}$$

$$V^{\mathrm{DC}}(r) = -\frac{1}{8\pi G\rho R^2}\frac{b}{(1+b)^2}\Omega_A^2\left(4R^2 r^2 - \frac{5}{2}r^4\right), \tag{7.62}$$

while the initial velocity is zero:

$$\dot{\boldsymbol{\xi}}^{\mathrm{DC}}(r,\theta) = 0. \tag{7.63}$$

The corresponding perturbed gravitational potential is

$$\delta\Phi^{\mathrm{CD}} = \frac{1}{2}\frac{K\Omega_A^2}{(1+K)^2} r^2 P_2(\cos\theta). \tag{7.64}$$

7.4 Projecting the initial data

In this section, we will take the calculated initial displacement field and project it against a basis of the eigenfunctions of Star D. In the current model where the star spins down to zero angular velocity before glitching, we can approximate Star D as spherical – this is shown in Appendix A. The eigenfunctions of D are then those of the spherical elastic star, calculated in Section 5.5.

This projection will give us the amplitudes of the modes excited. We will first outline how to do this, before moving on to discussing the results.

7.4.1 Theory

We will be projecting against a basis of eigenfunctions with the full, time-dependent form

$$\xi^{\alpha}(x,t) \equiv \xi^{\alpha}_{(0)}(x) e^{i\omega^{\alpha} t}. \tag{7.65}$$

Here, we have used the superscript α as a shorthand to label each mode, i.e. $\alpha \equiv (n,l,m)$. The initial data is then a sum over these modes, with each eigenfunction ξ^{α} excited by some amplitude b^{α}. The initial data is real, so to ensure that the sum over the eigenfunctions is also real we write it as

$$\xi^{\mathrm{ID}}(x) = \frac{1}{2}\sum_{\alpha}\left[b^{\alpha}\xi^{\alpha}_{(0)}(x) + b^{*\alpha}\xi^{*\alpha}_{(0)}(x)\right], \tag{7.66}$$

$$\dot{\xi}^{\mathrm{ID}}(x) = \frac{1}{2}\sum_{\alpha}\left[i\omega^{\alpha}b^{\alpha}\xi^{\alpha}_{(0)}(x) - i\omega^{\alpha}b^{*\alpha}\xi^{*\alpha}_{(0)}(x)\right]. \tag{7.67}$$

The complex conjugate is not really necessary in this chapter, where we are projecting against the real eigenfunctions of a nonrotating star. However, it will be required later when we extend to the rotating case and the eigenfunctions have an imaginary part, so for consistency we keep it in here.

We saw in Section 6.2 that these eigenfunctions are orthogonal with respect to the density ρ, which is constant throughout the star. We will scale our eigenfunctions so that they are orthonormal:

$$\left\langle \xi^{\beta}, \xi^{\alpha} \right\rangle = \delta^{\alpha\beta}. \tag{7.68}$$

Our aim is to find these amplitudes b^{α}, by using the orthogonality properties of the eigenfunctions ξ^{α}. First we take the inner product with one of the eigenfunctions, $\xi^{\beta}_{(0)}$:

$$\left\langle \xi^{\beta}_{(0)}, \xi^{\mathrm{ID}} \right\rangle = \frac{1}{2} \sum_{\alpha} \left[b^{\alpha} \left\langle \xi^{\beta}_{(0)}, \xi^{\alpha}_{(0)} \right\rangle + b^{*\alpha} \left\langle \xi^{\beta}_{(0)}, \xi^{*\alpha}_{(0)} \right\rangle \right], \tag{7.69}$$

$$\left\langle \xi^{\beta}_{(0)}, \dot{\xi}^{\mathrm{ID}} \right\rangle = \frac{1}{2} \sum_{\alpha} \left[i\omega^{\alpha} b^{\alpha} \left\langle \xi^{\beta}_{(0)}, \xi^{\alpha}_{(0)} \right\rangle - i\omega^{\alpha} b^{*\alpha} \left\langle \xi^{\beta}_{(0)}, \xi^{*\alpha}_{(0)} \right\rangle \right]. \tag{7.70}$$

Using orthogonality of the eigenfunctions,

$$\left\langle \xi^{\beta}_{(0)}, \xi^{\mathrm{ID}} \right\rangle = \frac{1}{2} \left(b^{\beta} + b^{*\beta} \right), \tag{7.71}$$

$$\left\langle \xi^{\beta}_{(0)}, \dot{\xi}^{\mathrm{ID}} \right\rangle = \frac{i}{2} \omega^{\beta} \left(b^{\beta} - b^{*\beta} \right). \tag{7.72}$$

Finally, we rearrange to get the amplitudes b^{β}. We have

$$b^{*\beta} = 2 \left\langle \xi^{\beta}_{(0)}, \xi^{\mathrm{ID}} \right\rangle - b^{\beta}, \tag{7.73}$$

so that eliminating $b^{*\beta}$ gives

$$\left\langle \xi^{\beta}_{(0)}, \dot{\xi}^{\mathrm{ID}} \right\rangle = \frac{i}{2} \omega^{\beta} b^{\beta} - \frac{i}{2} \omega^{\beta} \left(2 \left\langle \xi^{\beta}_{(0)}, \xi^{\mathrm{ID}} \right\rangle - b^{\beta} \right), \tag{7.74}$$

and the amplitudes are then

$$b^{\beta} = -\frac{i}{\omega^{\beta}} \left(\left\langle \xi^{\beta}_{(0)}, \dot{\xi}^{\mathrm{ID}} \right\rangle + i\omega^{\beta} \left\langle \xi^{\beta}_{(0)}, \xi^{\mathrm{ID}} \right\rangle \right). \tag{7.75}$$

7.4.2 Results

We can now use this result to project our initial displacement field (7.82) and (zero) velocity field against an orthonormal basis of the $l = 2$ spheroidal eigenfunctions (5.105) calculated in Section 5.5. We have shown that these have the form

$$\boldsymbol{\xi}_{2n}(x) = U_{2n}(x)P_2\,\mathbf{e}_x + V_{2n}(x)\frac{dP_2}{d\theta}\mathbf{e}_\theta, \tag{7.76}$$

where the radial functions U and V are

$$U_{2n}(x) = C_{2n}\left[2q_{2n}x + \frac{6}{k_{2n}x}j_2(k_{2n}x)\right], \tag{7.77}$$

$$V_{2n}(x) = C_{2n}\left[q_{2n}x + \frac{1}{k_{2n}x}j_2(k_{2n}x) + j_2'(k_{2n}x)\right]. \tag{7.78}$$

The C_{2n} are constants fixed by normalisation, and q_{2n} is the constant

$$q_{2n} = \frac{1}{2}\left[2j_2'(k_{2n}) + \left(\frac{10}{k_{2n}} - k_{2n}\right)\right]j_2(k_{2n}), \tag{7.79}$$

with

$$k_{2n} = \omega_{2n}\sqrt{\frac{\rho}{\mu}}\,. \tag{7.80}$$

Here we have scaled the eigenfunctions so that x is the fractional radius, $x = \frac{r}{R}$. The frequencies ω_{2n} are scaled so that $\omega_K = 1$, where ω_K is the $l = 2$ fundamental Kelvin mode of a fluid star; this is equivalent to specifying that

$$\sqrt{\frac{16\pi G\rho}{15}} = 1. \tag{7.81}$$

We also need to rescale our initial data (7.82) in the same way. After rescaling we have

$$\boldsymbol{\xi}^{\mathrm{DC}}(x,\theta) = U^{\mathrm{DC}}(x)P_2(\cos\theta)\mathbf{e}_r + V^{\mathrm{DC}}(x)\boldsymbol{\nabla}P_2, \tag{7.82}$$

where

$$U^{\mathrm{DC}}(x) = -\frac{2}{15}\frac{b}{(1+b)^2}\,\Omega_A^2\left(8x - 3x^3\right), \tag{7.83}$$

$$V^{\mathrm{DC}}(x) = -\frac{2}{15}\frac{b}{(1+b)^2}\,\Omega_A^2\left(4x^2 - \frac{5}{2}x^4\right). \tag{7.84}$$

The remaining free parameter is Ω_A^2. We will choose to scale our initial data so that

$$\Omega_A = 1. \tag{7.85}$$

We can now project the scaled initial data against our basis of eigenfunctions, obtaining the amplitudes b^α (7.75) using the methods of the last section.

Physically, we are more interested in the energy in each mode than its amplitude. As the modes we are interested in are all $m = 0$ modes, there is a point in each oscillation where the star is spherical and all the energy is kinetic. This means that we can use the kinetic energy in each mode to calculate energy in each mode,

$$E^\alpha = \frac{1}{2}(\omega^\alpha)^2 |b^\alpha|^2 \int_V |\xi^\alpha|^2 \, dV. \tag{7.86}$$

As our eigenfunctions are orthonormal, this just becomes

$$E^\alpha = \frac{1}{2}(\omega^\alpha)^2 |b^\alpha|^2. \tag{7.87}$$

Figure 7.2 shows the results of the projection for different values of $\frac{B}{A}$, ranging from the high value of $\frac{B}{A} = 0.1$ 7.2(a) down to the physical range of $\frac{B}{A} = 10^{-5}$ 7.2(e) and $\frac{B}{A} = 10^{-6}$ 7.2(f). The x-axis shows the radial number of the mode, while the y-axis shows the energy in that mode. In all of these plots, the most energy goes into the hybrid fluid-elastic mode discussed in Section 5.5; this is the mode with the frequency closest to the fundamental Kelvin mode of a purely fluid star. For the higher values of $\frac{B}{A}$, a significant proportion of the energy also goes into the lowest order modes: these are the shear modes with the lowest number of radial nodes. However, for physical values of $\frac{B}{A}$, almost all the energy (99.99% for $\frac{B}{A} = 10^{-5}$) goes into the fluid-elastic mode.

Finally, we can also check that we are reproducing the initial data correctly by reconstructing the sum over the eigenfunctions (7.65) with our calculated amplitudes b^α. We should expect to converge to the initial data as we add more modes in to the sum. Figure 7.3 shows the results of this for the illustrative case $\frac{B}{A} = 0.1$. The U and V parts of the initial data are plotted in the top row 7.3(a),7.3(b).

The middle row shows the results of summing progressively more eigenfunctions with our calculated amplitudes: defining the partial sum

$$\xi^{\text{partial}}(N, x) = \frac{1}{2} \sum_{\alpha=1}^{N} \left[b^\alpha \xi^\alpha_{(0)}(x) + b^{*\alpha} \xi^{*\alpha}_{(0)}(x) \right], \tag{7.88}$$

we have plotted $U^{\text{partial}}(N, x)$ 7.3(c) and $V^{\text{partial}}(N, x)$ 7.3(d) for $N = 1, \ldots, 10$. The largest contribution is from the $N = 3$ mode: this is the hybrid fluid-elastic mode for $\frac{B}{A} = 0.1$.

To test how the partial sums converge with increased N, in the last row we have plotted the U 7.3(e) and V 7.3(f) parts of the absolute value of the difference between $\xi^{\text{partial}}(N, x)$ and the initial data,

$$\xi^{\text{converge}}(N, x) = \left| \xi^{\text{partial}}(N, x) - \xi^{\text{ID}}(x) \right| \tag{7.89}$$

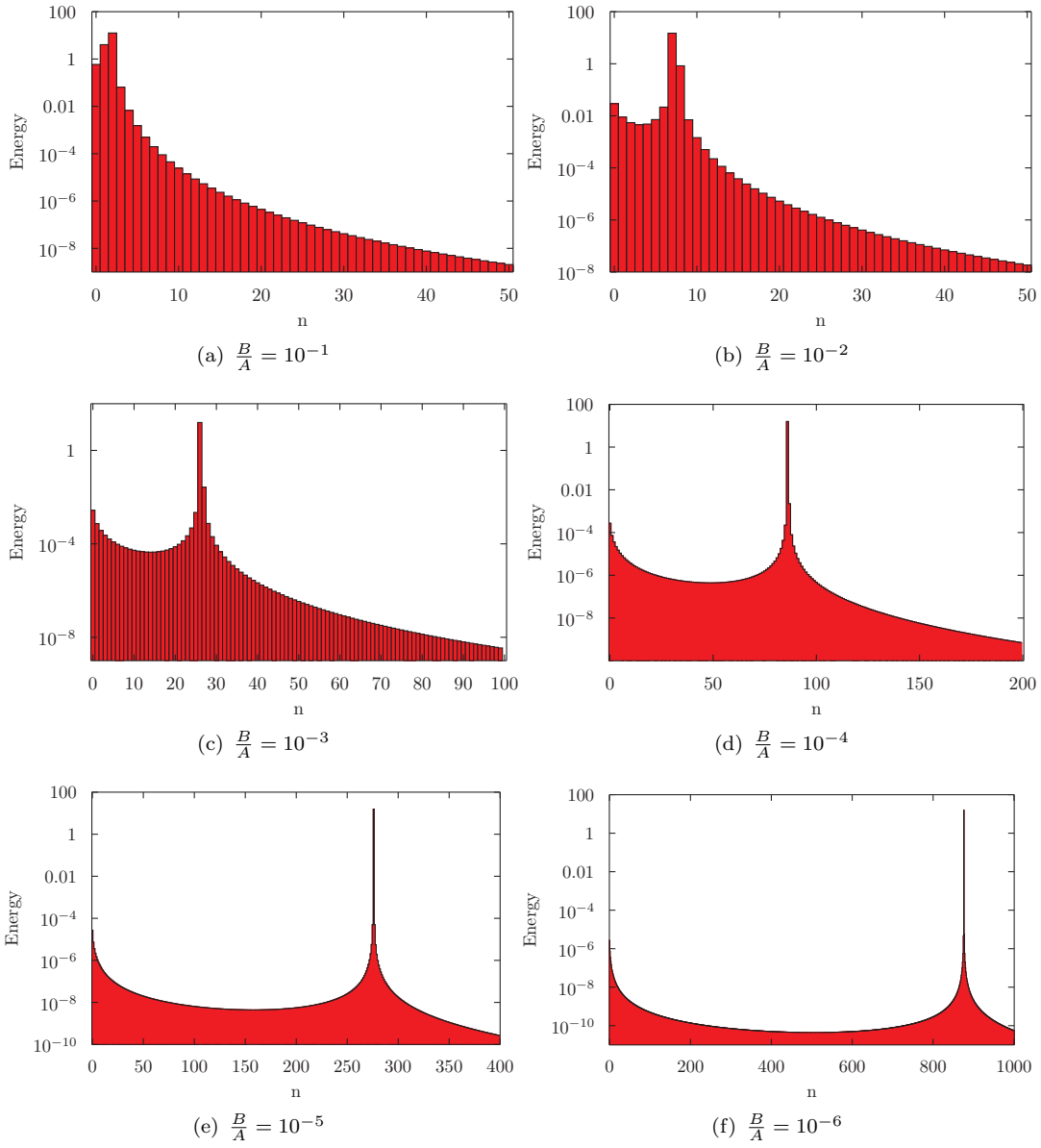

(a) $\frac{B}{A} = 10^{-1}$ (b) $\frac{B}{A} = 10^{-2}$

(c) $\frac{B}{A} = 10^{-3}$ (d) $\frac{B}{A} = 10^{-4}$

(e) $\frac{B}{A} = 10^{-5}$ (f) $\frac{B}{A} = 10^{-6}$

Figure 7.2: Figure showing the results of the projection for different values of $\frac{B}{A}$. The x-axis shows the radial number of the mode, while the y-axis shows the energy in that mode. The largest amount of energy goes into the hybrid fluid-elastic mode; this becomes more pronounced as $\frac{B}{A}$ is made smaller.

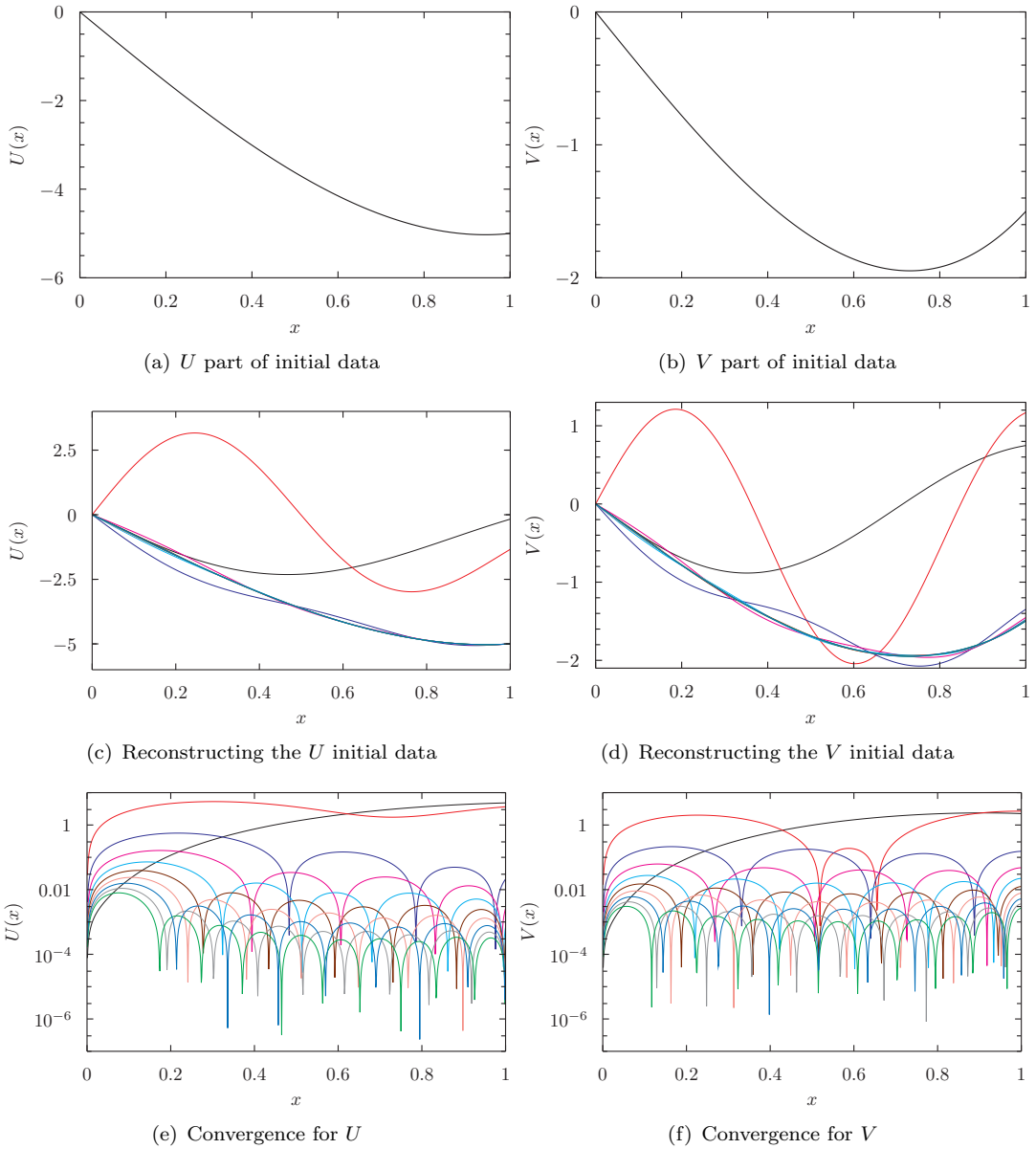

(a) U part of initial data

(b) V part of initial data

(c) Reconstructing the U initial data

(d) Reconstructing the V initial data

(e) Convergence for U

(f) Convergence for V

Figure 7.3: Figure showing the reproduction of the initial data as a sum of eigenfunctions for the case $\frac{B}{A} = 0.1$. The U and V parts of the initial data are shown in the top row. In the middle row, the partial sums $U^{\text{partial}}(N, x)$ and $V^{\text{partial}}(N, x)$ are shown for $N = 1$ (black line) up to $N = 10$ (green line); largest contribution is from the $N = 3$ eigenfunction (dark blue), which is the fluid-elastic hybrid mode. The bottom row plots the absolute value of the difference between the partial sums and the initial data, $U^{\text{converge}}(N, x)$ and $V^{\text{converge}}(N, x)$.

We can see that the contributions become progressively smaller as N increases.

Chapter 8

Oscillation modes: adding rotation

To model mode excitation of a glitching star, we will also need to account for the fact that the star is rotating. In this chapter we will add the effects of rotation in to our computation of the oscillation modes of our model.

We will assume that the star is rotating slowly, in the sense that the centrifugal force is small compared to the gravitational force at the surface of the star; this is a reasonable assumption for most pulsars. This approach was used for fluid stars by Cowling and Newing [25], and has also been developed in the geophysics literature [13, 67, 56]. Here we will mainly use the method of Strohmayer [80]. However, for consistency with previous chapters we will use somewhat different notation, so it will be useful to rederive some of the main results of the paper in our notation.

For a slowly rotating star of mass M, radius R and angular velocity Ω, we have that

$$\Omega^2 R \ll \frac{GM}{R^2}, \tag{8.1}$$

so that we can define a small dimensionless quantity

$$\varepsilon = \frac{\Omega}{\omega_*} \ll 1, \tag{8.2}$$

where

$$\omega_* = \sqrt{\frac{GM}{R^3}}. \tag{8.3}$$

We then expand our mode equation for the nonrotating star in this small parameter, keeping only terms up to first order. In general rotation at angular velocity $\mathbf{\Omega}$ will

introduce a Coriolis force $-\mathbf{\Omega} \times \dot{\boldsymbol{\xi}}$ and a centrifugal force $\mathbf{\Omega} \times (\mathbf{\Omega} \times \boldsymbol{\xi})$ in the rotating frame of the star. At first order in $\mathbf{\Omega}$ the centrifugal force can be neglected, so that the star can still be treated as spherical.

We will later be projecting our initial data against this set of modes; the initial data will be second order in the angular velocity Ω. However, we can still get consistent results up to first order in Ω by projecting against the rotation modes we have calculated to first order in this chapter.

8.1 Rotational corrections to the eigenfunctions

8.1.1 The mode equation for a rotating star

First, we write the mode equation of a nonrotating elastic incompressible star (5.31) as

$$A\ddot{\boldsymbol{\xi}} + C\boldsymbol{\xi} = 0, \tag{8.4}$$

where the operators A (6.79) and C (6.80) are defined as in Chapter 6,

$$A\boldsymbol{\xi} \equiv \rho\boldsymbol{\xi} \tag{8.5}$$

$$C\boldsymbol{\xi} \equiv \mu\boldsymbol{\nabla}^2\boldsymbol{\xi} - \boldsymbol{\nabla}\delta p - \rho\boldsymbol{\nabla}\Phi. \tag{8.6}$$

Next, we transform to a frame R rigidly rotating with the star. The velocity in the rotating frame can be defined with respect to the inertial frame I as

$$\left[\frac{d\boldsymbol{\xi}}{dt}\right]^R \equiv \left[\frac{d\boldsymbol{\xi}}{dt}\right]^I + \mathbf{\Omega} \times \boldsymbol{\xi}^I \tag{8.7}$$

The acceleration in the rotating frame is then

$$\left[\frac{d^2\boldsymbol{\xi}}{dt^2}\right]^R = \left[\frac{d^2\boldsymbol{\xi}}{dt^2}\right]^I + 2\,\mathbf{\Omega} \times \left[\frac{d\boldsymbol{\xi}}{dt}\right]^I + \mathbf{\Omega} \times \mathbf{\Omega} \times \boldsymbol{\xi}^I \tag{8.8}$$

The second term is the Coriolis force and the third term the centrifugal force. Dropping the I label, we can then write the mode equation (8.4) as

$$A\ddot{\boldsymbol{\xi}} + B\dot{\boldsymbol{\xi}} + C\boldsymbol{\xi} = 0, \tag{8.9}$$

where the new operator B is defined by

$$B\dot{\boldsymbol{\xi}} \equiv 2\rho\,\boldsymbol{\Omega} \times \frac{d\boldsymbol{\xi}}{dt} + \rho\,\boldsymbol{\Omega} \times \boldsymbol{\Omega} \times \boldsymbol{\xi}. \tag{8.10}$$

We will be looking for normal mode solutions of the form $\boldsymbol{\xi}(x,t) = e^{i\omega t}\boldsymbol{\xi}(x)$, so that

$$-\omega^2 A\boldsymbol{\xi} + i\omega B\boldsymbol{\xi} + C\boldsymbol{\xi} = 0. \tag{8.11}$$

First, though, we will make the slow rotation approximation, linearising in the small parameter ε (8.2).

8.1.2 Perturbations about the nonrotating star

We will now write the eigenfunction ξ and eigenvalue ω as

$$\xi = \xi_{(0)} + \varepsilon\xi_{(1)}, \tag{8.12}$$

$$\omega = \omega_{(0)} + \varepsilon\omega_{(1)}. \tag{8.13}$$

where we use the subscripts (0), (1) to indicate the order of the expansion in the rotational parameter ε.

The operators become

$$A = A_{(0)}, \tag{8.14}$$

$$B = \varepsilon B_{(1)}, \tag{8.15}$$

$$C = C_{(0)}. \tag{8.16}$$

To first order, our operator B (8.10) only retains the Coriolis term, i.e.

$$\varepsilon B_1 \xi_{(0)} = 2\rho\Omega\,\left(\hat{z} \times \xi_{(0)}\right), \tag{8.17}$$

or, using the definition of ε (8.2),

$$B_1 \xi_{(0)} = 2\omega_*\rho\,\left(\hat{z} \times \xi_{(0)}\right). \tag{8.18}$$

We can now put these definitions into the mode equation (8.11). To zeroth order in ε we get

$$-\omega_{(0)}^2 A_{(0)}\xi_{(0)} + C_{(0)}\xi_{(0)} = 0, \tag{8.19}$$

i.e. the mode equation for the nonrotating star, as expected. To first order in ε we have

$$-\omega_{(0)}^2 A_{(0)}\xi_{(1)} - 2\omega_{(0)}\omega_{(1)}A_{(0)}\xi_{(0)} + i\omega_{(0)}B_{(1)}\xi_{(0)} + C_{(0)}\xi_{(1)} = 0. \tag{8.20}$$

These two equations hold for any eigenfunction $\xi^\alpha_{(0)}$ and corresponding eigenvalue $\omega^\alpha_{(0)}$ of the nonrotating star. With the mode labels made explicit, the zeroth and first order equations in ε become

$$-\left(\omega^\alpha_{(0)}\right)^2 A_{(0)}\xi^\alpha_{(0)} + C_{(0)}\xi^\alpha_{(0)} = 0, \tag{8.21}$$

and

$$-\left(\omega^\alpha_{(0)}\right)^2 A_{(0)}\xi^\alpha_{(1)} - 2\omega^\alpha_{(0)}\omega^\alpha_{(1)}A_{(0)}\xi^\alpha_{(0)} + i\omega^\alpha_{(0)}B_{(1)}\xi^\alpha_{(0)} + C_{(0)}\xi^\alpha_{(1)} = 0. \tag{8.22}$$

The eigenfunctions $\xi_{(0)}$ form a complete set for the nonrotating star. We will write $\xi_{(1)}$ as a sum over this set as

$$\xi^\alpha_{(1)} = \sum_\beta \lambda^{\alpha\beta}_{(1)}\xi^\beta_{(0)}, \tag{8.23}$$

where the $\lambda_{(1)}$ are constants. Substituting this into the first order equation (8.20) gives

$$-\sum_\beta \lambda^{\alpha\beta}_{(1)}\left(\omega^\alpha_{(0)}\right)^2 A_{(0)}\xi^\beta_{(0)} - 2\omega^\alpha_{(0)}\omega^\alpha_{(1)}A_{(0)}\xi^\alpha_{(0)} + i\omega^\alpha_{(0)}B_{(1)}\xi^\alpha_{(0)} + \sum_\beta \lambda^{\alpha\beta}_{(1)}C_{(0)}\xi^\beta_{(0)} = 0. \tag{8.24}$$

Now we utilise the zeroth order equation (8.21), writing

$$C_{(0)}\xi^\beta_{(0)} = \left(\omega^\beta_{(0)}\right)^2 A_{(0)}\xi^\beta_{(0)}. \tag{8.25}$$

The first order equation (8.26) becomes

$$-\sum_\beta \lambda^{\alpha\beta}_{(1)}\left(\omega^\alpha_{(0)}\right)^2 A_{(0)}\xi^\beta_{(0)} - 2\omega^\alpha_{(0)}\omega^\alpha_{(1)}A_{(0)}\xi^\alpha_{(0)} + i\omega^\alpha_{(0)}B_{(1)}\xi^\alpha_{(0)} + \sum_\beta \lambda^{\alpha\beta}_{(1)}\left(\omega^\beta_{(0)}\right)^2 A_{(0)}\xi^\beta_{(0)} = 0. \tag{8.26}$$

Rearranging we get

$$-\sum_\beta \left(\left(\omega^\alpha_{(0)}\right)^2 - \left(\omega^\beta_{(0)}\right)^2\right)\lambda^{\alpha\beta}_{(1)}A_{(0)}\xi^\beta_{(0)} - 2\omega^\alpha_{(0)}\omega^\alpha_{(1)}A_{(0)}\xi^\alpha_{(0)} + i\omega^\alpha_{(0)}B_{(1)}\xi^\alpha_{(0)} = 0. \tag{8.27}$$

At this point, we can put the operators $A_{(0)}$ (8.5) and $B_{(1)}$ (8.18) back in. This gives

$$-\sum_{\beta}\left(\left(\omega^{\alpha}_{(0)}\right)^2-\left(\omega^{\beta}_{(0)}\right)^2\right)\lambda^{\alpha\beta}_{(1)}\xi^{\beta}_{(0)}-2\omega^{\alpha}_{(0)}\omega^{\alpha}_{(1)}\xi^{\alpha}_{(0)}+2i\omega_*\omega^{\alpha}_{(0)}\left(\hat{z}\times\xi^{\alpha}_{(0)}\right)=0. \quad (8.28)$$

We can use this equation to find rotational corrections to the eigenfunctions and eigenvalues.

8.1.3 Rotational corrections to the eigenvalues

To find the corrections to the eigenvalues, we can take an inner product of our equation (8.27) with $\xi^{\alpha}_{(0)}$:

$$\begin{aligned}-\sum_{\beta}\left(\left(\omega^{\alpha}_{(0)}\right)^2-\left(\omega^{\beta}_{(0)}\right)^2\right)\lambda^{\alpha\beta}_{(1)}\left\langle\xi^{\alpha}_{(0)},A_{(0)}\xi^{\beta}_{(0)}\right\rangle-2\omega^{\alpha}_{(0)}\omega^{\alpha}_{(1)}\left\langle\xi^{\alpha}_{(0)},A_{(0)}\xi^{\alpha}_{(0)}\right\rangle\\ +i\omega^{\alpha}_{(0)}\left\langle\xi^{\alpha}_{(0)},B_{(1)}\xi^{\alpha}_{(0)}\right\rangle=0.\end{aligned} \quad (8.29)$$

We have shown in Section 6.5 that the eigenfunctions are orthogonal with respect to the operator $A_{(0)}$:

$$\left\langle\xi^{\alpha}_{(0)},A_{(0)}\xi^{\beta}_{(0)}\right\rangle=0,\quad \alpha\neq\beta. \quad (8.30)$$

Using this, we find that all terms of the sum are zero, and

$$-2\omega^{\alpha}_{(1)}\left\langle\xi^{\alpha}_{(0)},A_{(0)}\xi^{\alpha}_{(0)}\right\rangle+i\left\langle\xi^{\alpha}_{(0)},B_{(1)}\xi^{\alpha}_{(0)}\right\rangle=0. \quad (8.31)$$

Rearranging, we get an expression for the corrections to the eigenvalues,

$$\omega^{\alpha}_{(1)}=\frac{i}{2}\frac{\left\langle\xi^{\alpha}_{(0)},B_{(1)}\xi^{\alpha}_{(0)}\right\rangle}{\left\langle\xi^{\alpha}_{(0)},A_{(0)}\xi^{\alpha}_{(0)}\right\rangle}. \quad (8.32)$$

Substituting in the operators $A_{(0)}$ (8.5) and $B_{(1)}$, (8.18), we have

$$\omega^{\alpha}_{(1)}=i\omega_*\frac{\left\langle\xi^{\alpha}_{(0)},\rho\left(\hat{z}\times\xi^{\alpha}_{(0)}\right)\right\rangle}{\left\langle\xi^{\alpha}_{(0)},\rho\xi^{\alpha}_{(0)}\right\rangle}. \quad (8.33)$$

8.1.4 Rotational corrections to the eigenfunctions

To reproduce the results for corrections to the eigenfunctions, we will instead take the inner product of our equation (8.27) with another eigenfunction $\xi^{\gamma}_{(0)}$, with $\gamma\neq\alpha$:

$$-\sum_{\beta}\left(\left(\omega^{\alpha}_{(0)}\right)^2-\left(\omega^{\beta}_{(0)}\right)^2\right)\lambda^{\alpha\beta}_{(1)}\left\langle\xi^{\gamma}_{(0)},A_{(0)}\xi^{\beta}_{(0)}\right\rangle-2\omega^{\alpha}_{(0)}\omega^{\alpha}_{(1)}\left\langle\xi^{\gamma}_{(0)},A_{(0)}\xi^{\alpha}_{(0)}\right\rangle \\ +i\omega^{\alpha}_{(0)}\left\langle\xi^{\gamma}_{(0)},B_{(1)}\xi^{\alpha}_{(0)}\right\rangle=0. \tag{8.34}$$

The second term is zero, as $\gamma\neq\alpha$. Also all terms of the sum except $\beta=\gamma$ are zero, leaving

$$\left(\left(\omega^{\alpha}_{(0)}\right)^2-\left(\omega^{\gamma}_{(0)}\right)^2\right)\lambda^{\alpha\gamma}_{(1)}\left\langle\xi^{\gamma}_{(0)},A_{(0)}\xi^{\gamma}_{(0)}\right\rangle+i\omega^{\alpha}_{(0)}\left\langle\xi^{\gamma}_{(0)},B_{(1)}\xi^{\alpha}_{(0)}\right\rangle=0. \tag{8.35}$$

This gives us a formula for the first order corrections to the eigenfunctions for $\alpha\neq\gamma$,

$$\lambda^{\alpha\gamma}_{(1)}=\frac{i\omega^{\alpha}_{(0)}}{\left(\omega^{\alpha}_{(0)}\right)^2-\left(\omega^{\gamma}_{(0)}\right)^2}\frac{\left\langle\xi^{\gamma}_{(0)},B_{(1)}\xi^{\alpha}_{(0)}\right\rangle}{\left\langle\xi^{\gamma}_{(0)},A_{(0)}\xi^{\gamma}_{(0)}\right\rangle}. \tag{8.36}$$

Next, we will demonstrate that for $\alpha=\gamma$, we can choose the coefficient $\lambda^{\alpha\alpha}_{(1)}$ to be zero. Here we follow an argument of Rae [72]. First, suppose we have taken an orthonormal set of zeroth order eigenfunctions:

$$\left\langle\xi^{\gamma}_{(0)},\rho\xi^{\gamma}_{(0)}\right\rangle=1, \tag{8.37}$$

and we want each rotationally corrected eigenfunction to be normalised in the same way, i.e.

$$\langle\xi^{\gamma},\rho\xi^{\gamma}\rangle=1, \tag{8.38}$$

$$\xi^{\gamma}=\xi^{\gamma}_{(0)}+\varepsilon\sum_{\alpha}\lambda^{\gamma\alpha}_{(1)}\xi^{\alpha}_{(0)}. \tag{8.39}$$

Writing out the inner product in full, we have

$$\left\langle\xi^{\gamma}_{(0)},\rho\xi^{\gamma}_{(0)}\right\rangle+\varepsilon\sum_{\alpha}(\lambda^{\gamma\alpha}_{(1)})^*\left\langle\xi^{\alpha}_{(0)},\rho\xi^{\gamma}_{(0)}\right\rangle+\varepsilon\sum_{\alpha}\lambda^{\gamma\alpha}_{(1)}\left\langle\xi^{\gamma}_{(0)},\rho\xi^{\alpha}_{(0)}\right\rangle+O(\lambda^{\gamma\alpha}_{(1)})^2=1. \tag{8.40}$$

The first term is 1 as the zeroth order eigenfunctions are orthonormal (8.37). In the sums, only the $\gamma=\alpha$ terms are nonzero, which leaves

$$(\lambda^{\alpha\alpha}_{(1)})^*=-\lambda^{\alpha\alpha}_{(1)}. \tag{8.41}$$

This means that the constant $\lambda^{\alpha\alpha}_{(1)}$ is purely imaginary:

$$\lambda_{(1)}^{\alpha\alpha} = ib \tag{8.42}$$

where b is real. Then we can write our eigenfunction ξ^γ as

$$\xi^\gamma = (1 + ib)\,\xi_{(0)}^\gamma + \varepsilon \sum_{\alpha\neq\gamma} \lambda_{(1)}^{\gamma\alpha}\xi_{(0)}^\alpha \tag{8.43}$$

To first order in b, we have $\exp(ib) \approx 1 + ib$, so that to the same order

$$\xi^\gamma = e^{ib}\xi_{(0)}^\gamma + \varepsilon \sum_{\alpha\neq\gamma} \lambda_{(1)}^{\gamma\alpha}\xi_{(0)}^\alpha \tag{8.44}$$

The $\exp(ib^\gamma)$ is just an overall phase factor in the definition of $\xi_{(0)}^\gamma$, which can be chosen arbitrarily. We will pick

$$b = 0, \tag{8.45}$$

so that our coefficients $\lambda_{(1)}^{\alpha\alpha}$ are zero.

8.2 Specialising to spheroidal and toroidal corrections

When calculating explicit values for the eigenfunctions and eigenvalues, it will be necessary to consider the spheroidal and toroidal parts separately. We will call the spheroidal zeroth order eigenfunctions $S_{(0)}^\alpha$, with

$$S_{(0)}^\alpha(r) = U^{nl}(r)Y_{lm}\hat{r} + V^{nl}\boldsymbol{\nabla}Y_{lm} \tag{8.46}$$

as in previous chapters. The toroidal zeroth order eigenfunctions $T_{(0)}^\alpha$ are

$$T_{(0)}^\alpha(r) = W^{nl}(r)\hat{r} \times \boldsymbol{\nabla}Y_{lm}. \tag{8.47}$$

8.2.1 Eigenvalue corrections

The formula (8.33) for the corrections to the eigenvalues becomes

$$(\omega_{(1)})_S^\alpha = i\omega_* \frac{\left\langle S_{(0)}^\alpha, \rho\left(\hat{z} \times S_{(0)}^\alpha\right)\right\rangle}{\left\langle S_{(0)}^\alpha, \rho S_{(0)}\right\rangle}, \tag{8.48}$$

for corrections to spheroidal eigenvalues and

$$(\omega_{(1)})^{\alpha}_{T} = i\omega_{*}\frac{\left\langle T^{\alpha}_{(0)}, \rho\left(\hat{z}\times T^{\alpha}_{(0)}\right)\right\rangle}{\left\langle T^{\alpha}_{(0)}, \rho T_{(0)}\right\rangle}. \tag{8.49}$$

for corrections to toroidal eigenvalues.

Full derivations of these corrections and those for the eigenfunctions can be found in Strohmayer [79]; here we will just state the results,

$$(\omega_{(1)})^{nlm}_{S} = m\omega^{*}\frac{\int_0^R \left[2rU_{nl}V_{nl} + (V_{nl})^2\right]\rho(r)dr}{\int_0^R \left[(U_{nl})^2r^2 + l(l+1)(V_{nl})^2\right]\rho(r)dr} \tag{8.50}$$

for the spheroidal corrections and

$$(\omega_{(1)})^{nlm}_{T} = \frac{m\omega^{*}}{l(l+1)}. \tag{8.51}$$

for the toroidal corrections.

8.2.2 Eigenfunction corrections

For the eigenfunctions, we will also need to separate out the spheroidal and toroidal corrections. We will write the full spheroidal eigenfunctions $S = S_{(0)} + \varepsilon S_{(1)}$ as

$$S^{\alpha} = S^{\alpha}_{(0)} + \varepsilon\sum_{\gamma}\left([SS]^{\alpha\gamma}_{(1)}S^{\gamma}_{(0)} + [ST]^{\alpha\gamma}_{(1)}T^{\gamma}_{(0)}\right), \tag{8.52}$$

specialising our formula for the corrections $\lambda^{\alpha\gamma}_{(1)}$ (8.36) where the $[SS]^{\alpha\gamma}_{(1)}$ are spheroidal corrections to the spheroidal eigenfunctions,

$$[SS]^{\alpha\gamma}_{(1)} = \frac{i\omega^{\alpha}_{S}\left\langle S^{\gamma}_{(0)}, \rho\left(\hat{z}\times S^{\alpha}_{(0)}\right)\right\rangle}{\left(\left(\omega^{\alpha}_{S}\right)^2 - \left(\omega^{\gamma}_{S}\right)^2\right)\left\langle S^{\alpha}_{(0)}, \rho S_{(0)}\right\rangle}, \quad \alpha\neq\gamma, \tag{8.53}$$

and the $[ST]^{\alpha\gamma}_{(1)}$ are toroidal corrections to the spheroidal eigenfunctions,

$$[ST]^{\alpha\gamma}_{(1)} = \frac{i\omega^{\alpha}_{T}\left\langle S^{\gamma}_{(0)}, \rho\left(\hat{z}\times T^{\alpha}_{(0)}\right)\right\rangle}{\left(\left(\omega^{\alpha}_{T}\right)^2 - \left(\omega^{\gamma}_{S}\right)^2\right)\left\langle S^{\alpha}_{(0)}, \rho S_{(0)}\right\rangle}, \quad \alpha\neq\gamma. \tag{8.54}$$

Again, we will just state the results of Strohmayer. A spheroidal zeroth order eigenfunctions with mode label $\alpha = (n, l, m)$ only couples to spheroidal modes with the same l and m value, and to toroidal modes with the same m and $l' = l-1$ or $l' = l+1$. Specifically, the corrected spheroidal eigenfunctions are

$$(S^{nlm}) = S^{nlm}_{(0)} + \varepsilon \sum_{n=1}^{\infty} \Big([SS]^{nlm,n'lm}_{(1)} S^{n'lm}_{(0)} + [ST]^{nlm,n'l-1m}_{(1)} T_{n'l-1m} + [ST]^{nlm,n'l+1m}_{(1)} T_{n'l+1m} \Big), \tag{8.55}$$

where

$$[SS]^{nlm,n'lm}_{(1)} = \frac{2m\omega_* \omega_S^{nlm} \int_0^R \left[V_{nl} U_{n'l} + U_{nl} V_{n'l} + V_{nl} V_{n'l} \right] \rho r^2 dr}{(\omega_S^{nlm})^2 - (\omega_T^{n'lm})^2 \int_0^R \left[(U_{n'l})^2 + l(l+1) \left(V_{n'l} \right)^2 \right] \rho r^2 dr} \tag{8.56}$$

$$[ST]^{nlm,n'l-1m}_{(1)} = -\frac{2i\omega_* \omega_S^{nlm} (l+m) \int_0^R \left[W_{n'l-1} (U_{nl} + (l+1) V_{nl}) \right] \rho r^2 dr}{l(2l+1) \left((\omega_S^{nlm})^2 - (\omega_T^{n'l-1m})^2 \right) \int_0^R \left(W_{n'l-1} \right)^2 \rho r^2 dr} \tag{8.57}$$

$$[ST]^{nlm,n'l+1m}_{(1)} = -\frac{2i\omega_* \omega_S^{nlm} (l-m+1) \int_0^R \left[W_{n'l+1} (l V_{nl} - U_{nl}) \right] \rho r^2 dr}{(l+1)(2l+1) \left((\omega_S^{nlm})^2 - (\omega_T^{n'l+1m})^2 \right) \int_0^R \left(W_{n'l+1} \right)^2 \rho r^2 dr} \tag{8.58}$$

Note that the second and third of these have a different sign to those of Strohmayer; this is because of an opposite sign convention to his for the toroidal eigenfunctions.

In the same way, we will write the full toroidal eigenfunctions as

$$T^{\alpha} = T^{\alpha}_{(0)} + \varepsilon \sum_{\gamma} \left([TS]^{\alpha\gamma}_{(1)} S^{\gamma}_{(0)} + [TT]^{\alpha\gamma}_{(1)} T^{\gamma}_{(0)} \right), \tag{8.59}$$

where the spheroidal corrections to the toroidal eigenfunctions are

$$[TS]^{\alpha\gamma}_{(1)} = \frac{i\omega_S^{\alpha} \left\langle T^{\gamma}_{(0)}, \rho \left(\hat{z} \times S^{\alpha}_{(0)} \right) \right\rangle}{\left(\left(\omega_S^{\alpha} \right)^2 - \left(\omega_T^{\gamma} \right)^2 \right) \left\langle T^{\gamma}_{(0)}, \rho T^{\gamma}_{(0)} \right\rangle}, \quad \alpha \neq \gamma, \tag{8.60}$$

and the toroidal corrections to the toroidal eigenfunctions are

$$[TT]^{\alpha\gamma}_{(1)} = \frac{i\omega_T^{\alpha} \left\langle T^{\gamma}_{(0)}, \rho \left(\hat{z} \times T^{\alpha}_{(0)} \right) \right\rangle}{\left(\left(\omega_T^{\alpha} \right)^2 - \left(\omega_T^{\gamma} \right)^2 \right) \left\langle T^{\gamma}_{(0)}, \rho T^{\gamma}_{(0)} \right\rangle}, \quad \alpha \neq \gamma. \tag{8.61}$$

The toroidal eigenfunctions only couple to spheroidal eigenfunctions with the same m value and $l = l - 1$ or $l = l + 1$; the coefficients $[TT]^{\alpha\gamma}_{(1)}$ are all zero. In full, we have

$$T^{nlm} = T^{nlm}_{(0)} + \varepsilon \sum_{n'=1}^{\infty} \left[[TS]^{nlm,n'l-1m}_{(1)} S^{n'l-1m}_{(0)} + [TS]^{nlm,n'l+1m}_{(1)} S^{n'l+1m}_{(0)} \right], \tag{8.62}$$

where

$$[TS]^{nlm,n'l-1m}_{(1)} = \frac{2i\omega_* \omega_T^{nlm}(l+1)(l+m)}{(2l+1)\left((\omega_T^{nlm})^2 - (\omega_S^{n'l-1m})^2\right)} \cdot \frac{\int_0^R \left[W_{nl}(U_{n'l-1} - (l-1)V_{n'l-1})\right] \rho r^2 dr}{\int_0^R \left[(U_{n'l-1})^2 + l(l-1)\left(V_{n'l-1}\right)^2\right] \rho dr}, \tag{8.63}$$

$$[TS]^{nlm,n'l+1m}_{(1)} = -\frac{2i\omega_* \omega_T^{nlm} l(l-m+1)}{(2l+1)\left((\omega_T^{nlm})^2 - (\omega_S^{n'l+1m})^2\right)} \cdot \frac{\int_0^R \left[W_{nl}(U_{n'l+1} + (l+2)V_{n'l+1})\right] \rho r^2 dr}{\int_0^R \left[(U_{n'l+1})^2 + (l+1)(l+2)\left(V_{n'l+1}\right)^2\right] \rho r^2 dr}. \tag{8.64}$$

Again, these have the opposite sign to those of Strohmayer.

8.3 Numerical investigation of the eigenfunctions

Our initial data for the glitch will still be axisymmetric for the rotating case, so we can specialise to $m = 0$. The toroidal and spheroidal corrections to the eigenvalues (8.50),(8.51) both vanish in this case.

As in our previous numerical work in Chapters 5 and 7, we will scale the equations so that the radius $R = 1$. We will also scale the frequencies so that the $l = 2$ fluid Kelvin mode $\omega_K = 1$ (7.81), i.e.

$$\frac{16\pi}{15} G\rho = 1. \tag{8.65}$$

With this choice, the parameter σ_* (8.3) becomes

$$\sigma_* = \frac{\sqrt{5}}{2}. \tag{8.66}$$

In spherical coordinate components, the full eigenfunctions (8.52), (8.62) for $m = 0$ look like

$$S^{nl0} = \begin{pmatrix} U^{nl0} P_l \\ V^{nl0} \frac{dP_l}{d\theta} \\ 0 \end{pmatrix} + \varepsilon \sum_{n'=1}^{\infty} \begin{pmatrix} 0 \\ 0 \\ [ST]^{nl0,n'l-10}_{(1)} W^{n'l-10} P_{l-1} + [ST]^{nl0,n'30}_{(1)} W^{n'l+10} P_{l+1} \end{pmatrix}. \tag{8.67}$$

and

$$T^{nl0} = \begin{pmatrix} 0 \\ 0 \\ W^{nl0} P_2 \end{pmatrix} + \varepsilon \sum_{n'=1}^{\infty} \begin{pmatrix} [TS]^{nl0,n'l-10}_{(1)} U^{n'l-10}_{(0)} P_{l-1} + [TS]^{nl0,n'l+10}_{(1)} U^{n'l+10}_{(0)} P_{l+1} \\ [TS]^{nl0,n'l-10}_{(1)} V^{n'l-10}_{(0)} \frac{dP_{l-1}}{d\theta} + [TS]^{nl0,n'l+10}_{(1)} V^{n'l+10}_{(0)} \frac{dP_{l+1}}{d\theta} \\ 0 \end{pmatrix}. \tag{8.68}$$

To calculate these eigenfunctions numerically, we will have to truncate the infinite sums over the radial eigenvalue n' at some finite number. It will be useful to define the partial sum

$$\left(S^{\text{partial}}\right)^{nl0}_{N} \equiv \begin{pmatrix} U^{nl0} P_l \\ V^{nl0} \frac{dP_l}{d\theta} \\ 0 \end{pmatrix} + \varepsilon \sum_{n'=1}^{N} (\text{correction terms...}), \tag{8.69}$$

where the sum is taken up to the mode with $n' = N$; similarly, for the toroidal eigenfunctions we define

$$\left(T^{\text{partial}}\right)^{nl0}_{N} = \begin{pmatrix} 0 \\ 0 \\ W^{nl0} P_2 \end{pmatrix} + \varepsilon \sum_{n'=1}^{N} (\text{correction terms...}). \tag{8.70}$$

As an initial test of our glitch model for the rotating case, we will only investigate the case $\frac{B}{A} = 0.1$. Although this is not a realistic physical value, it is a useful first test case for how to carry out the projection, because the hybrid fluid-elastic mode in this case is at a low radial eigenvalue number of $n = 3$. This means that we can truncate at a relatively low n' in the sum and still retain this mode. Specifically, we will choose to truncate at $n' = 10$.

For the spheroidal eigenfunctions, the rotational corrections are to the ϕ component only. To see the convergence of these corrections, we will calculate the partial sums $\left(S^{\text{partial}}\right)^{nl0}_{N}$ for $N = 1, \ldots, 10$. We then plot the ϕ component of the functions $(S^{\text{converge}})^{nl0}_{N}$, defined as

$$(S^{\text{converge}})^{nl0}_{N} \equiv \left| \left(S^{\text{partial}}\right)^{nl0}_{N} - \left(S^{\text{partial}}\right)^{nl0}_{10} \right|, \tag{8.71}$$

for $N = 1, \ldots, 9$, to show that the absolute value of the corrections decreases as more modes are included.

This is shown in Figure 8.1 for $l = 2$ and $n = 1, 2, 3$. The $l = 2$ spheroidal modes are of greatest interest to us, because this is the form of the displacement field in our initial data, and so we can expect these to be excited the most.

The corrections to the toroidal eigenfunctions are in the r and θ components only. To show the convergence of these corrections, we plot the r-components of the functions $(T^{\text{converge}})_N^{nl0}$, defined similarly as

$$(T^{\text{converge}})_N^{nl0} \equiv \left| \left(T^{\text{partial}}\right)_N^{nl0} - \left(T^{\text{partial}}\right)_{10}^{nl0} \right|. \tag{8.72}$$

This is shown in Figure 8.2, again for the cases of $l = 2$ and $n = 1, 2, 3$.

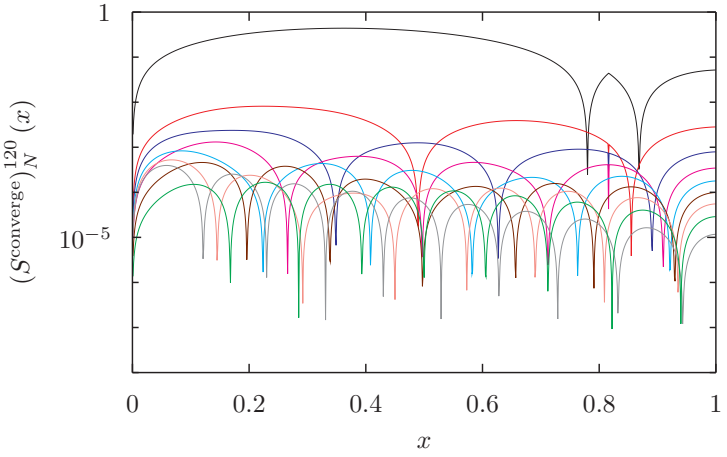

(a) Corrections to spheroidal eigenfunctions for $l = 2$, $n = 1$

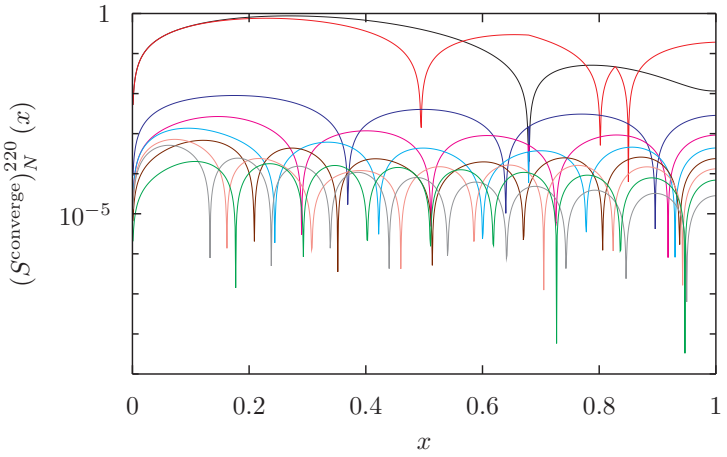

(b) Corrections to spheroidal eigenfunctions for $l = 2$, $n = 2$

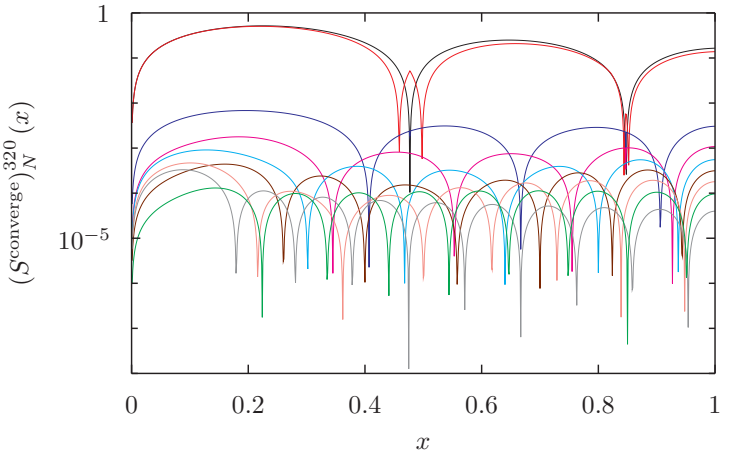

(c) Corrections to spheroidal eigenfunctions for $l = 2$, $n = 3$

Figure 8.1: Figure showing the convergence of the rotational corrections to the spheroidal $l = 2$ eigenfunctions for a) $n = 1$, b) $n = 2$, c) $n = 3$, as the corrections are truncated at progressively higher values of the radial eigenvalue N. In particular, the ϕ component of the functions $(S^{\text{converge}})^{n20}_N$ (8.71) is plotted for $N = 1$ (plotted in black) up to $N = 9$ (plotted in green).

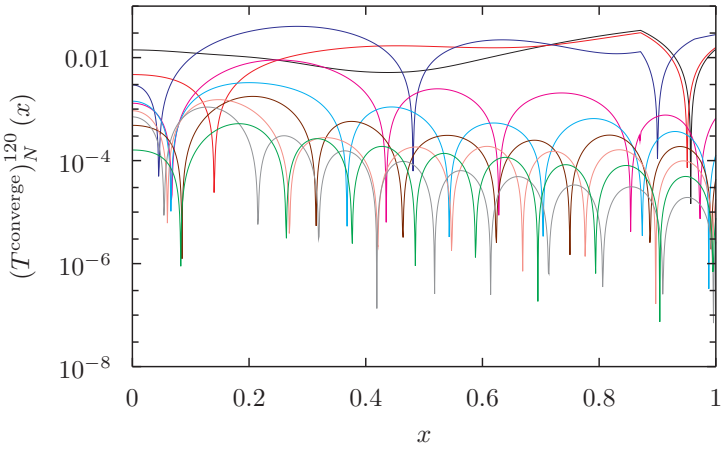

(a) Corrections to toroidal eigenfunctions for $l = 2$, $n = 1$

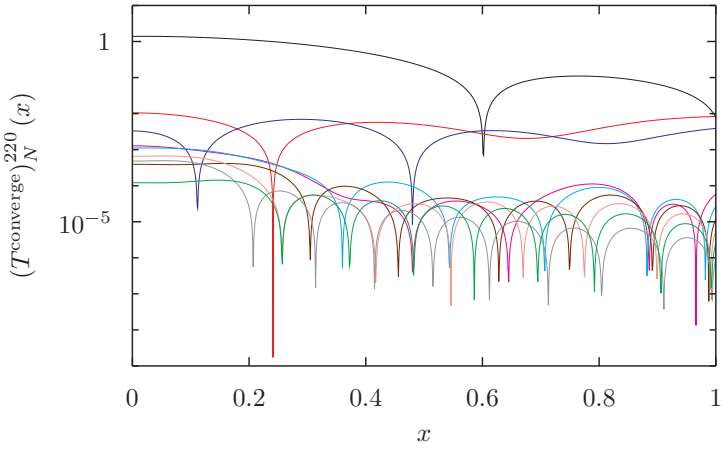

(b) Corrections to toroidal eigenfunctions for $l = 2$, $n = 2$

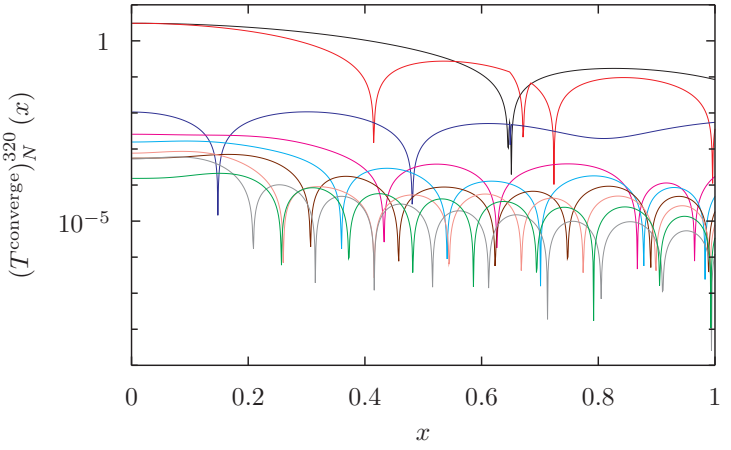

(c) Corrections to toroidal eigenfunctions for $l = 2$, $n = 3$

Figure 8.2: Figure showing the convergence of the rotational corrections to the toroidal $l = 2$ eigenfunctions for a) $n = 1$, b) $n = 2$, c) $n = 3$, as the corrections are truncated at progressively higher values of the radial eigenvalue N. In particular, the r component of the functions $(T^{\text{converge}})_N^{n20}$ (8.72) is plotted for $N = 1$ (plotted in black) up to $N = 9$ (plotted in green).

Chapter 9

Extending the toy model: adding rotation

In this chapter, we extend the glitch model to the more realistic case where the star does not spin down to zero angular velocity before glitching, but instead glitches at some known angular velocity which we label Ω_B. This extended toy model is summarised in Figure 9.1.

As in the zero glitch case, we are able to calculate the displacement field ξ^{AB} between the unstrained Star A and the configuration before the glitch, Star B, using the results of Chapter 4. We then model the glitch, as before, as a sudden loss of all strain from the star. The star will then settle to a new, less oblate equilibrium state, Star D, spinning at a new angular velocity Ω_D. Because angular momentum is conserved at the glitch, the star must now be spinning faster: $\Omega_D > \Omega_B$.

We start by making some estimates of the energy released in the glitch, and the amplitudes of the modes excited, before moving on to make a detailed calculation of the initial data: this time, this will include a nonzero velocity field as well as the displacement field. We then discuss how to project this initial data against the modes of Star D, given that it is now rotating and so the modes are no longer orthogonal.

9.1 Energy estimates for the glitch model

As in the zero-spin model of the previous chapter, we will start by making some order-of-magnitude estimates for the change in energy of the star at the glitch. This will be similar to the analysis of Chapter 3, except that the change in energy in our model is only that between Star C and Star D.

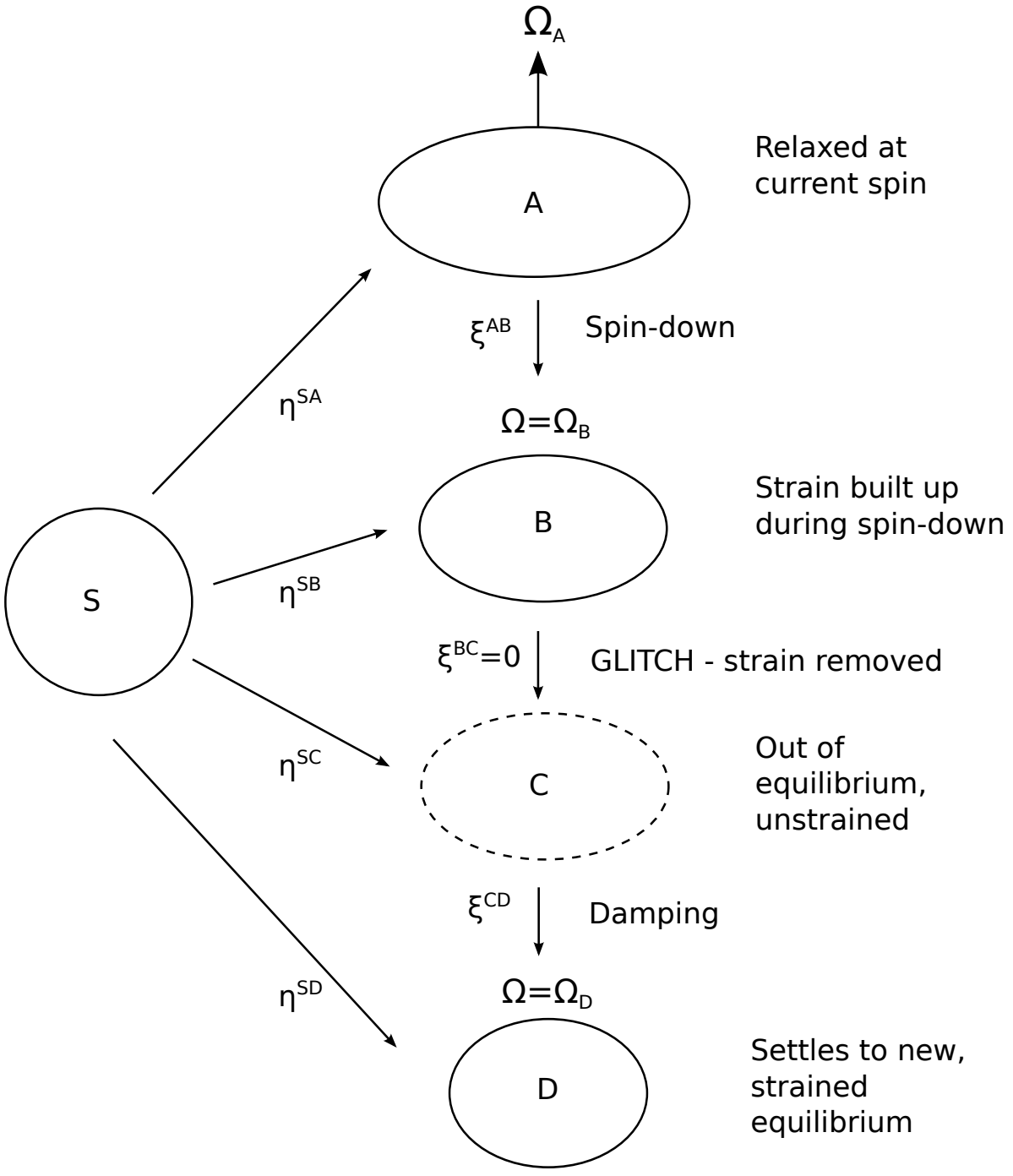

Figure 9.1: Diagram showing the main stages of the glitch model, this time for the general case where Star B is still rotating with angular velocity Ω_B at the glitch. After the glitch the star settles to a new equilibrium rotating at angular velocity Ω_D.

The energy of Star C differs from that of Star B (3.26) in that the strain energy has been removed, so that it has energy

$$E_C = E_{\rm S} + A\left[\frac{1}{2}t(1+\varepsilon_B) + \varepsilon_B^2\right] \tag{9.1}$$

The star still has the same ellipticity as Star B, (3.10):

$$\varepsilon_C = \varepsilon_B = \frac{t}{4}\left(1 + bx\right). \tag{9.2}$$

We then use conservation of angular momentum (3.14) as before to find the ellipticity of Star D up to second order in both b and t, (3.24), which we repeat here:

$$\varepsilon_D = \frac{t}{4}. \tag{9.3}$$

The energy of Star D is then (3.29)

$$E_D = E_{\rm S} + A\left[\frac{1}{2}t(1+\varepsilon_D) + \varepsilon_D^2 + b(\varepsilon_D - \varepsilon_B)^2\right], \tag{9.4}$$

We can then find the change in energy $\Delta E_{CD} = E_D - E_C$. The lowest order term is fourth order in the small parameters,

$$\Delta E_{CD} = \frac{1}{16} A\, b^2 X^2 t^2. \tag{9.5}$$

Note the extra factor of b compared to the energy change ΔE_{BD} (3.31) in Chapter 3; this means that the energy released in our model will be considerably less than that in our earlier upper estimate.

Next, we can estimate the amplitude of the oscillation modes by putting the change in energy at the glitch ΔE_{CD} into kinetic energy of the form

$$E_{\rm mode} \sim I_S \omega^2 \alpha^2 \tag{9.6}$$

where, as before, ω is the frequency of the oscillations and α is a dimensionless number characterising their amplitude.

Equating this to the energy in the initial data ΔE (7.8), we find that

$$I_S \omega^2 \alpha^2 \sim A\, b^2 X^2 t^2, \tag{9.7}$$

i.e.

$$\alpha \sim \sqrt{\frac{A}{I_S}}\frac{btX}{\omega}. \tag{9.8}$$

Substituting back in the original variables,

$$\alpha \sim \frac{1}{\omega}\left(\frac{B}{A}\right)\sqrt{\frac{A}{I_S}}\frac{I_S\Omega_B^2}{A}\left(\frac{\Omega_A^2}{\Omega_B^2}-1\right), \tag{9.9}$$

which can be rewritten in a more useful form as

$$\alpha \sim \left(\frac{B}{A}\right)\sqrt{\frac{I_S\Omega_A^2}{A}}\left(\frac{\Omega_A}{\omega}\right)\left(1-\frac{\Omega_B^2}{\Omega_A^2}\right) \tag{9.10}$$

We can see that this reduces to the previous expression (7.10) for the case where the star spins down completely before 'glitching': $\Omega_B = 0$. Later we will compare this to the results from the detailed calculation carried out in the next section.

9.2 Calculation of initial data

We will now move on to making a full calculation of the initial data. Our initial data will still take the form of a displacement and velocity field connecting Stars C and D. The first difference is that the velocity field $\dot{\xi}^{\mathrm{DC}}$ is no longer zero. Instead there is a change in angular velocity from Ω_B to Ω_D at the glitch, so that the velocity field is

$$\dot{\boldsymbol{\xi}}^{\mathrm{DC}} = r\Delta\Omega\mathbf{e}_\phi, \tag{9.11}$$

where

$$\Delta\Omega = (\Omega_D - \Omega_B). \tag{9.12}$$

Star B is an equilibrium configuration spinning at Ω_B and relaxed at Ω_A. Using the results of Chapter 4 we can calculate the surface shape of Star B:

$$(\eta^r)^{\mathrm{SB}}(R,\theta) = -\frac{5R}{8\pi G\rho}\frac{1}{1+b}\left(\Omega_B^2 + b\Omega_A^2\right)P_2(\cos\theta), \tag{9.13}$$

where we are again using the shorthand notation $b = \frac{B}{A}$. This is (4.106) with $\Omega = \Omega_B$, $\Omega_0 = \Omega_A$, We again assume that the surface shape of Star C is the same as that of B, $\eta_r^{\mathrm{SB}}(R) = \eta_r^{\mathrm{SC}}(R)$. The difference in the new model is that the star is still rotating after the glitch, so that the equation of motion for Star D is

$$-\rho\nabla_i(\Omega_D^2 r^2\cos^2\theta) = -\nabla_i\Delta p^{\mathrm{SD}} - \rho\nabla_i\Delta\Phi^{\mathrm{SD}} + 2\mu\nabla_j u_{ij}^{\mathrm{CD}}. \tag{9.14}$$

We also have the usual surface boundary conditions (7.22)

$$-\left(\Delta p^{\mathrm{SD}}(R)\right)\delta_{ir} + 2\mu u_{ir}^{\mathrm{CD}}(R) = 0, \tag{9.15}$$

while conditions on the gravitational potential at the surface (7.23),(7.24) mean that at the surface $\Delta\Phi^{\mathrm{SD}}$ has the form

$$\Delta\Phi^{\mathrm{SD}}(R) = \frac{8\pi G\rho}{15} R\left(\eta_r'^{\mathrm{SB}}(R) + U^{\mathrm{CD}}(R)\right) P_2(\cos\theta). \tag{9.16}$$

We define

$$\mu h^{\mathrm{SD}} = -\Delta p^{\mathrm{SD}} - \rho\Delta\Phi^{\mathrm{SD}} + \rho\nabla_i(\Omega_D^2 r^2\cos^2\theta), \tag{9.17}$$

and substitute it back into the equation of motion (9.14), finding that

$$\nabla^2 h^{\mathrm{SD}} = 0. \tag{9.18}$$

We can rewrite the centrifugal potential using the fact that

$$\cos^2\theta = \frac{1}{3}\left(1 - P_2(\cos\theta)\right), \tag{9.19}$$

and so we expect h^{SD} to have the same symmetries,

$$h^{\mathrm{SD}} = H_2 r^2 P_2(\cos\theta) + H_0, \tag{9.20}$$

for H_2 and H_0 constant. We decompose the displacement vector ξ_i^{CD} as

$$\boldsymbol{\xi}^{\mathrm{CD}} = U^{\mathrm{CD}}(r)P_2(\cos\theta)\boldsymbol{e}_r + V^{\mathrm{CD}}(r)\boldsymbol{\nabla}P_2(\cos\theta). \tag{9.21}$$

Substituting this back into the force equation (9.14) and using incompressibility, we find that

$$U^{\mathrm{CD}}(r) = Cr - \frac{1}{7}H_2 r^3, \tag{9.22}$$

$$V^{\mathrm{CD}}(r) = \frac{1}{2}Cr^2 - \frac{5}{42}H_2 r^4, \tag{9.23}$$

where C is another constant. We can then use our surface boundary conditions to fix C and H_2. The $(r\theta)$ component of the traction condition (9.15) still gives $C = \frac{8}{21}H_2R^2$, so that

$$U^{\mathrm{CD}}(r) = \frac{H_2}{21}\left(8R^2 r - 3r^3\right), \tag{9.24}$$

$$V^{\mathrm{CD}}(r) = \frac{H_2}{21}\left(4R^2 r^2 - \frac{5}{2}r^4\right), \tag{9.25}$$

but the expression for Δp^{SD} in the (rr) component is now more complicated, because of the extra centrifugal force:

$$-\Delta p^{\mathrm{SD}} = \mu h^{\mathrm{SD}} + \rho\Delta\Phi^{\mathrm{SD}} - \rho\Omega_D^2\frac{r^2}{3}\left(1 - P_2(\cos\theta)\right). \tag{9.26}$$

We can then substitute this into the (rr) component along with our boundary condition for the gravitational potential $\Delta\Phi^{\mathrm{SD}}$ (9.16), obtaining

$$\mu H_0 = \frac{\rho}{3}\Omega_D^2 R^2. \tag{9.27}$$

for the constant part and

$$\frac{19\mu H_2}{21}R^2 + \frac{8\pi G\rho^2 R}{15}\left(\eta_r'^{\mathrm{SC}}(R) + \frac{5H_2}{21}R^3\right) + \frac{\rho}{3}\Omega_D^2 R^2 = 0. \tag{9.28}$$

for the terms proportional to $P_2(\cos\theta)$. Rearranging for H_2,

$$H_2 = -\frac{21}{57\mu R^2 + 8\pi G\rho^2 R^4}\cdot\left(\rho\Omega_D^2 R^2 + \frac{8\pi G\rho^2 R}{5}\eta_r'^{\mathrm{SC}}(R)\right). \tag{9.29}$$

It remains to include the shape of Star C at the surface, $\eta_r'^{\mathrm{SC}}(R)$ (9.13). Inserting this in we have

$$H_2 = -\frac{21}{57\mu R^2 + 8\pi G\rho^2 R^4}\cdot\left(\Omega_D^2\rho R^2 - \frac{\rho R^2}{1+b}\left(\Omega_B^2 + b\Omega_A^2\right)\right), \tag{9.30}$$

For a homogeneous star

$$b = \frac{57\mu}{8\pi G\rho^2 R^2}, \tag{9.31}$$

so H_2 simplifies to

$$H_2 = -\frac{21}{8\pi G\rho R^2}\frac{1}{1+b}\left(\Omega_D^2 - \frac{\Omega_B^2 + b\Omega_A^2}{1+b}\right). \tag{9.32}$$

9.2.1 Displacement field

We now have our final form for the radial part of the displacement field (9.24), (9.25):

$$U^{\mathrm{CD}}(r) = -\frac{1}{8\pi G\rho R^2}\frac{1}{1+b}\left(\Omega_D^2 - \frac{\Omega_B^2 + b\Omega_A^2}{1+b}\right)\left(8R^2 r - 3r^3\right), \tag{9.33}$$

$$V^{\mathrm{CD}}(r) = -\frac{1}{8\pi G\rho R^2}\frac{1}{1+b}\left(\Omega_D^2 - \frac{\Omega_B^2 + b\Omega_A^2}{1+b}\right)\left(4R^2 r^2 - \frac{5}{2}r^4\right). \tag{9.34}$$

Along with the velocity field (9.11), this completes our set of initial data for the glitch.

We can check that this is consistent with the previous, spin zero glitch model. This is the special case where $\Omega_B = \Omega_D = 0$, so

$$U^{\mathrm{CD}}_{\mathrm{zero}}(r) = \frac{1}{8\pi G\rho R^2}\frac{b\Omega_A^2}{(1+b)^2}\left(8R^2 r - 3r^3\right), \tag{9.35}$$

$$V^{\mathrm{CD}}_{\mathrm{zero}}(r) = \frac{1}{8\pi G\rho R^2}\frac{b\Omega_A^2}{(1+b)^2}\left(4R^2 r^2 - \frac{5}{2}r^4\right), \tag{9.36}$$

which agrees with our previous result (7.51), (7.52).

Our initial data is still written in terms of the angular velocity Ω_D, so to complete this we need to express Ω_D in terms of the known angular velocities Ω_A and Ω_B. In Section 3.1.1 we did this by using the fact that angular momentum is conserved. We found that

$$\Omega_D = \left(1 + \frac{1}{4}tbX\right)\Omega_B. \tag{9.37}$$

where we have also used the assumptions

$$b \ll 1, \tag{9.38}$$

$$t \ll 1, \tag{9.39}$$

$$\frac{\Omega_D - \Omega_B}{\Omega_B} \ll 1. \tag{9.40}$$

To first order in b we have

$$\frac{1}{1+b}\left(\Omega_D^2 - \frac{\Omega_B^2 + b\Omega_A^2}{1+b}\right) = \left(\Omega_D^2 - \Omega_B^2\right) + b\left(2\Omega_B^2 - \Omega_A^2 - \Omega_D^2\right). \tag{9.41}$$

Substituting in Ω_D (9.37),

$$\frac{1}{1+b}\left(\Omega_D^2 - \frac{\Omega_B^2 + b\Omega_A^2}{1+b}\right) = b\left(\frac{t}{2}X + \Omega_B^2 - \Omega_A^2\right), \tag{9.42}$$

again to first order in b. We can then expand in t as well, using the fact that for a homogeneous star we have [16]

$$A = \frac{16\pi^2}{75} G\rho^2 R^5, \tag{9.43}$$

$$I_S = \frac{8\pi}{15} \rho R^5, \tag{9.44}$$

so that

$$t = \frac{5}{2\pi G\rho} \Omega_B^2. \tag{9.45}$$

Then we can write

$$U^{\mathrm{CD}}(r) = -\frac{5bt}{4R^2\Omega_B^2} \left(\frac{t}{2} x + \Omega_B^2 - \Omega_A^2 \right) \left(8R^2 r - 3r^3 \right), \tag{9.46}$$

$$V^{\mathrm{CD}}(r) = -\frac{5bt}{4R^2\Omega_B^2} \left(\frac{t}{2} x + \Omega_B^2 - \Omega_A^2 \right) \left(4R^2 r^2 - \frac{5}{2} r^4 \right). \tag{9.47}$$

Keeping terms up to second order in t and b, we finally obtain

$$U^{\mathrm{CD}}(r) = \frac{5btX}{4R^2} \left(8R^2 r - 3r^3 \right), \tag{9.48}$$

$$V^{\mathrm{CD}}(r) = \frac{5btX}{4R^2} \left(4R^2 r^2 - \frac{5}{2} r^4 \right). \tag{9.49}$$

We can write this in terms of the change in angular velocity at the glitch $z = \frac{\Omega_B - \Omega_D}{\Omega_D}$ (3.16) as

$$U^{\mathrm{CD}}(r) = \frac{5z}{R^2} \left(8R^2 r - 3r^3 \right), \tag{9.50}$$

$$V^{\mathrm{CD}}(r) = \frac{5z}{R^2} \left(4R^2 r^2 - \frac{5}{2} r^4 \right). \tag{9.51}$$

As a measure of the amplitude of oscillations produced by this initial data we can take

$$\frac{U^{\mathrm{CD}}(R)}{R} = \frac{25btx}{4}. \tag{9.52}$$

For oscillations which scale like the fundamental fluid mode, $\omega \sim \sqrt{G\rho}$ we have

$$\frac{1}{\omega} \sqrt{\frac{A}{I_S}} \sim O(1), \tag{9.53}$$

so this is consistent with our estimate α (9.8) from the preceding energy argument.

9.2.2 Surface shape of Star D

We can also find the surface shape of Star D, using the known surface shape of Star C (9.13). To first order in b this is

$$(\eta^r)^{\mathrm{SC}}(R,\theta) = -\frac{5R}{8\pi G\rho}\left(\Omega_B^2 + b\left(\Omega_A^2 - \Omega_B^2\right)\right) P_2(\cos\theta), \tag{9.54}$$

or in terms of our new notation

$$(\eta^r)^{\mathrm{SC}}(R,\theta) = -\frac{R}{4}t\,(1+bx)\,P_2(\cos\theta), \tag{9.55}$$

so that the surface shape of D is

$$\eta_r^{\mathrm{SD}}(R) = Rt\left(-\frac{1}{4} + \frac{21}{4}bx\right) P_2(\cos\theta). \tag{9.56}$$

9.2.3 Gravitational potential perturbation

Finally, we can find the gravitational potential perturbation $\delta\Phi^{\mathrm{CD}}$ corresponding to the initial data $(\xi)_i^{\mathrm{CD}}$. As in the previous chapter we have that

$$\delta\Phi^{\mathrm{SD}}(r,\theta) = -\left(\frac{4\pi G\rho}{5R}\eta_r^{\mathrm{SD}}(R)\right) r^2 P_2(\cos\theta), \tag{9.57}$$

so that

$$\delta\Phi^{\mathrm{SD}}(r,\theta) = \left(\frac{\pi G\rho t}{5}\,(1-21bx)\right) r^2 P_2(\cos\theta), \tag{9.58}$$

Substituting in t (9.45),

$$\delta\Phi^{\mathrm{SD}}(r,\theta) = \left(\frac{\Omega_B^2}{2}\,(1-21bx)\right) r^2 P_2(\cos\theta), \tag{9.59}$$

We can then find $\delta\Phi^{\mathrm{CD}}$ by subtracting $\delta\Phi^{\mathrm{SC}}$, calculated in Chapter 4 (4.95). To first order in b this is

$$\delta\Phi^{\mathrm{SC}} = \frac{1}{2}\left(\Omega_B^2 + b\left(\Omega_D^2 - \Omega_B^2\right)\right) r^2 P_2(\cos\theta). \tag{9.60}$$

Substituting in Ω_D^2 (9.37), we find that to first order we just have

$$\delta\Phi^{\mathrm{SC}} = \frac{1}{2}\Omega_B^2 r^2 P_2(\cos\theta). \tag{9.61}$$

9.2.4 Velocity field

The initial velocity field of the star takes the form of a rigid rotation: the angular velocity is the difference in velocity between Stars D and C,

$$\Omega_{DC} = \Omega_B - \Omega_D = -\Omega_B z \tag{9.62}$$

where $z = \frac{\Omega_D - \Omega_B}{\Omega_B}$ (3.16). The velocity field is then

$$\dot{\boldsymbol{\xi}}^{\mathrm{DC}} = -\Omega_B z\, r \sin\theta\, \hat{\phi}. \tag{9.63}$$

We can show that this has the form of an $l = 1$, $m = 0$ toroidal mode. These modes have the form

$$T^{n10} = \frac{W_{n1}(r)}{r} \frac{dP_{10}(\cos\theta)}{d\theta} \hat{\phi}. \tag{9.64}$$

We have

$$P_{10}(x) = x, \tag{9.65}$$

so that

$$\dot{\xi}^{\mathrm{DC}} = \Omega_B z\, r \frac{dP_{10}(\cos\theta)}{d\theta}\, \hat{\phi}, \tag{9.66}$$

and

$$W_{11}(r) = \Omega_B z\, r^2. \tag{9.67}$$

We can write Ω_B in terms of the rotational parameter t, so that

$$\Omega_B = \sqrt{\frac{3}{8}}\sqrt{t} \tag{9.68}$$

and the velocity field becomes

$$\dot{\xi}^{\mathrm{DC}}(x) = \sqrt{\frac{3}{8}}\, \sqrt{t}\, zx \frac{dP_{10}(\cos\theta)}{d\theta}\, \hat{\phi}. \tag{9.69}$$

9.2.5 Summary

Here we summarise the main results of the section. The initial data we want to project takes the form of a displacement field $\xi^{\rm DC}$ and velocity field $\dot{\xi}^{\rm DC}$. The displacement field has the form

$$\boldsymbol{\xi}^{\rm DC} = U^{\rm DC}(r)P_l(\cos\theta)\hat{r} + V^{\rm DC}(r)\boldsymbol{\nabla}P_l, \tag{9.70}$$

where the functions $U^{\rm DC}(r)$ (9.50) and $V^{\rm DC}(r)$ (9.50) are

$$U^{\rm DC}(r) = -\frac{5z}{R^2}\left(8R^2r - 3r^3\right), \tag{9.71}$$

$$V^{\rm DC}(r) = -\frac{5z}{R^2}\left(4R^2r^2 - \frac{5}{2}r^4\right). \tag{9.72}$$

The velocity field looks like (9.66)

$$\dot{\boldsymbol{\xi}}^{\rm DC} = W(r)\left(\hat{r}\times\boldsymbol{\nabla}P_l\right), \tag{9.73}$$

where

$$W(r) = -\sqrt{\frac{3}{8}}\,\sqrt{t}\,zr\sin\theta. \tag{9.74}$$

9.3 Projecting the initial data

To project our initial data against the modes of the rotating star, we have to take into account a number of new factors that did not affect us in the nonrotating case. One of these is that the eigenfunctions of the rotating star are no longer orthogonal; we will describe a scheme that allows us to nonetheless carry out the projection.

Another is the existence of the zero eigenvalue $l = 1$ toroidal mode (9.64) that our velocity initial data is built from. As this mode is zero frequency, it will not have the $e^{i\omega t}$ time-dependence of the other modes and we will have to consider it separately. We will deal with this problem first.

9.3.1 The zero eigenvalue mode

To find the time-dependence of the zero eigenvalue eigenfunction, we need to go back to the governing equation for the zeroth order equations (8.19)

$$A_{(0)}\frac{\partial^2 \xi_{(0)}}{\partial t^2} + C_{(0)}\xi_{(0)} = 0. \tag{9.75}$$

Making a separation of variables $\xi_{(0)}(x,t) = \xi_{(0)}(x)T(t)$,

$$A_{(0)}\xi_{(0)}\frac{d^2 T}{dt^2} + C_{(0)}\xi_{(0)}T = 0, \tag{9.76}$$

To separate these, we can take the divergence,

$$\frac{1}{T}\frac{d^2 T}{dt^2}\nabla\cdot[A_{(0)}\xi_{(0)}] + \nabla\cdot[C_{(0)}\xi_{(0)}] = 0, \tag{9.77}$$

so that

$$\frac{1}{T}\frac{d^2 T}{dt^2} = -\frac{\nabla\cdot[C_{(0)}\xi_{(0)}]}{\nabla\cdot[A_{(0)}\xi_{(0)}]} = \lambda. \tag{9.78}$$

For the non-zero frequency modes, we will take the case where λ is negative, $\lambda^\alpha = -(\omega^\alpha)^2$ for $\alpha > 2$. Then

$$\frac{d^2 T}{dt^2} = -(\omega^\alpha)^2 T, \tag{9.79}$$

with general solution

$$T(t) = \mathrm{Re}\left[c^\alpha e^{i\omega^\alpha t}\right], \tag{9.80}$$

c^α a complex constant. To show explicitly that the solution is real, we will instead write

$$T(t) = \frac{1}{2}\left(b^\alpha e^{i\omega^\alpha t} + (b^\alpha)^* e^{-i\omega^\alpha t}\right). \tag{9.81}$$

For the spatial dependence, we obtain

$$(\omega^\alpha)^2 A_{(0)}\xi_{(0)} = C_{(0)}\xi_{(0)}, \tag{9.82}$$

i.e. we regain our normal eigenvalue equation.

Next we look at the zero frequency case. For now it will be convenient to label this eigenvalue as ω^1, with $\omega^1 = 0$ and corresponding eigenfunction ξ^1.

For the zero frequency eigenvalue ω^1, we take $\lambda^1 = 0$. The T equation of the separation of variables (9.78) becomes

$$\frac{d^2 T}{dt^2} = 0, \tag{9.83}$$

so the solutions are

$$T(t) = C^1 t + D^1, \tag{9.84}$$

C^1 and D^1 real. We can write this in a similar way to the $\lambda < 0$ case by labelling

$$D^1 = \frac{1}{2}\left(b^1 + \left(b^1\right)^*\right), \tag{9.85}$$

$$C^1 = \frac{i}{2}\left(b^1 - \left(b^1\right)^*\right), \tag{9.86}$$

where b^1 is a complex constant. The spatial part of $\xi^1_{(0)}$ satisfies

$$C_{(0)}\xi^1_{(0)} = 0. \tag{9.87}$$

We can also look at the first-order corrections $\xi^1_{(1)} = \sum_\beta \lambda^{1\beta}_{(1)}\xi^\beta_{(0)}$ to this mode. These satisfy the equation

$$C_{(0)}\xi^1_{(1)} = 0, \tag{9.88}$$

which has the same form as the equation for the zeroth order modes. This means that we can absorb them into the zeroth order mode $\xi^0_{(1)}$, so that the corrections $\lambda^{1\beta}_{(1)} = 0$.

9.3.2 The projection scheme

We saw in Chapter 8 that we can write the modes of the rotating star as

$$\xi^\alpha = \xi^\alpha_{(0)} + \sum_\beta \varepsilon\lambda^{\alpha\beta}_{(1)}\xi^\beta_{(0)}, \tag{9.89}$$

where $\xi^\alpha_{(0)}$ are the modes of the nonrotating star and the $\lambda^{\alpha\beta}_{(1)}$ are correction coefficients. These eigenfunctions have the time dependence

$$\xi^\alpha = \xi^\alpha(x,t) = e^{i\omega^\alpha t}\xi^\alpha(x). \tag{9.90}$$

The full displacement field (with time-dependence) can then be written as a sum over these modes

$$\xi(x,t) = \left[\frac{i}{2}\left(b^1 - \left(b^1\right)^*\right)t + \frac{1}{2}\left(b^1 + \left(b^1\right)^*\right)\right]\xi^1_{(0)}(x) + \frac{1}{2}\sum_{\alpha=2}^{\infty}\left[b^\alpha\xi^\alpha(x,t) + b^{*\alpha}\xi^{*\alpha}(x,t)\right]. \tag{9.91}$$

Here we have included the zero eigenvalue mode (9.84) – note that it has no first order corrections so we can just use its zeroth order form. To make sure that the data is real we have added on the complex conjugate. The complex coefficients b^α contain the amplitude and phase of each mode. Similarly, the velocity field is

$$\dot{\xi}(x,t) = \frac{1}{2}\left(b^1 + \left(b^1\right)^*\right)\xi^1_{(0)}(x) + \frac{1}{2}\sum_{\alpha=2}^{\infty}\left[i\omega^\alpha_{(0)}b^\alpha\xi^\alpha(x,t) - i\omega^\alpha_{(0)}b^{*\alpha}\xi^{*\alpha}(x,t)\right], \tag{9.92}$$

where we have used the fact that there are no rotational corrections to the zeroth order eigenvalues $\omega_{(0)}$ in the $m = 0$ case we are interested in.

To obtain the initial data, we just specialise to $t = 0$. We can also combine $\xi^1_{(0)}$ with the other eigenfunctions by making the definition

$$\tilde{\omega}^\alpha_{(0)} = \begin{cases} 1 & \alpha = 1, \\ \omega^\alpha_{(0)} & \text{otherwise.} \end{cases} \tag{9.93}$$

Then we can write the initial data as

$$\xi^{\mathrm{ID}}(x) \equiv \xi(x,0) = \frac{1}{2}\sum_\alpha\left[b^\alpha\xi^\alpha(x) + \text{c.c.}\right], \tag{9.94}$$

$$\dot{\xi}^{\mathrm{ID}}(x) \equiv \dot{\xi}(x,0) = \frac{1}{2}\sum_\alpha\left[i\omega^\alpha_{(0)}b^\alpha\xi^\alpha(x) + \text{c.c.}\right]. \tag{9.95}$$

Now we expand the eigenfunctions in the sum to first order in rotation, so that

$$\xi^\alpha = \xi^\alpha_{(0)} + \sum_{\beta=2}^{\infty}\lambda^{\alpha\beta}_{(1)}\xi^\beta_{(0)}. \tag{9.96}$$

We then have

$$\xi^{\mathrm{ID}}(x) = \sum_{\alpha=1}^{\infty}\left[\frac{b^\alpha}{2}\left(\xi^\alpha_{(0)}(x) + \sum_{\beta=1}\lambda^{\alpha\beta}_{(1)}\xi^\beta_{(0)}\right) + \frac{(b^\alpha)^*}{2}\left(\xi^\alpha_{(0)}(x) + \sum_{\beta=1}(\lambda^*)^{\alpha\beta}_{(1)}\xi^\beta_{(0)}\right)\right], \tag{9.97}$$

$$\dot{\xi}^{\mathrm{ID}}(x) = \sum_{\alpha=1}^{\infty}\left[i\tilde{\omega}^\alpha\frac{b^\alpha}{2}\left(\xi^\alpha_{(0)}(x) + \sum_{\beta=1}\lambda^{\alpha\beta}_{(1)}\xi^\beta_{(0)}\right) - i\tilde{\omega}^\alpha\frac{(b^\alpha)^*}{2}\left(\xi^\alpha_{(0)}(x) + \sum_{\beta=1}(\lambda^*)^{\alpha\beta}_{(1)}\xi^\beta_{(0)}\right)\right], \tag{9.98}$$

where the corrections to $\xi^1_{(0)}$ are $\lambda^{1\beta} = 0$. Now we can take an inner product with another zeroth order eigenfunction $\xi^\gamma_{(0)}$ to obtain

$$\left\langle \xi^\gamma_{(0)}, \xi^{\mathrm{ID}}(x) \right\rangle = \sum_{\alpha=1}^{\infty} \left[\frac{b^\alpha}{2} \left(\delta^{\alpha\gamma} + \lambda^{\alpha\gamma}_{(1)} \right) + \frac{(b^\alpha)^*}{2} \left(\delta^{\alpha\gamma} + (\lambda^*)^{\alpha\gamma}_{(1)} \right) \right], \tag{9.99}$$

$$\left\langle \xi^\gamma_{(0)}, \dot{\xi}^{\mathrm{ID}}(x) \right\rangle = \sum_{\alpha=1}^{\infty} \left[i\tilde{\omega}^\alpha \frac{b^\alpha}{2} \left(\delta^{\alpha\gamma} + \lambda^{\alpha\gamma}_{(1)} \right) - i\tilde{\omega}^\alpha \frac{(b^\alpha)^*}{2} \left(\delta^{\alpha\gamma} + (\lambda^*)^{\alpha\gamma}_{(1)} \right) \right]. \tag{9.100}$$

In practice, when carrying out a projection numerically we will only consider a finite sum, cutting off at some sufficiently large $\beta = N$. We can then view (9.99) and (9.100) as vectors of N equations, so that we can rewrite them as

$$\mathbf{x} = \frac{1}{2} \left(\Lambda^T \mathbf{b} + \left(\Lambda^T \right)^* \mathbf{b}^* \right), \tag{9.101}$$

$$\dot{\mathbf{x}} = \frac{1}{2} \left(\Omega^T \mathbf{b} + \left(\Omega^T \right)^* \mathbf{b}^* \right), \tag{9.102}$$

where the vectors $\mathbf{x}$ and $\dot{\mathbf{x}}$ are defined by

$$x^\beta \equiv \left\langle \xi^\beta, \xi^{\mathrm{ID}}(x) \right\rangle \tag{9.103}$$

$$\dot{x}^\beta \equiv \left\langle \xi^\beta, \dot{\xi}^{\mathrm{ID}}(x) \right\rangle, \tag{9.104}$$

and the matrices Λ and Ω are built from the matrix of correction coefficients λ as

$$\Lambda \equiv I + \lambda, \tag{9.105}$$

$$\Omega \equiv D\Lambda, \tag{9.106}$$

$$D \equiv \mathrm{diag}\left[i\tilde{\omega}^1, i\tilde{\omega}^2, \ldots, i\tilde{\omega}^N \right]. \tag{9.107}$$

To solve for $\mathbf{b}$, we first calculate

$$2 \left[(\Lambda^*)^{\mathrm{T}} \right]^{-1} \mathbf{x} = \left[(\Lambda^*)^{\mathrm{T}} \right]^{-1} \Lambda^{\mathrm{T}} \mathbf{b} + \mathbf{b}^* \tag{9.108}$$

$$2 \left[(\Omega^*)^{\mathrm{T}} \right]^{-1} \dot{\mathbf{x}} = \left[(\Omega^*)^{\mathrm{T}} \right]^{-1} \Omega^{\mathrm{T}} \mathbf{b} + \mathbf{b}^*, \tag{9.109}$$

so that

$$2 \left[(\Lambda^*)^{\mathrm{T}} \right]^{-1} \mathbf{x} - 2 \left[(\Omega^*)^{\mathrm{T}} \right]^{-1} \dot{\mathbf{x}} = \left[(\Lambda^*)^{\mathrm{T}} \right]^{-1} \Lambda^{\mathrm{T}} \mathbf{b} - \left[(\Omega^*)^{\mathrm{T}} \right]^{-1} \Omega^{\mathrm{T}} \mathbf{b}. \tag{9.110}$$

Inverting for $\mathbf{b}$, we have

$$\mathbf{b} = 2\mathrm{A}^{-1}\left\{\left[(\Lambda^*)^{\mathrm{T}}\right]^{-1}\mathbf{x} - \left[(\Omega^*)^{\mathrm{T}}\right]^{-1}\dot{\mathbf{x}}\right\} \tag{9.111}$$

where A is the matrix

$$\mathrm{A} = \left[(\Lambda^*)^{\mathrm{T}}\right]^{-1}\Lambda^{\mathrm{T}} - \left[(\Omega^*)^{\mathrm{T}}\right]^{-1}\Omega^{\mathrm{T}}. \tag{9.112}$$

9.3.3 Carrying out the projection numerically

To use this projection scheme, we first need to construct the matrix Λ. To do this, we will need to decide which modes $\alpha = (n, l, m)$ we are keeping in the projection, and choose an ordering for the mode indices α.

We have previously found that the corrected spheroidal eigenfunctions have the form

$$S^{nl0} = S^{nl0}_{(0)} + \varepsilon\sum_{n'=1}^{\infty}\left([ST]^{nl0,n'l-10}_{(1)}T^{n'l-10} + [ST]^{nl0,n'l+10}_{(1)}T^{n'l+10}\right), \tag{9.113}$$

i.e. the only nonzero correction terms are $l' = l-1$ and $l' = l+1$ toroidal corrections. For each of these there is an infinite set of radial eigenmodes n; we will need to cut off these contributions at some finite number.

We can write this out in components as

$$S^{nl0} = \begin{pmatrix} U^{nl0}P_l \\ V^{nl0}\frac{dP_l}{d\theta} \\ 0 \end{pmatrix} + \varepsilon\sum_{n'=1}^{\infty}\begin{pmatrix} 0 \\ 0 \\ [ST]^{nl0,n'l-10}_{(1)}W^{n'10}P_{l-1} + [ST]^{nl0,n'l+10}_{(1)}W^{n'l+10}P_{l+1} \end{pmatrix}. \tag{9.114}$$

Similarly, the corrected toroidal eigenfunctions look like

$$T^{nl0} = T^{nl0}_{(0)} + \varepsilon\sum_{n'=1}^{\infty}\left([TS]^{nl0,n'l-10}_{(1)}S^{n'l-10}_{(0)} + [TS]^{nl0,n'l+10}_{(1)}S^{n'l+10}_{(0)}\right), \tag{9.115}$$

which in components is

$$T^{nl0} = \begin{pmatrix} 0 \\ 0 \\ W^{nl0}P_l \end{pmatrix} + \varepsilon\sum_{n'=1}^{\infty}\begin{pmatrix} [TS]^{nl0,n'l-10}_{(1)}U^{n'l-10}_{(0)}P_{l-1} + [TS]^{nl0,n'l+10}_{(1)}U^{n'l+10}_{(0)}P_{l+1} \\ [TS]^{nl0,n'l-10}_{(1)}V^{n'l-10}_{(0)}\frac{dP_{l-1}}{d\theta} + [TS]^{nl0,n'l+10}_{(1)}V^{n'l+10}_{(0)}\frac{dP_{l+1}}{d\theta} \\ 0 \end{pmatrix}. \tag{9.116}$$

Looking at the initial data we are projecting, we can see that the displacement field (9.70) is spheroidal $l = 2$ and $m = 0$. This can be expected to couple to $l = 1$ and $l = 3$ toroidal $m = 0$ modes. The velocity field (9.73) is built from the toroidal $l = 1$, $m = 0$ zero frequency mode, which has no first order corrections. However the $l = 2$ spheroidal eigenfunctions can be expected to couple to this mode.

Motivated by this, we will choose to consider only $m = 0$ and also to cut off at $l = 3$, including only $l = 1, 2, 3$ (the $l = 0$ radial modes are all zero for an incompressible star). This is illustrated in Figure 9.2.

As with Chapter 8 we will also consider only the case $\frac{B}{A} = 0.1$. For this value, the fluid-elastic mode is at $n = 3$. As we have seen that this mode is preferentially excited in the non-rotating case, we can expect the same here, so that $n = 10$ is a reasonable cut-off.

Schematically, we can then write all the zeroth order eigenfunctions we plan to use as a vector

$$\begin{pmatrix} S1 \\ T1 \\ S2 \\ T2 \\ S3 \\ T3 \end{pmatrix}, \tag{9.117}$$

where $S1$ is a vector of the first 10 spheroidal $l = 1$ eigenfunctions, $T1$ is a vector of the first 10 toroidal $l = 1$ eigenfunctions, etc.

The corrected eigenfunctions are then obtained by acting on this vector with the matrix Λ (9.105), which schematically looks like

$$\begin{pmatrix} I & 0 & 0 & \varepsilon[ST12] & 0 & 0 \\ 0 & I & \varepsilon[TS12] & 0 & 0 & 0 \\ 0 & \varepsilon[ST21] & I & 0 & 0 & \varepsilon[ST23] \\ \varepsilon[TS21] & 0 & 0 & I & \varepsilon[TS23] & 0 \\ 0 & 0 & 0 & \varepsilon[ST32] & I & 0 \\ 0 & 0 & \varepsilon[TS32] & 0 & 0 & I \end{pmatrix}. \tag{9.118}$$

Each entry represents an $n \times n$ matrix. Most off-diagonal entries are zero apart from a few blocks. For $l = 2$ these are the $l = 1$ and 3 toroidal corrections to the spheroidal eigenfunctions, $[ST21]_n$ and $[ST23]_n$, and the $l = 1$ and 3 spheroidal corrections to the toroidal eigenfunctions, $[TS21]_n$ and $[TS23]_n$. For $l = 1$ there are only $l = 2$ corrections; this is also true for $l = 3$ as we are not including $l = 4$. The structure of the matrix is

shown in more detail in Figure 9.3, where the absolute value of the matrix coefficients is plotted (a darker colour indicates a larger value of the coefficient).

The modes have been scaled so that $R = 1$, so we must do the same for the initial data. Writing $x = \frac{r}{R}$, the displacement field is

$$\dot{\xi}^{\mathrm{DC}}(x) = U^{\mathrm{DC}}(x) P_{20}(\cos\theta) + \frac{V^{\mathrm{DC}}(x)}{x} \frac{dP_{20}(\cos\theta)}{d\theta} \tag{9.119}$$

with

$$U^{\mathrm{DC}}(x) = -5z\left(8x - 3x^3\right), \tag{9.120}$$

$$V^{\mathrm{DC}}(x) = -5z\left(4x^2 - \frac{5}{2}x^4\right), \tag{9.121}$$

The velocity field becomes

$$\dot{\xi}^{\mathrm{DC}}(x) = \sqrt{\frac{3}{8}}\,\sqrt{t}\,zx \frac{dP_{10}(\cos\theta)}{d\theta}\,\hat{\phi}. \tag{9.122}$$

We can also scale the rotational parameter ε (8.2) in the modes by relating it to t; we have

$$\varepsilon = \Omega_B \sqrt{\frac{R^3}{GM}}, \tag{9.123}$$

which in our code units becomes

$$\varepsilon = \sqrt{\frac{3}{10}}\sqrt{t}. \tag{9.124}$$

There are then two free parameters in the initial data, t and z. This is as expected: they correspond to the two free parameters Ω_A and Ω_B of the model.

Given our matrix Λ, we want to calculate the amplitudes of the excited modes b^α using our projection formula (9.111), and use these to reconstruct the initial displacement and velocity fields.

We have recently used this scheme to reproduce the displacement field and velocity, and are now in the process of analysing how the amplitudes b^α change as the free parameters t and z are varied in the initial data.

As a rough sketch of our current findings, we see that the $l = 2$ spheroidal fluid-elastic mode is still excited as in the nonrotating model of Chapter 7. The rotational corrections mean that the $l = 1$ and $l = 3$ toroidal modes are also excited to a lesser extent, while the velocity field also excites the zero frequency $l = 1$ toroidal mode.

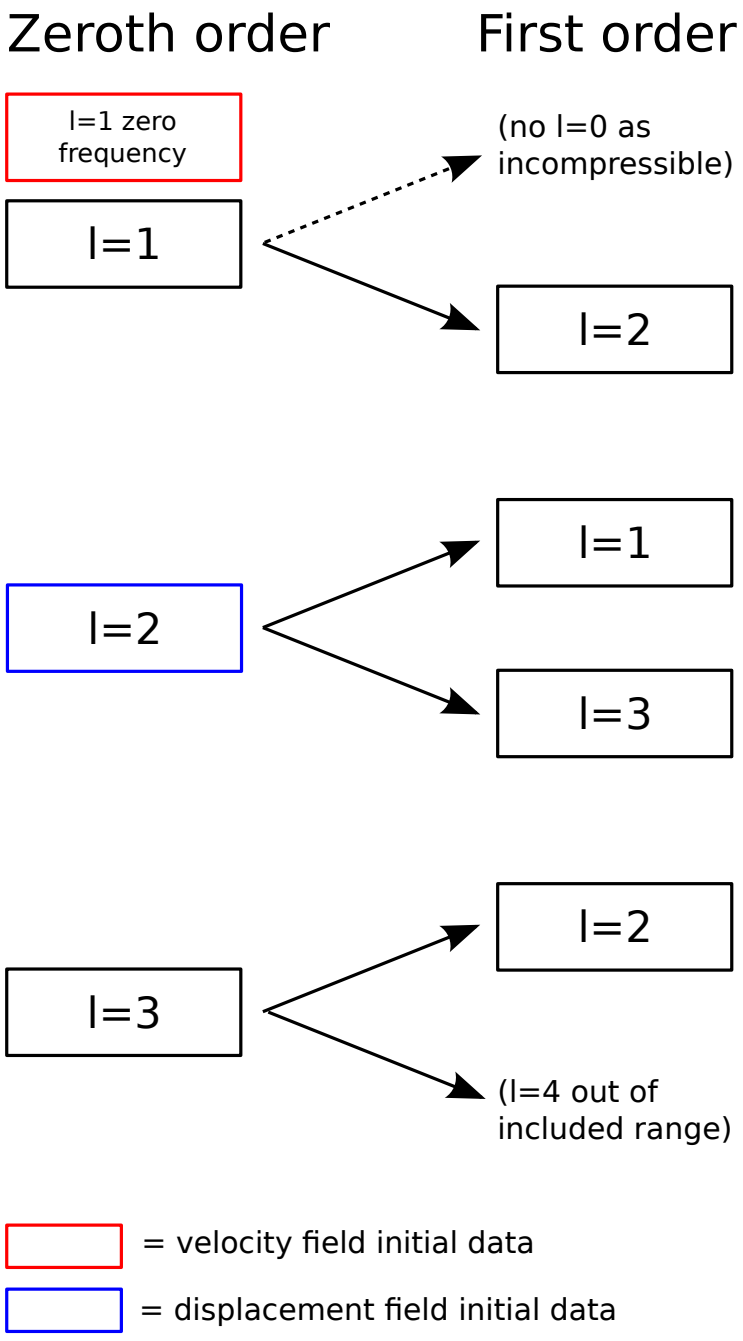

Figure 9.2: Schematic showing how the zeroth order modes couple to other modes at first order in rotation. The displacement field has an $l = 2$ form and couples to $l = 1$ and $l = 3$; this is shown in blue. The velocity field, shown in read, has the form of a zero frequency $l = 1$ mode; it has no rotational corrections. The other modes in the range we are considering are also shown. The $l = 1$ modes only couple to $l = 2$, while for the $l = 3$ modes, only the $l = 2$ coupling falls into the range we are considering.

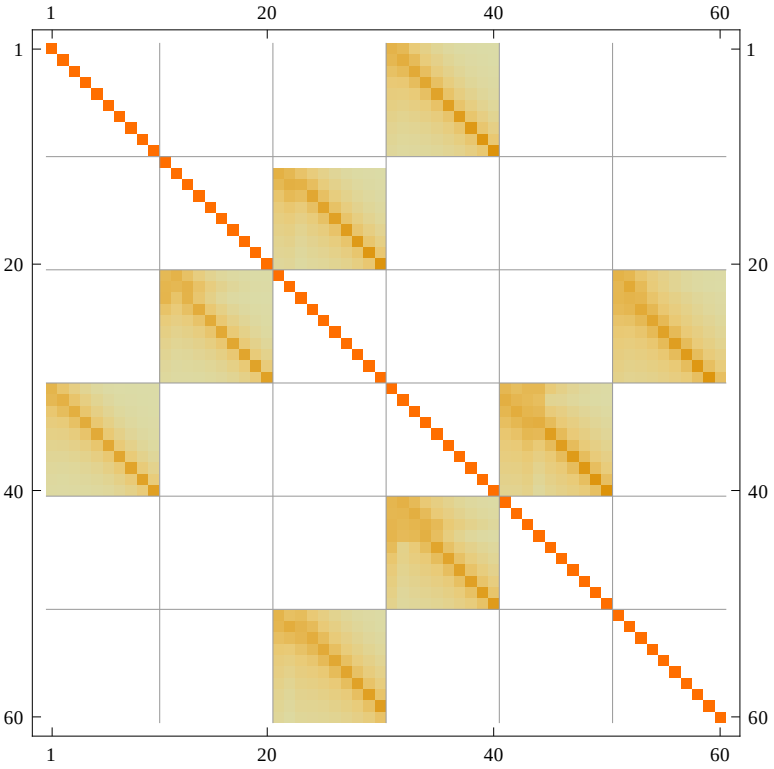

Figure 9.3: Plot of the matrix Λ, which we are using to act on a vector of our zeroth order eigenfunctions to obtain the rotationally corrected eigenfunctions. Each coloured box represents a component of the matrix; a darker orange indicates a larger absolute value of the component.

Chapter 10

Discussion

Neutron star glitches have the potential to excite global oscillations of the star, a potential source of gravitational waves. The amplitude of these oscillations, and the type of modes that are excited, is strongly dependent on the specific physics of the glitch mechanism. In this thesis we have investigated mode excitation for the specific case of a glitch caused by a starquake.

After covering some introductory material relating to neutron stars and glitches in the first two chapters, we give some order-of-magnitude upper estimates of the oscillation amplitudes in Chapter 3. In this chapter we first calculate the energy released by a starquake. At this stage, we do not specify a detailed model of how the energy is put into oscillations at the glitch, but just obtain an upper estimate by assuming that all the energy released goes into oscillation modes. For this general model we find a dimensionless mode amplitude of around 10^{-6}, corresponding to a characteristic strain of around $10^{-24}\ \sqrt{\text{Hz}}$, a level expected to be detectable by third generation detectors. We also make some estimates for the more exotic scenario of a glitch in a completely solid quark star: in this case our model is able to account for much larger glitches, giving rise to a characteristic strain of up to around $10^{-22}\ \sqrt{\text{Hz}}$.

For the rest of the thesis, we specialise to a particular model of what happens at the starquake. Given this, we can then tackle the problem of self-consistently constructing initial data describing how the star changes at the glitch, and projecting this against a basis of its normal modes of oscillation. Our model for the glitch is that all strain is lost from the star at the glitch, and also that particles immediately after the glitch (Star C of our model) are not displaced from their positions in Star B.

To construct our toy model, we make the further assumption that the star is completely solid and incompressible. This allows us to carry out a large proportion of the work analytically. In our initial model, the star also spins down completely to zero angular velocity before glitching.

The next three chapters contain the preliminary work needed to carry out this projection. In Chapter 4 we calculate analytic equilibrium solutions for a rotating elastic incompressible star. The solution depends on the current angular velocity of the star, and also the angular velocity at which it was relaxed. An analytic solution for this problem exists in the literature [16]; here we fill in the details of the calculation, which will be used later in the thesis for constructing our initial data for the starquake.

The main focus of Chapter 5 is a calculation of the normal modes of oscillation of the star in our toy model, an elastic, incompressible self-gravitating star. This is an old problem, first investigated analytically by Bromwich in 1898 [19]. We reproduce his analytic results for the eigenvalues of this system and also extend it slightly by obtaining an analytic form for the eigenfunctions.

We then carry out a numerical investigation of the problem. Focussing on the $l = 2$ spheroidal modes (the most important for our problem), we find that the star has an infinite set of equally spaced elastic modes scaling with the shear modulus μ, and also one mode with a frequency close to that of the $l = 2$ fundamental ('Kelvin') mode of a fluid star. The corresponding eigenfunction has a hybrid fluid-elastic character, approximating that of the fluid Kelvin mode in the limit of small μ.

In Chapter 6 we discuss a series of simpler toy models of mode excitation, with the aim of building up to our starquake model and developing the necessary mathematical framework. The main new result of the chapter is a demonstration that the eigenfunctions of an elastic incompressible star found in Chapter 5 are orthogonal, by showing that the equations they satisfy constitute a self-adjoint boundary value problem.

We are then in a position to construct the full glitch toy model in Chapter 7. First we construct initial data describing the change in the star at the glitch, in the form of a displacement field connecting the new equilbrium state of the star that the star settles down to (Star D) with that immediately after the glitch. To do this we use the equilibrium solutions of Chapter 4, along with the prescription that particles in Star C are not displaced from their positions immediately before the glitch in Star B (only the strain is lost).

Next, we project this initial data against our orthogonal basis of normal modes calculated in Chapter 5. We do this for different values of the ratio of strain to gravitational energy, $\frac{B}{A}$, for $\frac{B}{A} = 0.1$ down to realistic values of $\frac{B}{A} = 10^{-5} - 10^{-6}$. We find that the majority of the glitch energy goes into the hybrid fluid-elastic mode. For realistic values of $\frac{B}{A}$, where this mode is very similar to the purely fluid Kelvin mode, this is extremely pronounced, with more that 99.9% of the energy going into this mode.

The final two chapters of the thesis deal with the extension of the model to the more realistic case where the star is still rotating at the glitch. The first complication this adds is that we have to take this rotation into account in order to calculate the oscillation

modes of Star D. We do this in Chapter 8, using the formalism of Strohmayer [80] to find the eigenvalues and eigenfunctions correct to first order in the rotational parameter. There is now a coupling of modes of different l values, so that the $l = 2$ spheroidal modes excited by our initial data in the zero spin problem now couple to $l = 1$ and $l = 3$ toroidal modes.

In the first part of Chapter 9 we calculate the initial data for the rotating model. There are now two free parameters in the initial data: the anglular velocity Ω_A that the star was relaxed at, and the angular velocity Ω_B at which the glitch occurs. We are able to calculate the increase in spin rate at the glitch, which gives us a nonzero velocity field as a new part of the initial data along with the displacement field. We show that this velocity field can be represented as an $l = 1$ toroidal mode of the nonrotating star with zero frequency.

A second complication added by rotation is that the modes of the rotating star are no longer orthogonal, so that we can no longer carry out a projection of the initial data against these modes in the same way as before. Instead, we develop a new scheme that relies on the fact that the oscillation modes are orthogonal to zeroth order in rotation, and that the first-order rotational corrections can be written as a sum over these zeroth-order modes. We can then project our initial data against the modes of the rotating star, including the zero frequency $l = 1$ toroidal mode representing rotation. We sketch the process of how to carry this out for the test case of $\frac{B}{A} = 0.1$. This is a useful test value because in this case the hybrid fluid-elastic mode is at the low radial eigenvalue number of $n = 3$. By analogy with the zero spin case we expect this mode to be excited most and then contributions from higher modes to drop off. This allows us to make a cut-off at $n = 10$.

Currently we are able to reproduce the displacement field but not the velocity using our method. We are still investigating what the problem is.

To extend this work, we need to test the model further and produce more robust results. For the $\frac{B}{A} = 0.1$ case we need to show that we can reproduce both the initial data and velocity accurately given the amplitudes of the excited modes. We would expect the $l = 2$ fluid-elastic mode to still be excited in a similar way to the glitch at zero spin model, plus small excitations of $l = 1$ and $l = 3$ toroidal modes. We would also expect the $l = 1$ zero frequency toroidal mode to be excited.

We also need to extend to more realistic values of $\frac{B}{A}$. One problem we expect to run into is that the eigenvalues may become very close together for high n. This near-degeneracy will mean that we will need to adapt the perturbation scheme that we use.

In terms of extending the model itself, there are a number of possibilities. One obvious one is to extend to the more realistic case where there is a fluid core and an elastic crust. This would complicate the spectrum of oscillation modes by adding extra ones

connected to the fluid-elastic interface. We could also consider using a more realistic equation of state rather than our incompressible model, introducing new p- and g-modes to the mode spectrum.

Another interesting direction would be to consider more realistic models for the starquake itself. At the moment we have an acausal mechanism in which all strain is lost from the star instantaneously. In a realistic model the quake would propagate across the star over time, possibly in the form of surface cracks. The new timescale introduced here could strongly affect which modes of the star are excited. However, this timescale is not well constrained observationally.

The oscillations produced by a starquake would be expected to shake the magnetosphere at the surface of the star. This could lead to radio emission connected with the starquake, possibly at a level that could be resolved with the new generation of radio telescopes. It would be worthwhile to try to make some estimates of this with a toy model of how the pulsar could shake magnetic field lines in the magnetosphere.

Appendix A

Approximating Star D as spherical

To find out which oscillation modes are excited in our first glitch model where the glitch occurs at zero spin, we first need to know the spectrum of possible oscillation modes of the new equilibrium configuration of the star after the glitch. This is Star D of our model.

This star is not completely spherical, because of the residual strain left after the glitch; instead, the surface shape S can be described by

$$S_D(\theta) = R(1 + a_2 P_2(\cos\theta)), \tag{A.1}$$

where a_2 is a small parameter. This is approximately an ellipse, to first order in the difference between the major and minor axes, as shown in Section 4.3.2. We would like to show that to first order in a_2 we can approximate the oscillation modes of Star D by those of the spherical background star S. To do this, we want to show that up to $O(a_2)$, the equations and boundary conditions governing the modes of Star D are the same as those of S.

In general, we would have two relevant small quantities in this problem: the perturbations δP and ξ^i, and the rotation shape parameterised by a_2. However, the case of our model the perturbations are generated by the initial data ξ^{CD} (7.82), whose components are also proportional to a_2: comparing with $(\eta_r)^{\mathrm{SD}}$ at the surface (7.54) we find

$$a_2 = \frac{5}{8\pi G\rho} \frac{\left(\frac{B}{A}\right)^2}{\left(1 + \frac{B}{A}\right)^2} \Omega_0^2 \,, \tag{A.2}$$

so that we can write the displacement ξ^{CD} as

$$(\xi^{\mathrm{CD}})^r(r,\theta) = \frac{1}{5R^2}\frac{a_2}{K}\left(3r^3 - 8R^2 r\right) P_2(\cos\theta), \tag{A.3}$$

$$(\xi^{\mathrm{CD}})^\theta(r,\theta) = \frac{1}{5R^2}\frac{a_2}{K}\left(\frac{5}{2}r^4 - 4R^2 r^2\right)\frac{dP_2}{d\theta}. \tag{A.4}$$

Similarly, we can show that δp and $\delta\Phi$ are also first order in the oblateness parameter a_2.

To find the normal modes, we start by making some arbitrary small perturbation ξ to Star D. This perturbation will induce some extra strain in the star, and the equations of motion become

$$-\rho_D\omega^2\xi_i = -\nabla_i\delta P + \mu\nabla^2\xi_i - \rho_D\nabla_i\delta\Phi. \tag{A.5}$$

Here ρ_D is the density of the background star. We also have Poisson's equation

$$\nabla^2\delta\Phi = 4\pi G\delta\rho. \tag{A.6}$$

First, we can write $\delta\rho$ as

$$\delta\rho = -\xi^i\nabla_i\rho_D. \tag{A.7}$$

Writing ρ_D in terms of a Heaviside step function, we have

$$\rho_D = \rho[1 - H(r - R(1 + a_2P_2(\cos\theta)))], \tag{A.8}$$

so that

$$\frac{\partial\rho_D}{\partial r} = -\delta(r - R(1 + a_2P_2(\cos\theta))) \tag{A.9}$$

$$\frac{\partial\rho_D}{\partial\theta} = a_2R\sin\theta\,\frac{dP_2}{d\theta}\delta(r - R(1 + a_2P_2(\cos\theta))). \tag{A.10}$$

This gives

$$\delta\rho = \xi^r\delta(r - R(1 + a_2P_2(\cos\theta))) + \xi^\theta a_2R\sin\theta\,\frac{dP_2}{d\theta}\delta(r - R(1 + a_2P_2(\cos\theta))), \tag{A.11}$$

and so inserting this back into Poisson's equation (A.6) gives

$$\nabla^2\delta\Phi = 4\pi G\left[\xi^r\delta(r - R(1 + a_2P_2(\cos\theta)) + \xi^\theta a_2R\sin\theta\,\frac{dP_2}{d\theta}\delta(r - R(1 + a_2P_2(\cos\theta)))\right]. \tag{A.12}$$

Integrating this over the volume V of the star, and using Stokes' theorem on the LHS, we get

$$\begin{aligned}\int_{S_D} \nabla_i \delta\Phi dS^i = 4\pi G \int_V \xi^r \delta(r - R(1 + a_2 P_2(\cos\theta)) \\ + \xi^\theta a_2 R \sin\theta \frac{dP_2}{d\theta} \delta(r - R(1 + a_2 P_2(\cos\theta)))\end{aligned} \tag{A.13}$$

$$= 4\pi G \left([\xi^r]_{S_D} + a_2 R \sin\theta \frac{dP_2}{d\theta} [\xi^\theta]_{S_D} \right). \tag{A.14}$$

We see that the second term is $O(a_2)$, and so this term will not contribute. This leaves

$$\int_{S_D} \nabla_i \delta\Phi dS^i = 4\pi G [\xi^r]_{S_D}. \tag{A.15}$$

The surface traction boundary condition is

$$(-\Delta P \delta_{ij} + 2\mu u_{ij})\, n^i = 0, \tag{A.16}$$

imposed at the surface of D, defined by (A.1). The normal to D, n^i, is only slightly different to that of S, so we can write $n^i = r^i + \epsilon^i$ for a small vector ϵ^i. As ΔP and u_{ij} are already first order in a_2, we can just write

$$(-\Delta P \delta_{ij} + 2\mu u_{ij})\, r^i = 0 \tag{A.17}$$

as for the spherical star.

References

[1] J. Abadie, B. P. Abbott, R. Abbott, T. D. Abbott, M. Abernathy, T. Accadia, F. Acernese, C. Adams, R. Adhikari, C. Affeldt, and et al. All-sky search for gravitational-wave bursts in the second joint LIGO-Virgo run. *Physical Review D*, 85(12):122007, June 2012.

[2] J. Abadie, B. P. Abbott, R. Abbott, M. Abernathy, T. Accadia, F. Acernese, C. Adams, R. Adhikari, P. Ajith, B. Allen, and et al. Search for gravitational waves from compact binary coalescence in LIGO and Virgo data from S5 and VSR1. *Physical Review D*, 82(10):102001, November 2010.

[3] J. Abadie, B. P. Abbott, R. Abbott, R. Adhikari, P. Ajith, B. Allen, G. Allen, E. Amador Ceron, R. S. Amin, S. B. Anderson, and et al. Search for gravitational waves associated with the August 2006 timing glitch of the Vela pulsar. *Physical Review D*, 83(4):042001, February 2011.

[4] B. Abbott, R. Abbott, R. Adhikari, P. Ajith, B. Allen, G. Allen, R. Amin, S. B. Anderson, W. G. Anderson, M. A. Arain, and et al. Beating the Spin-Down Limit on Gravitational Wave Emission from the Crab Pulsar. *ApJ Letters*, 683:L45–L49, August 2008.

[5] B. P. Abbott, R. Abbott, F. Acernese, R. Adhikari, P. Ajith, B. Allen, G. Allen, M. Alshourbagy, R. S. Amin, S. B. Anderson, and et al. An upper limit on the stochastic gravitational-wave background of cosmological origin. *Nature*, 460:990–994, August 2009.

[6] B. P. Abbott, R. Abbott, R. Adhikari, P. Ajith, B. Allen, G. Allen, R. S. Amin, S. B. Anderson, W. G. Anderson, M. A. Arain, and et al. LIGO: the Laser Interferometer Gravitational-Wave Observatory. *Reports on Progress in Physics*, 72(7):076901, July 2009.

[7] M. Aizenman, P. Smeyers, and A. Weigert. Avoided Crossing of Modes of Non-radial Stellar Oscillations. *Astronomy and Astrophysics*, 58:41, June 1977.

[8] M. A. Alpar, D. Pines, P. W. Anderson, and J. Shaham. Vortex creep and the internal temperature of neutron stars. I - General theory. *The Astrophysical Journal*, 276:325–334, January 1984.

[9] P. W. Anderson and N. Itoh. Pulsar glitches and restlessness as a hard superfluidity phenomenon. *Nature*, 256:25–27, July 1975.

[10] N. Andersson. TOPICAL REVIEW: Gravitational waves from instabilities in relativistic stars. *Classical and Quantum Gravity*, 20:105, April 2003.

[11] G. B. Arfken and H. J. Weber. *Mathematical Methods for Physicists*. Elsevier Academic Press, 2005.

[12] W. Baade and F. Zwicky. Cosmic Rays from Super-novae. *Proceedings of the National Academy of Science*, 20:259–263, May 1934.

[13] G. Backus and F. Gilbert. The Rotational Splitting of the Free Oscillations of the Earth. *Proceedings of the National Academy of Science*, 47:362–371, March 1961.

[14] G. Baym and C. Pethick. Neutron stars. *Annual Review of Nuclear and Particle Science*, 25:27–77, 1975.

[15] G. Baym, C. Pethick, and D. Pines. Superfluidity in Neutron Stars. *Nature*, 224:673–674, November 1969.

[16] G. Baym and D. Pines. Neutron starquakes and pulsar speedup. *Annals of Physics*, 66:816–835, 1971.

[17] G. Birkhoff and G. Rota. *Ordinary Differential Equations*. Ginn and Company, 1962.

[18] R. Blandford and K. Thorne. *Applications of Classical Physics*. http://www.pma.caltech.edu/Courses/ph136/yr2008/, 2008.

[19] T. Bromwich. On the influence of gravity on elastic waves, and in particular on the vibrations of an elastic globe. *Proc. of the London Mathematical Society*, 30, 1898.

[20] S. Chandrasekhar. The Maximum Mass of Ideal White Dwarfs. *The Astrophysical Journal*, 74:81, July 1931.

[21] S. Chandrasekhar. A General Variational Principle Governing the Radial and the Non-Radial Oscillations of Gaseous Masses. *The Astrophysical Journal*, 139:664, February 1964.

[22] S. Chandrasekhar and N. R. Lebovitz. Non-Radial Oscillations of Gaseous Masses. *The Astrophysical Journal*, 140:1517, November 1964.

[23] W.-Y. Chau. Gravitational Radiation from Neutron Stars. *The Astrophysical Journal*, 147:664–+, February 1967.

[24] T. G. Cowling. The non-radial oscillations of polytropic stars. *MNRAS*, 101:367–+, 1941.

[25] T. G. Cowling and R. A. Newing. The Oscillations of a Rotating Star. *The Astrophysical Journal*, 109:149, January 1949.

[26] J. P. Cox. *Theory of stellar pulsations.* Princeton University Press, 1983.

[27] P. B. Demorest, T. Pennucci, S. M. Ransom, M. S. E. Roberts, and J. W. T. Hessels. A two-solar-mass neutron star measured using Shapiro delay. *Nature*, 467:1081–1083, October 2010.

[28] T. Ersek. *RootSearch.* http://library.wolfram.com/infocenter/Demos/4482, 2008.

[29] C. M. Espinoza, A. G. Lyne, B. W. Stappers, and M. Kramer. A study of 315 glitches in the rotation of 102 pulsars. *MNRAS*, 414:1679–1704, June 2011.

[30] L. M. Franco, B. Link, and R. I. Epstein. Quaking Neutron Stars. *Astrophysical Journal*, 543:987–994, November 2000.

[31] J. L. Friedman and B. F. Schutz. Lagrangian perturbation theory of nonrelativistic fluids. *The Astrophysical Journal*, 221:937–957, May 1978.

[32] K. Glampedakis and N. Andersson. Hydrodynamical Trigger Mechanism for Pulsar Glitches. *Physical Review Letters*, 102(14):141101, April 2009.

[33] N. K. Glendenning. *Compact Stars.* 1996.

[34] T. Gold. Rotating Neutron Stars as the Origin of the Pulsating Radio Sources. *Nature*, 218:731–732, May 1968.

[35] P. Haensel, A. Y. Potekhin, and D. G. Yakovlev, editors. *Neutron Stars 1 : Equation of State and Structure*, volume 326 of *Astrophysics and Space Science Library*, 2007.

[36] B. Haskell, N. Andersson, D. I. Jones, and L. Samuelsson. Are Neutron Stars with Crystalline Color-Superconducting Cores Relevant for the LIGO Experiment? *Physical Review Letters*, 99(23):231101, December 2007.

[37] A. Hewish, S. J. Bell, J. D. H. Pilkington, P. F. Scott, and R. A. Collins. Observation of a Rapidly Pulsating Radio Source. *Nature*, 217:709–713, February 1968.

[38] C. J. Horowitz and K. Kadau. Breaking Strain of Neutron Star Crust and Gravitational Waves. *Physical Review Letters*, 102(19):191102, May 2009.

[39] R. A. Hulse and J. H. Taylor. Discovery of a pulsar in a binary system. *ApJ Letters*, 195:L51–L53, January 1975.

[40] Richard A. Isaacson. Gravitational radiation in the limit of high frequency. i. the linear approximation and geometrical optics. *Phys. Rev.*, 166:1263–1271, Feb 1968.

[41] Richard A. Isaacson. Gravitational radiation in the limit of high frequency. ii. nonlinear terms and the effective stress tensor. *Phys. Rev.*, 166:1272–1280, Feb 1968.

[42] M. Kramer, I. H. Stairs, R. N. Manchester, M. A. McLaughlin, A. G. Lyne, R. D. Ferdman, M. Burgay, D. R. Lorimer, A. Possenti, N. D'Amico, J. M. Sarkissian, G. B. Hobbs, J. E. Reynolds, P. C. C. Freire, and F. Camilo. Tests of general relativity from timing the double pulsar. *Science*, 314(5796):97–102, 2006.

[43] L. D. Landau and E. M. Lifschitz. *Theory of Elasticity.* Pergamon, 1986.

[44] L. D. Landau and E. M. Lifshitz. *Fluid mechanics.* 1959.

[45] E. R. Lapwood and T. Usami. *Free Oscillations of the Earth.* Cambridge University Press, 1981.

[46] J. M. Lattimer and M. Prakash. The Physics of Neutron Stars. *Science*, 304:536–542, April 2004.

[47] J. M. Lattimer and M. Prakash. What a Two Solar Mass Neutron Star Really Means. *ArXiv e-prints*, December 2010.

[48] James M. Lattimer. The nuclear equation of state and neutron star masses. *Annual Review of Nuclear and Particle Science*, 62(1):485–515, 2012.

[49] L. Lindblom. Determining the nuclear equation of state from neutron-star masses and radii. *The Astrophysical Journal*, 398:569–573, October 1992.

[50] D. R. Lorimer. What's new in the pulsar world? In J. F. Nieves, editor, *Particle Physics and Cosmology*, volume 540 of *American Institute of Physics Conference Series*, pages 247–262, October 2000.

[51] D. R. Lorimer. Binary and Millisecond Pulsars. *Living Reviews in Relativity*, 8:7–+, November 2005.

[52] A. Love. *A Treatise on the Mathematical Theory of Elasticity.* Dover, 1927.

[53] D. Lynden-Bell and J. P. Ostriker. On the stability of differentially rotating bodies. *MNRAS*, 136:293, 1967.

[54] A. G. Lyne and F. Graham-Smith. *Pulsar Astronomy.* Cambridge University Press, 1998.

[55] A. G. Lyne, F. G. Smith, and R. S. Pritchard. Spin-up and recovery in the 1989 glitch of the Crab pulsar. *Nature*, 359:706, October 1992.

[56] G. J. F. MacDonald and N. F. Ness. A Study of the Free Oscillations of the Earth. *Journal of Geophysical Research*, 66:1865–1911, June 1961.

[57] R. N. Manchester, G. B. Hobbs, A. Teoh, and M. Hobbs. The Australia Telescope National Facility Pulsar Catalogue. *The Astronomical Journal*, 129:1993–2006, April 2005.

[58] P. M. McCulloch, P. A. Hamilton, G. W. R. Royle, and R. N. Manchester. Daily observations of a large period jump of the VELA pulsar. *Nature*, 302:319–321, March 1983.

[59] P. N. McDermott, H. M. van Horn, and C. J. Hansen. Nonradial oscillations of neutron stars. *The Astronphysical Journal*, 325:725–748, February 1988.

[60] A. Melatos, C. Peralta, and J. S. B. Wyithe. Avalanche Dynamics of Radio Pulsar Glitches. *The Astrophysical Journal*, 672:1103–1118, January 2008.

[61] P. Olver. *Introduction to Partial Differential Equations.* http://www.math.umn.edu/ olver/pdn.html, 2012.

[62] J. R. Oppenheimer and G. M. Volkoff. On Massive Neutron Cores. *Physical Review*, 55:374–381, February 1939.

[63] B. J. Owen. Maximum Elastic Deformations of Compact Stars with Exotic Equations of State. *Physical Review Letters*, 95(21):211101, November 2005.

[64] F. Pacini. Rotating Neutron Stars, Pulsars and Supernova Remnants. *Nature*, 219:145–146, July 1968.

[65] V. R. Pandharipande, D. Pines, and R. A. Smith. Neutron star structure: theory, observation, and speculation. *The Astrophysical Journal*, 208:550–566, September 1976.

[66] J. Papaloizou and J. E. Pringle. Non-radial oscillations of rotating stars and their relevance to the short-period oscillations of cataclysmic variables. *MNRAS*, 182:423–442, February 1978.

[67] C. L. Pekeris, Z. Alterman, and H. Jarosch. Rotational multiplets in the spectrum of the earth. *Phys. Rev.*, 122:1692–1700, Jun 1961.

[68] C. J. Pethick, A. Akmal, V. R. Pandharipande, and D. G. Ravenhall. Neutron star structure. *Nuclear Physics B Proceedings Supplements*, 80:C1114+, January 2000.

[69] M. Pitkin, S. Reid, S. Rowan, and J. Hough. Gravitational Wave Detection by Interferometry (Ground and Space). *Living Reviews in Relativity*, 14:5–+, July 2011.

[70] M. Punturo. Et sensitivities. 2009.

[71] V. Radhakrishnan and R. N. Manchester. Detection of a Change of State in the Pulsar PSR 0833-45. *Nature*, 222:228–229, April 1969.

[72] A. I. M. Rae. *Quantum Mechanics, Fourth edition.* IOP Publishing, 2002.

[73] P. E. Reichley and G. S. Downs. Observed Decrease in the Periods of Pulsar PSR 0833-45. *Nature*, 222:229–230, April 1969.

[74] M. Ruderman. Neutron Starquakes and Pulsar Periods. *Nature*, 223:597–598, August 1969.

[75] B. Schutz. *A First Course in General Relativity.* Cambridge University Press, 2009.

[76] S. L. Shapiro and S. A. Teukolsky. *Black Holes, White Dwarfs, and Neutron Stars.* John Wiley & Sons, 1983.

[77] D. Shoemaker. Ligo document t0900288-v3. 2009.

[78] T. Sidery, A. Passamonti, and N. Andersson. The dynamics of pulsar glitches: contrasting phenomenology with numerical evolutions. *MNRAS*, 405:1061–1074, June 2010.

[79] T. Strohmayer, H. M. van Horn, S. Ogata, H. Iyetomi, and S. Ichimaru. The shear modulus of the neutron star crust and nonradial oscillations of neutron stars. *The Astrophysical Journal*, 375:679–686, July 1991.

[80] T. E. Strohmayer. Oscillations of rotating neutron stars. *The Astrophysical Journal*, 372:573–591, May 1991.

[81] J. H. Taylor and J. M. Weisberg. A new test of general relativity - Gravitational radiation and the binary pulsar PSR 1913+16. *ApJ Letters*, 253:908–920, February 1982.

[82] W. Thomson. On the rigidity of the earth. *Phil. Trans. Roy. Soc. London*, 153:573–582, 1863.

[83] W. Unno, Y. Osaki, H. Ando, H. Saio, and H. Shibahashi. *Nonradial oscillations of stars.* 1989.

[84] C. A. van Eysden and A. Melatos. Gravitational radiation from pulsar glitches. *Classical and Quantum Gravity*, 25(22):225020, November 2008.

[85] R. M. Wald. *General relativity.* 1984.

[86] T. Wong, D. C. Backer, and A. G. Lyne. Observations of a Series of Six Recent Glitches in the Crab Pulsar. *The Astrophysical Journal*, 548:447–459, February 2001.

[87] R. X. Xu. Solid Quark Stars? *The Astrophysical Journal*, 596:L59–L62, October 2003.

[88] A. Y Potekhin. The physics of neutron stars. *Physics Uspekhi*, 53:1235–1256, December 2010.